NEXT GENERATION PEPTIDE NUCLEIC ACIDS FOR CHARGE AND SPIN TRANSPORT STUDIES

by

Selma Ulku

A dissertation submitted in partial fulfillment of the requirements for the degree of

Doctor of Philosophy in Chemistry

Carnegie Mellon University
Pittsburgh, Pennsylvania
April 2017

To my family,

My love Evren, and My Kids, Arda & Beliz

ACKNOWLEDGMENTS

I would like to express my most sincere appreciation and profound gratitude to my advisor Dr. Catalina Achim for her valuable advice, continuous guidance, and unforgettable encouragement and understanding throughout my studies. Catalina, you have not only been a great mentor but also a very good friend for me and my family. I feel fortunate to have completed my Ph.D. under your supervision.

Sincere thanks are extended to the other members of my Dissertation Committee. I am highly grateful to Dr. Armitage and Dr. Ly for providing invaluable suggestions and advice. I am also thankful to Dr. Liu for agreeing to be an external examiner and constructive comments. Special thanks to my undergraduate advisor, Dr. Ender Erdik for the inspiration to pursue higher studies.

I wish to thank our collaborators, Dr. Waldeck and his group; especially Ed Beall and Dr. Emil Wierzbinski for the conductance results; Dr. Beratan and his group for their theoretical calculations; Dr. Naaman and his group members Dr. Nirit Kantor and Dr. Francesco Tassinari for SAM, solid device preparation and magnetoresistance data; Dr. Zacharias and Paul for Mott Polarimeter data. My work could not be completed without their contribution.

I would like to express my deep gratitude to Chemistry Department of Carnegie Mellon University for their generous funding throughout my graduate study. I would like to thank my current and past group member coworkers, especially Dilhara, Yookie, Heather and Artur for all their kindness, help and being like a family during my time at CMU. I wish all of them the best of luck in their future careers. I also would like to thank

all the undergraduate students whom I had a chance to teach and train. They gave me the biggest smile on my face every time I worked with them.

I would like to thank my family; my parents, my mother Emine and father Ahmet (Mom I could not have been who I am today without your endless support during all my studies, thank you for being the best mom ever); sister Belma and brother Özgür for their love, patience, encouragement and continuous support throughout my studies. They have done their best to make rough times manageable. This has been a long and difficult journey and none of these could have been possible without them.

Last but not least, my biggest thanks go to the love of my life Dr. Evren Ülkü, without your tremendous love, support and help I could not have achieved my goals. I should admit when I struggled the most, I gave you the hardest time, but hey we made it together. My two precious ones Arda and Beliz, you both suffered from having a graduate student mommy. Arda, you went through every challenging step with me. I am sorry for stealing from your time; I hope I can make you a little proud of what your mom could achieve.

Being a mother of two and a graduate student was the most challenging assignment I've had so far in my life. My dream could not have been real if I did not have the support from the people I was surrounded with. I will always have extra sympathy for the women with a family trying to achieve their goals.

ABSTRACT

Next Generation PNA for Charge and Spin Transport Studies

By: Selma Ulku

Advisor: Professor Catalina Achim

PNA is a synthetic analog of DNA in which the sugar diphosphate backbone is replaced by a polyamide one consisting of repeating N-(2-aminoethyl)-glycine (aeg) units. PNA serves as a good scaffold for organic and inorganic compounds with a variety of magnetic, electronic and photophysical properties and of potential applications. Though the synthesis of non-modified, aeg-PNA as well as of PNA with modifications in the backbone or nucleobases is relatively straightforward, the synthesis of long modified PNA strands is time consuming and relatively low yield, and thus costly. Research in this thesis describes the use of the template method for the synthesis of long modified PNAs and their use in spectroscopic, electronic and magnetic studies. The focus was on the hybridization of short 10-base PNA single strands on a long 20-bp PNA or DNA template strand to form long PNA duplexes. The 20-bp duplex can be formally seen as the concatenation of two 10-base pair duplexes.

The spin-selective transmission of electrons through self-assembled monolayers of stitched γ-modified and non-modified PNA duplexes on Au was measured. Variable temperature UV-vis, CD spectroscopy and fluorescence spectroscopy were used to evaluate the stitching protocol for the synthesis of 20-bp PNA duplexes. Self-assembled monolayers (SAMs) of the stitched PNA duplexes with thiol linkers have been characterized by Ellipsometry and PM-IRRAS. The observed spin polarizations for the SAMs of stitched aeg-PNA and γ-PNA duplexes were approximately +20% and -5% at

room temperature, respectively. This remarkable spin polarization of γ-PNAs establishes dsPNA as a candidate for room-temperature spin filter.

Scanning tunneling microscope-break junction measurements have been used to examine how the molecular conductance of nucleic acids depends on the chemical nature of their backbone and on the linker group that connects the PNA to the electrodes. The molecular conductance was measured for 10-base pair long homo-duplexes of DNA, aeg-PNA, γ-PNA, and a hetero-duplex of DNA/aeg-PNA; all duplexes had the same sequence of nucleobases. The molecular conductance was found to vary by 12 to 13 times with the change in backbone. Computational studies showed that the molecular conductance differences between nucleic acids of different backbones correlate with differences in backbone structural flexibility. The molecular conductance was also measured for duplexes connected to the electrode through two different linkers, one directly to the PNA backbone and one directly to the nucleobase stack. The linker caused an order of magnitude variation in the conductance of a particular duplex. The differences in the electrical conductance due to the chemical nature of the backbone manifested irrespective of the linker. The highest molecular conductance value, 0.06 G_0, was measured for aeg-PNA duplexes with a base stack linker. These findings reveal an important new strategy for creating longer and more complex electroactive, nucleic acid assemblies.

Finally, the stitching of the short PNA duplexes by coordination to a pair of a ligand (Q or Bpy) situated at adjacent ends of the short PNA strands hybridized on the template was examined. The stability and helical structure of the stitched duplexes in the absence of a metal and in the presence of a metal (Ni^{2+}, or Cu^{2+}) were determined by variable temperature UV-Vis and CD spectroscopy, respectively. The inclusion of ligands

at adjacent ends of two 10-base PNAs hybridized to a template had a very small effect on the stability of the stitched duplex. In contrast, the metal coordination increased the thermal stability of ligand-modified stitched PNA duplexes thus supporting the idea that the inter-strand metal complexes act as glue for the two short PNAs. UV titrations show that the bridging metal complexes have an ML_2 stoichiometry. In one case, the metal complex formed in the middle of the duplex affected the handedness of the stitched duplex. The stability constants of these complexes are similar to those which in past research have been formed between ligands situated in complementary position in the duplexes and acted as alternative base pair.

CONTENTS

TABLE OF CONTENTS

LIST OF FIGURES

CHAPTER I

CHAPTER II

CHAPTER III

LIST OF TABLES

CHAPTER III

CHAPTER IV

CHAPTER V

LIST OF SCHEMES

CHAPTER II

ABBREVIATIONS AND SYMBOLS

ACN	Acetonitrile
ALD	Atomic layer decomposition
Prolyl ACPC	prolyl-2-aminocyclopentanecarboxylic acid
Aeg	N-(2-aminoethyl)-glycine
Apg	aminopropylglycine
Boc	tert-Butyloxycarbonyl
Bn	Benzyl
Bpy	Bipyridin
Cbz	Carboxybenzyl
Cya	Cysteamine
Cys	Cysteine
CD	Circular dichroism
CPD	Contact potential difference
CT	Charge transfer
CV	Cyclic voltammetry
DCC	Dicyclohexylcarbodiimide
DCM	Dichloromethane
Dap	3-amino-L-Alanine
DhBtOh	3-Hydroxy-1,2,3-benzotriazin-4(3H)-one
DIAD	Diisopropyl azodicarboxylate
DIE	Diisopropyl ethyl amine
DME	Dimethoxyethane
DMF	Dimethylforamide
DMSO	Dimethylsulfoxide
DNA	Deoxyribonucleic acid
ds-	Double stranded
Fc	Ferrocene
Fmoc	Fluorenylmethyloxycarbonyl
HATU	1-[Bis(dimethylamino)methylene]-1H-1,2,3-triazolo[4,5-b]pyridinium 3-oxid hexafluorophosphate
HBTU	2-(1*H*-benzotriazol-1-yl)-1,1,3,3-tetramethyluronium hexafluorophosphate
HOBt	1-Hydroxybenzotriazole hydrate
HPLC	High pressure liquid chromatography
LDA	Lithium diisopropylamide
MALDI/TOF/MS	Matrix-assisted laser desorption/ionization time of flight mass spectrometry
MD	Molecular dynamics
MeOH	Methanol
M	Magnetoresitance
NaPi	Sodium phosphate
NMM	N-methylmorpholine
PM-IRRAS	Polarization modulation infrared reflection absorption spectroscopy
PL	Photoluminescence
PNA	Peptide nucleic acid
PT	Propylthiol
SPV	Surface photovoltage

HQ/Q	Hydroxyquinoline
SAMs	Self-assembled monolayers
ss-	Single stranded
STM-BJ	Scanning tunneling microscope break junction
TEMPO	2,2,6,6-tetramethylpiperidine-1-oxyl
TPP	Triphenylphosphine
Tpy	Terpyridine
BAIB	(Diacetoxyiodo)benzene
TBAF	Tetra-*n*-butylammonium fluoride
THF	Tetrahydrofuran
TFA	Trifluoroacetic acid
TFMSA	Trifluoromethanesulfonic acid
TMSCl	Trimethylsilyl chloride
T_m	Melting temperature
Tris	tris(hydroxymethyl)aminomethane
UV	Ultraviolet
Vis	Visible

CHAPTER I. INTRODUCTION

I.1. Chiral Peptide Nucleic Acid Monomers

PNA is a synthetic analog of DNA in which the sugar diphosphate backbone is replaced by a polyamide skeleton consisting of repeating N-(2-aminoethyl)-glycine (aeg) units linked by amide bonds.[1] The purine (adenine, guanine) and pyrimidine (cytosine and thymine) nucleobases are attached to the glycine secondary nitrogen through a methylene carbonyl linker. PNA forms duplexes by Watson-Crick base pairing (Figure I.1).[2]

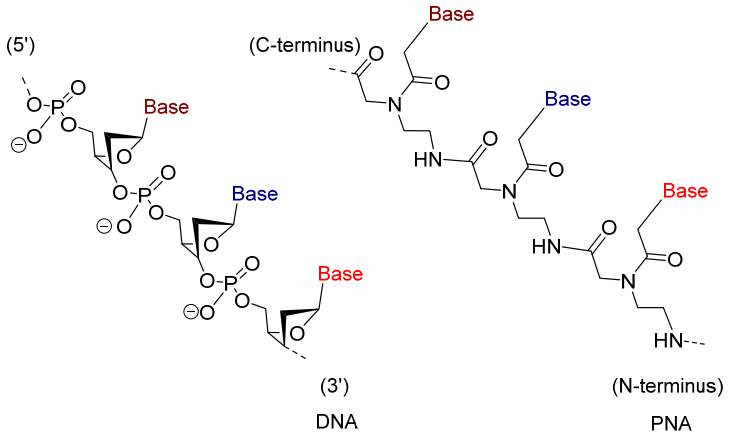

Figure I.1 Chemical Structure of DNA and PNA

The backbone of PNA is neutral and achiral. The neutral character of PNA is an important and significant feature. One of the most notable consequences of the neutral character is the stronger binding between complementary PNA/DNA strands than between complementary DNA/DNA strands due to lack of charge repulsion between the PNA and DNA strand. Therefore, PNA/DNA duplexes are more stable than the corresponding DNA/DNA duplexes. PNA does not only have strong binding affinity but it also has a strong selectivity toward DNA and RNA. The relative rigidity of the PNA backbone improves sequence selectivity on hybridization.[3] PNA is not prone to

degradation by proteases and nucleases as DNA and RNA are[4] and has low affinity for proteins.[5] A noteworthy feature of PNAs is their ability to invade dsDNA. In earlier reports,[6-10] it has been also shown that PNAs can target DNA duplexes in living cells by strand invasion. High stability of PNA/DNA duplexes enables strand invasion displacing DNA strand. Strand invasion requires high stability of PNA/DNA duplexes to compete with the displaced DNA strand. Preorganization of PNA increases binding affinity for DNA and RNA, thus increases antisense and antigene potency. One of the methods used in the literature to improve the binding affinity of the PNA towards DNA is to design and synthesize preorganized PNAs preferring a right-handed helical conformation.

Since the first discovery of PNA in 1991 by Nielsen, the great potential of PNA has stimulated chemists to develop new PNA analogues with superior properties to unmodified PNA. Many modified PNAs have been obtained by modifying the PNA aeg backbone, nucleobases, and the linker connecting a nucleobase to the backbone. These studies focused on the 'structural space' occupied by PNA, as well as to obtain a molecular understanding of the chemical parameters that determine the DNA and RNA mimicking properties of a peptide nucleic acid analogue. It was shown that preorganization can be achieved by cyclization of the PNA backbone or by adding substituents to the backbone.[11-12] The main drawbacks of the PNA are the solubility, biocompatibility and poor cellular uptake as compared to DNA and RNA. The elaboration of modified PNAs also aims to overcome these problems.

Since the PNA backbone is achiral, PNA duplexes form racemic mixture of right handed and left handed helices. A preferred handedness can be induced in PNA duplexes using a chiral molecular component, such as a chiral amino acid or a stereogenic center at

the α-, β- or γ- positions of the PNA aeg backbone (Figure I.2). For example, incorporation of a chiral L-lysine to the C-terminal base of the PNA results in a left-handed helix.[13] Ly et al. have shown that insertion of a (S)-Me chiral center at the γ-position induced the formation of a right-handed helix.[14] The handedness of the helix depends on the length of the PNA/PNA duplexes.[13] The nature of the side chain of the amino acid and the identity of the nucleobase closest to the chiral amino acid at the C-terminal end also play an important role for the preferred handedness.[13]

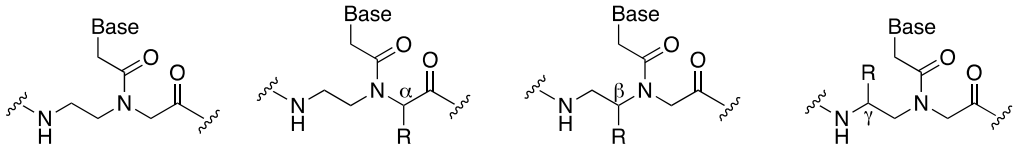

Figure I.2 Chemical structures of achiral and chiral PNA (α, β, γ) monomers

The question of accommodating functionality (and chirality) in the PNA backbone can be answered by constructing PNA monomers from α-amino acids other than glycine. However, these modifications should be carried out in a stereospecific manner; if not, one ends up with 2^n isomers for a PNA molecule with n monomers. By using natural amino acids, one can also take advantage of the enormous amount of information in the literature regarding the physical and chemical properties of various amino acids. This functionality would provide opportunities to tailor the hybridization behavior of PNA. The influences on other properties such as solubility and cell penetration have also been studied. PNA backbone or nucleobases provide convenient attachment points for various biologically active ligands.

First α-chiral PNA was reported by Nielsen in 1994, in which glycine moiety of the PNA backbone was replaced by alanine.[15] Both the L- and D- enantiomers of the

chiral monomers were synthesized from L- or D-alanine and integrated into oligomers. The lysine side chain of α-Lys monomer was used as a handle for site specific incorporation of functional molecules into PNA oligomers.[16] Synthesis of a series of α-PNAs bearing glycosylated side chains at the α-position and their selective biodistribution was reported by Nielsen in 2003.[17] Synthesis of *C*-linked glycosylated α-PNA and its successful incorporation into a PNA oligomer using Fmoc chemistry was demonstrated by Metzler-Nolte et al.[18] In addition to natural amino acids and carbohydrates, cyclobutyl-carbonyl-containing α-PNA monomer was stereoselectively synthesized from (+)-α-pinene.[19] Czerny et al. recently introduced phosphonic ester into the α-side chain (Figure I.3).[20]

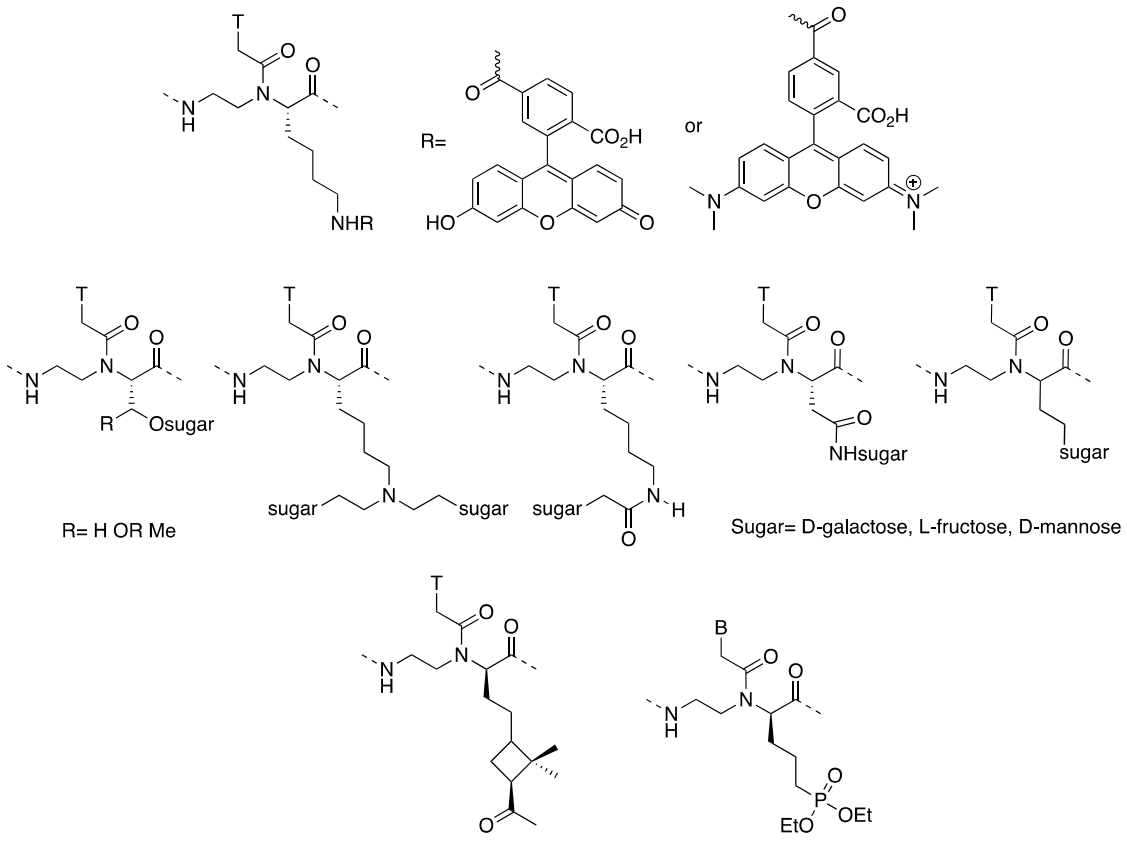

Figure I.3 Structures of α-PNAs bearing functional molecules

PNAs with a single substituent only at the β-position (β-PNAs) have recently been synthesized though some cyclic PNA analogues have a chiral center at the β-position.[21-24] Sugiyama et al. reported the first β-PNA bearing a methyl group at the β-position in 2011 (Figure I.4).[25]

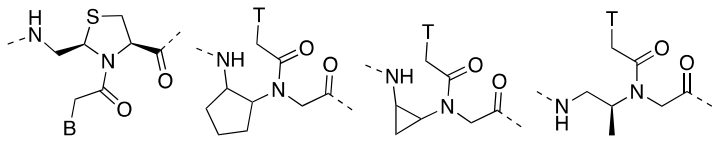

Figure I.4 Structures of β-PNAs bearing functional molecules

Oligomers carrying γ-chiral units were not reported until 2005 [26-29] although the first γ-chiral PNA monomer appeared in 1994.[30] Figure I.5 shows the some representative examples of γ-PNA monomers. In 2005, Appella et al. reported PNA oligomers carrying Lys and Lys side chain was used as a handle for fluorene incorporation aiming at developing quencher- free molecular PNA beacons.[27, 31] Cysteine-based PNA have been also reported. PNA oligomers carrying the Cys-based monomer at the *N*-terminus could be used for native chemical PNA ligation with thioesters of PNAs to yield long chain PNAs.[26] A variety of γ-PNAs bearing side chains derived from amino acids have been reported to improve solubility, rigidity and binding affinities towards DNA and RNA analogues.[32-34] Sulfate group bearing PNAs was aimed at making PNAs more DNA-like in terms of polarity and charge. [35]

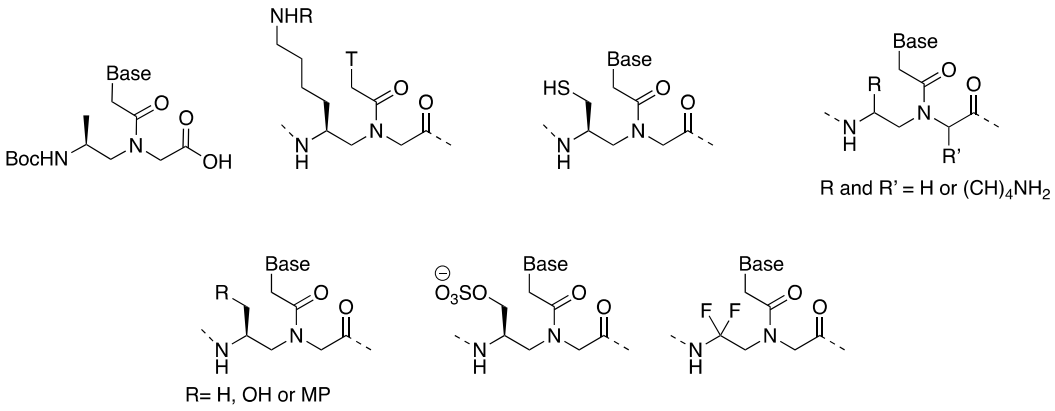

Figure I.5 Structures of γ-PNA bearing functional molecules[26-27, 29-31, 35-36]

I.2. Thesis Organization

An important part of this research is dedicated to PNA duplex formation between two 10-base PNA strands on a complementary PNA or DNA template and to their applications. To stitch PNA duplexes on a complementary template, different types of modifications were introduced on PNA strands including γ-modification, ligands, thiol linkers, and pyrene.

Chapter II describes the synthesis of small organic molecules which can be incorporated in PNA oligomers. Seven PNA monomers with different features have been prepared. They were used in research described in the thesis to study the properties of PNA/PNA and PNA/DNA duplexes such as stability and helical sense. Acetic acids of Tpy and Bpy ligands, were prepared and inserted into peptide nucleic acids through solid phase peptide synthesis. A new derivative of the acetic acid of C2-amino uracil was prepared. Propylthiol linkers were made in high yields and used to prepare N-end thiol modified peptide nucleic acids.

Chapter III examines the possibility of "stitching" short PNAs onto a PNA or DNA template and the spin filter properties of stitched Aeg- and γ-PNA/PNA homo-

duplexes. UV-vis melting profiles, CD spectroscopy and fluorescence spectroscopy were used to evaluate the stitching 20-base pair homo-PNA/PNA and hetero-PNA/DNA duplexes were formed by the hybridization of 10-base strands onto a PNA or DNA template. The thermal stability of stitched γPNA duplexes was similar to that of stitched pyrene PNAs. The stitched homo γ- and pyrene-containing PNA/PNA duplexes were right-handed. SAMs of these PNA duplexes with different type of thiol linkers, such as cysteamine (Cya), cysteine (Cys) and propylthiol (PT), have been prepared and characterized by ellipsometry and polarization modulation-infrared reflection-adsorption spectroscopy PM-IRAS. The magnetoresistance and spin polarization properties of the stitched PNA duplexes were measured using a solid-state device and a Mott polarimeter, respectively. The spin polarization at room temperature of SAMs containing γ-modified and non-modified PNA duplexes was approximately +20% and -5%, respectively, which correlates with the CD signals of these PNAs.

Chapter IV presents the results of scanning tunneling microscope-break junction (STM-BJ) measurements that provided the molecular conductance of nucleic acids. These studies showed that the conductance depends on the chemical nature of the nucleic acid backbone and the linker between the PNA and the electrodes. The molecular conductance was measured for 10-base pair long homoduplexes of DNA, aeg-PNA, γ-PNA, and of a DNA/aeg-PNA hetero-duplex of identical nucleobase sequence as well as for duplexes connected by two different linkers that connect the PNA to the electrode, one directly to the backbone and one directly to the nucleobase stack. The most probable molecular conductance of the 10-base pair nucleic acid duplexes with identical nucleobase sequence but different backbones covered a 200-fold range. The aeg-PNA has

a high mode conductance that is ~13 times higher than that of the corresponding DNA duplex when the linker is propylthiol linker and ~34 times higher than the DNA when the linker is amino-C2-thymidine. The G_H/G_M ratios for the thiol linker are in reasonable agreement with previous findings for both nucleic acid duplexes and for alkanedithiol, which suggest that the different conductance modes originate from linker-gold conformation.

Chapter V describes studies in which metal complexes based on Bpy and Q act as "glue" in stitched PNA duplexes. The inclusion of ligands at the adjacent ends of two 10-base PNAs hybridized to a template has a very small effect on the stability of the stitched duplex. Metal coordination to the ligand-containing stitched PNA duplexes increased the thermal stability of the duplexes, supporting the idea that metal complexes bridge the two short PNAs on the template. UV titrations indicated that ML_2 complexes bridged the ligand-containing 10 base PNA strands. The metal complex formed in the middle of the duplex can affect the handedness of the stitched duplex. The binding constants for the duplexes stitched by metal complexes are similar to that of duplexes that contain the same metal complexes as alternative base pairs.

I.3. References

1. Nielsen, P. E.; Egholm, M.; Berg, R. H.; Buchardt, O., Sequence-selective recognition of DNA by strand displacement with a thymine-substituted polyamide. *Science* **1991,** *254* (5037), 1497-1500.
2. Nielsen, P. E.; Egholm, M., An introduction to peptide nucleic acid. *Curr Issues Mol Biol* **1999,** *1* (1-2), 89-104.
3. Egholm, M.; Buchardt, O.; Christensen, L.; Behrens, C.; Freier, S. M.; Driver, D. A.; Berg, R. H.; Kim, S. K.; Norden, B.; Nielsen, P. E., PNA hybridizes to complementary oligonucleotides obeying the Watson-Crick hydrogen-bonding rules. *Nature* **1993,** *365* (6446), 566.
4. Demidov, V. V.; Potaman, V. N.; Frank-Kamenetskil, M. D.; Egholm, M.; Buchard, O.; Sönnichsen, S. H.; Nlelsen, P. E., Stability of peptide nucleic acids in human serum and cellular extracts. *Biochem. Pharmacol.* **1994,** *48* (6), 1310-1313.
5. Hamilton, S. E.; Iyer, M.; Norton, J. C.; Corey, D. R., Specific and nonspecific inhibition of transcription by DNA, PNA, and phosphorothioate promoter analog duplexes. *Bioorg. Med. Chem. Lett.* **1996,** *6* (23), 2897-2900.
6. Boffa, L.; Cutrona, G.; Cilli, M.; Matis, S.; Damonte, G.; Mariani, M.; Millo, E.; Moroni, M.; Roncella, S.; Fedeli, F., Inhibition of Burkitt's lymphoma cells growth in SCID mice by a PNA specific for a regulatory sequence of the translocated c-myc. *Cancer Gene Ther.* **2007,** *14* (2), 220-226.
7. Cogoi, S.; Codognotto, A.; Rapozzi, V.; Meeuwenoord, N.; van der Marel, G.; Xodo, L., Transcription inhibition of oncogenic KRAS by a mutation-selective peptide nucleic acid conjugated to the PKKKRKV nuclear localization signal peptide. *Biochemistry* **2005,** *44* (31), 10510-10519.
8. Cutrona, G.; Carpaneto, E. M.; Ulivi, M.; Roncella, S.; Landt, O.; Ferrarini, M.; Boffa, L. C., Effects in live cells of a c-myc anti-gene PNA linked to a nuclear localization signal. *Nat. Biotechnol.* **2000,** *18* (3), 300-303.
9. Janowski, B. A.; Kaihatsu, K.; Huffman, K. E.; Schwartz, J. C.; Ram, R.; Hardy, D.; Mendelson, C. R.; Corey, D. R., Inhibiting transcription of chromosomal DNA with antigene peptide nucleic acids. *Nat. Chem. Biol.* **2005,** *1* (4), 210-215.
10. Tonelli, R.; Purgato, S.; Camerin, C.; Fronza, R.; Bologna, F.; Alboresi, S.; Franzoni, M.; Corradini, R.; Sforza, S.; Faccini, A., Anti-gene peptide nucleic acid specifically inhibits MYCN expression in human neuroblastoma cells leading to cell growth inhibition and apoptosis. *Mol. Cancer Ther.* **2005,** *4* (5), 779-786.
11. Corradini, R.; Sforza, S.; Tedeschi, T.; Totsingan, F.; Manicardi, A.; Marchelli, R., Peptide nucleic acids with a structurally biased backbone. Updated review and emerging challenges. *Curr. Top. Med. Chem.* **2011,** *11* (12), 1535-1554.
12. Kumar, V. A.; Ganesh, K. N., Conformationally Constrained PNA Analogues: Structural Evolution toward DNA/RNA Binding Selectivity. *Acc. Chem. Res.* **2005,** *38* (5), 404-412.
13. Wittung, P.; Eriksson, M.; Lyng, R.; Nielsen, P. E.; Norden, B., Induced Chirality in PNA-PNA Duplexes. *J. Am. Chem. Soc.* **1995,** *117* (41), 10167-10173.
14. Rapireddy, S.; He, G.; Roy, S.; Armitage, B. A.; Ly, D. H., Strand invasion of mixed-sequence B-DNA by acridine-linked, γ-peptide nucleic acid (γ-PNA). *J. Am. Chem. Soc.* **2007,** *129* (50), 15596-15600.

15. Dueholm, K. L.; Petersen, K. H.; Jensen, D. K.; Egholm, M.; Nielsen, P. E.; Buchardt, O., Peptide nucleic acid (PNA) with a chiral backbone based on alanine. *Bioorg. Med. Chem. Lett.* **1994,** *4* (8), 1077-1080.
16. Dose, C.; Seitz, O., Single nucleotide specific detection of DNA by native chemical ligation of fluorescence labeled PNA-probes. *Bioorg. Med. Chem.* **2008,** *16* (1), 65-77.
17. Hamzavi, R.; Dolle, F.; Tavitian, B.; Dahl, O.; Nielsen, P. E., Modulation of the pharmacokinetic properties of PNA: preparation of galactosyl, mannosyl, fucosyl, N-acetylgalactosaminyl, and N-acetylglucosaminyl derivatives of aminoethylglycine peptide nucleic acid monomers and their incorporation into PNA oligomers. *Bioconjug. Chem.* **2003,** *14* (5), 941-954.
18. Hamzavi, R.; Meyer, C.; Metzler-Nolte, N., Synthesis of a C-linked glycosylated thymine-based PNA monomer and its incorporation into a PNA oligomer. *Org. Biomol. Chem.* **2006,** *4* (19), 3648-3651.
19. Aguado, G. P.; Rúa, F.; Branchadell, V.; Nielsen, P. E.; Ortuño, R. M., Cyclobutyl-carbonyl substituted PNA: synthesis and study of a novel PNA derivative. *Tetrahedron: Asymmetry* **2006,** *17* (17), 2499-2503.
20. Dorn, S.; Aghaallaei, N.; Jung, G.; Bajoghli, B.; Werner, B.; Bock, H.; Lindhorst, T.; Czerny, T., Side chain modified peptide nucleic acids (PNA) for knock-down of six3 in medaka embryos. *BMC Biotechnol.* **2012,** *12* (1), 50.
21. Bregant, S.; Burlina, F.; Vaissermann, J.; Chassaing, G., Synthesis and hybridization properties of thiazolidine PNAs. *Eur. J. Org. Chem.* **2001,** *2001* (17), 3285-3294.
22. Myers, M. C.; Witschi, M. A.; Larionova, N. V.; Franck, J. M.; Haynes, R. D.; Hara, T.; Grajkowski, A.; Appella, D. H., A cyclopentane conformational restraint for a peptide nucleic acid: Design, asymmetric synthesis, and improved binding affinity to DNA and RNA. *Org. Lett.* **2003,** *5* (15), 2695-2698.
23. Pokorski, J. K.; Myers, M. C.; Appella, D. H., Cyclopropane PNA: observable triplex melting in a PNA constrained with a 3-membered ring. *Tetrahedron Lett.* **2005,** *46* (6), 915-917.
24. Pokorski, J. K.; Witschi, M. A.; Purnell, B. L.; Appella, D. H., (S, S)-trans-cyclopentane-constrained peptide nucleic acids. A general backbone modification that improves binding affinity and sequence specificity. *J. Am. Chem. Soc.* **2004,** *126* (46), 15067-15073.
25. Sugiyama, T.; Imamura, Y.; Demizu, Y.; Kurihara, M.; Takano, M.; Kittaka, A., β-PNA: Peptide nucleic acid (PNA) with a chiral center at the β-position of the PNA backbone. *Bioorg. Med. Chem. Lett.* **2011,** *21* (24), 7317-7320.
26. Dose, C.; Seitz, O., Convergent synthesis of peptide nucleic acids by native chemical ligation. *Org. Lett.* **2005,** *7* (20), 4365-4368.
27. Englund, E. A.; Appella, D. H., Synthesis of γ-substituted peptide nucleic acids: a new place to attach fluorophores without affecting DNA binding. *Org. Lett.* **2005,** *7* (16), 3465-3467.
28. Ficht, S.; Dose, C.; Seitz, O., As Fast and Selective as Enzymatic Ligations: Unpaired Nucleobases Increase the Selectivity of DNA-Controlled Native Chemical PNA Ligation. *ChemBioChem* **2005,** *6* (11), 2098-2103.
29. Tedeschi, T.; Sforza, S.; Corradini, R.; Marchelli, R., Synthesis of new chiral PNAs bearing a dipeptide-mimic monomer with two lysine-derived stereogenic centres. *Tetrahedron Lett.* **2005,** *46* (48), 8395-8399.

30. Kosynkina, L.; Wang, W.; Liang, T. C., A convenient synthesis of chiral peptide nucleic acid (PNA) monomers. *Tetrahedron Lett.* **1994,** *35* (29), 5173-5176.
31. Englund, E. A.; Appella, D. H., γ-Substituted Peptide Nucleic Acids Constructed from L-Lysine are a Versatile Scaffold for Multifunctional Display. *Angew. Chem. Int. Ed.* **2007,** *46* (9), 1414-1418.
32. Dragulescu-Andrasi, A.; Rapireddy, S.; Frezza, B. M.; Gayathri, C.; Gil, R. R.; Ly, D. H., A Simple γ-Backbone Modification Preorganizes Peptide Nucleic Acid into a Helical Structure. *J. Am. Chem. Soc.* **2006,** *128* (31), 10258-10267.
33. Sahu, B.; Chenna, V.; Lathrop, K. L.; Thomas, S. M.; Zon, G.; Livak, K. J.; Ly, D. H., Synthesis of conformationally preorganized and cell-permeable guanidine-based γ-peptide nucleic acids (γGPNAs). *J. Org. Chem.* **2009,** *74* (4), 1509-1516.
34. Sahu, B.; Sacui, I.; Rapireddy, S.; Zanotti, K. J.; Bahal, R.; Armitage, B. A.; Ly, D. H., Synthesis and characterization of conformationally preorganized,(R)-diethylene glycol-containing γ-peptide nucleic acids with superior hybridization properties and water solubility. *J. Org. Chem.* **2011,** *76* (14), 5614-5627.
35. Avitabile, C.; Moggio, L.; Malgieri, G.; Capasso, D.; Di Gaetano, S.; Saviano, M.; Pedone, C.; Romanelli, A., γ Sulphate PNA (PNA S): highly selective DNA binding molecule showing promising antigene activity. *PloS One* **2012,** *7* (5), e35774.
36. Sforza, S.; Tedeschi, T.; Corradini, R.; Marchelli, R., Induction of helical handedness and DNA binding properties of peptide nucleic acids (PNAs) with two stereogenic centres. *Eur. J. Org. Chem.* **2007,** *2007* (35), 5879-5885.

CHAPTER II. SYNTHESIS OF γ-MODIFIED PNA MONOMERS, LIGANDS AND LINKERS

II.1. Introduction

To incorporate PNA aeg backbone to the solid phase peptide synthesis (SPPS) procedures, N-end and C-end of the backbone have to be protected. The protecting groups can be Fmoc- or Boc- at the N-end, protecting the primary amine, and *tert*-butyl or ethyl at the C-end, protecting the carboxylic group. The most efficient protecting group for the amine end is the Boc- group, because of the lower cost of the reagents, shorter reaction times and less aggregation problems during the oligomer synthesis by SPPS.[1] N-alkylation of Boc-protected ethylene diamine with ethyl α-bromo acetate or *t*-butyl α-chloro acetate is the procedure used by others and us to obtain aeg backbone (Figure II.1).

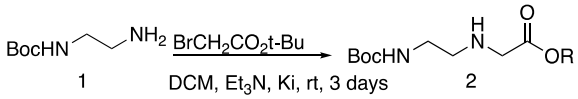

Figure II.1 (N-(2-aminoethyl)-glycine (PNA backbone-aeg)

To get an α-chiral aminoethyglycine backbone, reductive amination is the most commonly used procedure (Scheme II.1). A variety of α-chiral PNAs bearing side chains from amino acids have been prepared by this method.[2-4]

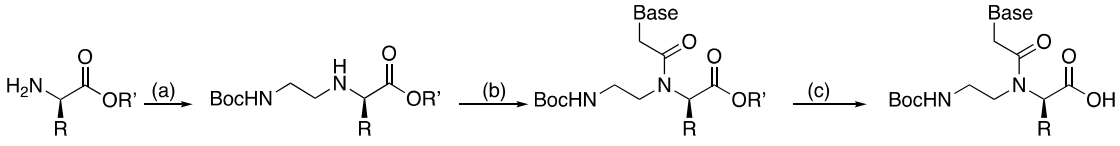

Scheme II.1 Synthesis of the monomers by amination: R' = benzyl, allyl or methyl a) $BocNHCH_2CHO$, $NaBH_3CN$, AcOH, MeOH; b) thymin-l-yl-acetic acid, DCC, DhbtOH, DMF; c) R': benzyl H_2, 10g Pd/C, MeOH; R': allyl $Pd(PPh_3)_4$, morpholine, THF; R': methyl $Ba(OH)_2$, THF, then aq. H_2SO_4.

Racemization of α-carbon during oligomer synthesis is a major problem in the

synthesis of chiral α-PNAs.[5] It is shown that the coupling reagent used in solid-phase synthesis has an effect on the optical purity of PNA oligomers. To avoid racemization DIC/HOBt is used and gives the best coupling results compared to HATU or HBTU. Especially, HATU gives rise to more rapid racemization.[6] Optically pure α-PNA oligomers can be obtained by eliminating the pre-activation step when using HATU. As an alternative route, sub-monomer solid-phase synthesis of chiral monomers has been reported. This method produces α-PNA oligomers with the highest optical purity among reported approaches (Scheme II.2).[7-8]

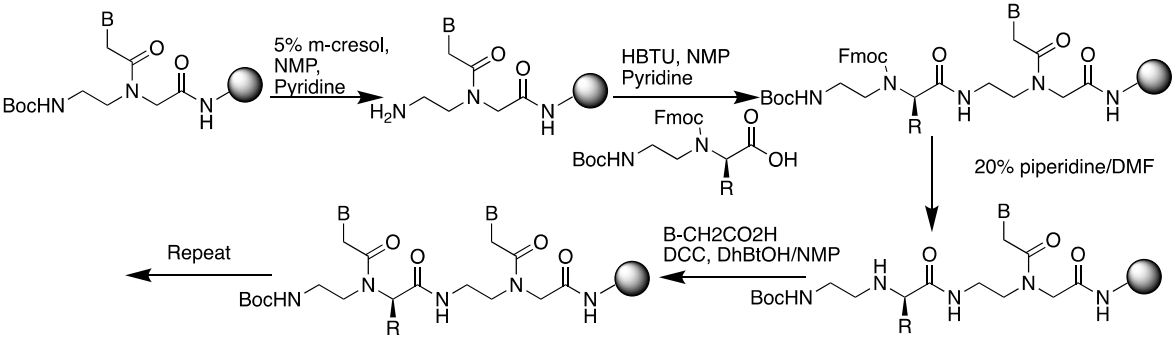

Scheme II.2 Sub-monomeric cycle for the insertion of a chiral monomer into a PNA chain on resin

At the α-position, introduction of a side chain destabilizes the PNA/DNA duplexes relative to the unmodified PNA to some extent.[3-4, 9-10] The extent was less for PNA oligomers carrying D-form monomers than for those carrying L-form monomers. On the other hand, D-Lys-based PNA showed higher melting temprature (T_m) than that of unmodified PNA. This was attributed to the electrostatic attraction between the ammonium group of lysine side chain and the phosphate groups of DNAs. The incorporation of a chiral center at the α-position of the PNA backbone restricts the capability of the PNA strands to adopt other conformations, thus enhancing the mismatch

discrimination ability.

The incorporation of a substituent at the β-position was anticipated to affect the conformation and the DNA binding properties of PNA oligomers greatly since the β-position of the PNA backbone corresponds to the C4' of the deoxyribose moiety of DNA and the C4' is a chiral carbon atom. Synthesis of a methyl group containing PNA monomer is outlined in (Scheme II.3).[11]

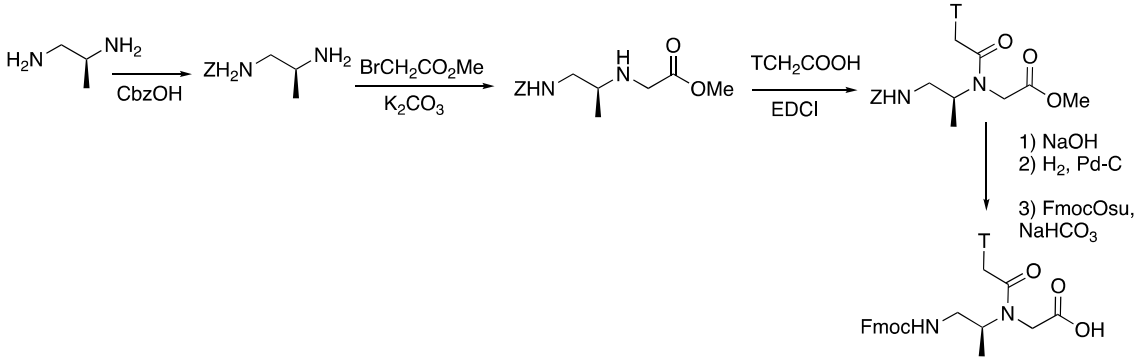

Scheme II.3 Synthesis of β-methyl PNA monomer

Unmodified PNA and β-PNA containing three *S*-form chiral units (derived from L-alanine) showed similar T_m values. On the other hand, three *R*-enantiomers (derived from D-alanine) carrying β-PNA did not bind to DNA. Accordingly, the stereochemistry of the β-carbon of the PNA backbone was crucial to the hybridization ability of PNA and strictly limited to *S*-configuration. This is in contrast to α-PNAs in which stereochemistry of the α-carbon arising from a methyl group hardly affected the DNA binding ability.

Most γ-chiral aminoethyglycine backbones were constructed by using reductive amination as a key step, as also in the case of α-PNAs. Further, the sub-monomeric approach originally developed for the synthesis of α-PNA was also adopted for γ-PNAs.[12] Mitsunobu-Fukuyama reaction is another route to prepare γ-PNAs. [13-15]

Ly et al. have reported a number of γ-PNAs bearing side chains derived from amino acids.[16] It was shown that the γ-position could accommodate various hindered side chains without bringing adverse effects on the hybridization properties of PNAs. This is in contrast to α-PNA, which is sensitive to steric hindrance arising from side chains at the α-position. Introduction of each chiral unit into the oligomer resulted in an increase in the T_m of the PNA/DNA duplex by ~4 °C. Detailed spectroscopic studies of serine- or alanine-based γ-PNAs carried out by Ly et al. revealed that a simple γ-backbone modification preorganized ssPNA oligomers into a right-handed helical structure that was very similar to that of PNA/DNA duplex. The γ-PNAs bound to DNA with very high affinity and high sequence selectivity. Helical induction was sterically driven and stabilized by base stacking.[17] Ly et al. also reported γ-minipeg (mp) modified PNA oligomers to improve solubility.[15]

PNA has been chemically modified in many ways some of which mentioned above to overcome the limitations it has. Even though first fluorinated PNA analogue was reported in 2003, olefinic PNA monomer in which the tertiary rotameric amide bond was replaced with a more rigid fluoro vinyl moiety, fluorine modified PNA monomers was not available until the report by Ellipilli et al. in 2015. Ellipilli et al. showed the multistep synthesis of γ-di-fluorinated PNA monomers (Scheme II.4).[18] Due to small size with higher electronegativity and low polarizability, substitution of hydrogen with fluorine affects the physiochemical properties like lipophilicity, solubility, acidity, basicity, hydrogen bonding and etc.[19] T_m of duplexes from fluorinated PNAs with DNA and RNA do not change very much; both apg and γ-CF_2-apg (apg: aminopropylglycine) PNAs are biased to bind RNA more than DNA. Notably, the efficiency of cellular entry

of fluorinated γ-CF_2-apg PNAs is better than its related non-fluorinated apg-PNA analogues. This intrinsic modification of backbone neither introduces chirality nor changes the conformational features of PNAs but improves the antisense activity.[20-21] Synthesis of γ-CF_2-apg was completed overall 14 steps and key step to construct the γ-CF_2-apg monomer was Reformatsky reaction with ethylbromodifluoroacetate which resulted in the difluoromethylene compound that was followed by several reduction, protection/deprotection, alkylation and oxidation steps to produce the γ-CF_2-apg monomer.

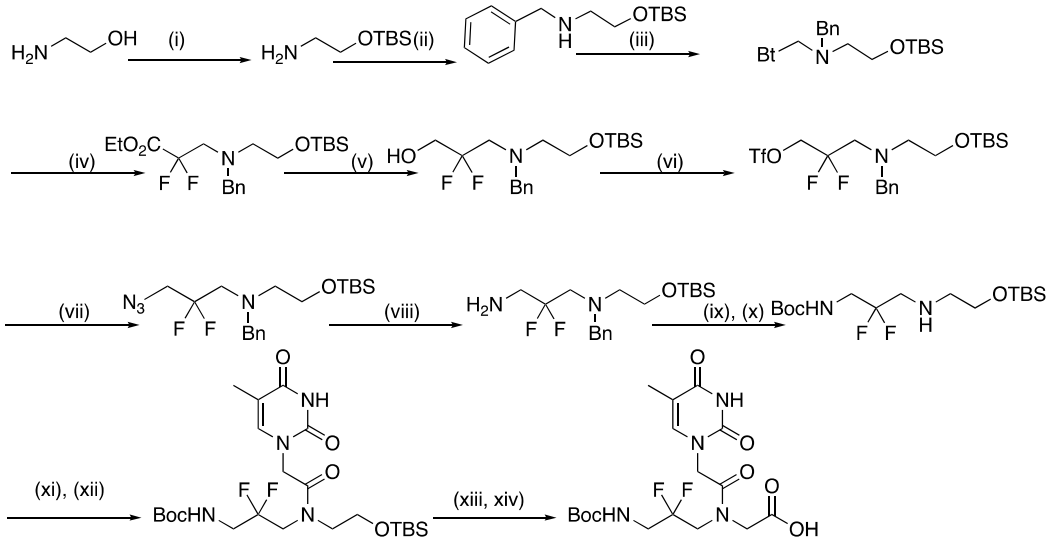

Scheme II.4 Synthesis of γ-CF_2 apg-PNA-T monomer (i) TBSCl, imidazole, DCM, rt, 12 h; (ii)BnBr/Et_3N, ACN, rt, 12 h; (iii) 1*H*-benzo[*d*][1,2,3]triazole, HCHO, Et_2O, rt, 12 h; (iv)$BrCF_2COOEt$, Zn, TMSCl, THF, reflux, 6 h; (v) $NaBH_4$, EtOH, rt, 12 h; (vi) Tf_2O, Et_3N, DCM, -78 ^oC, 1 h; (vii) NaN_3, DMF, rt, 16 h; (viii) PPh_3/THF, H_2O, 12 h; (ix)$(Boc)_2O$, Et_3N, 6 h; (x) Pd/C, EtOH, H_2, 1 h; (xi) $ClCOCH_2Cl$, $NaHCO_3$, (1:1) Dioxane/H_2O, 2 h, (xii) 5-methylpyrimidine-2,4(1*H*,3*H*)-dione, K_2CO_3, DMF, 12 h; (xiii) TBAF, THF, 3 h; (xiv) TEMPO, BAIB, (1:1) ACN/H_2O, rt, 2 h

In the absence of chiral sugars in the backbone, the helical sense of antiparallel 3′→5′ directionality of DNA duplex, a very significant aspect of natural DNA, is compromised in PNA. A variety of aforementioned chiral PNA modifications were

studied to enhance the discrimination of parallel/antiparallel binding. The positively charged chiral PNA analogues containing amino- and guanidino-functionalities[22-23] and the negatively charged PNA analogues containing carboxy-[24] and sulfate-[25] groups have been studied to improve PNA properties depending on the charges on the backbone and experimental conditions. The prolyl-(ACPC) PNA[26-27] (prolyl-2-aminocyclopentanecarboxylic acid backbone) and its homologues[28] are unique examples in which an entirely new backbone comprising alternating α- and β-amino acids exhibited strong preference of binding with complementary antiparallel DNA and thus indicated optimized internucleoside geometries to bind antiparallel DNA but comparatively less so, with complementary RNA (Figure II.2). To extend the binding affinity and sequence-specificity only to the antiparallel complementary RNA and DNA polyamide analogues of nucleic acids 3′-NH-g-CO-5′amide-DNAs was synthesized.[29-30] The amide-DNA behaved very comparable to the natural DNA with similar properties such as effective mismatch discrimination and directional specificity in addition to its special features being better binding with RNA compared to DNA. Furthermore, in the absence of the electrostatic repulsions arising from the phosphate negative charges of natural DNA/RNA duplexes, it binds to both DNA/RNA duplexes with better strength.

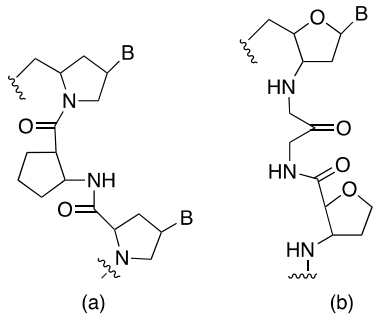

Figure II.2 Polyamide possessing DNA analogues (a) prolyl-(ACPC)-PNA (b) Glycine-liked nucleoside-β-amino acids; 3′-NH-g-CO-5′amide-DNA.

Attaching a substituent to the PNA backbone is a basic approach but has demonstrated to be effective in enhancing DNA binding properties and the sequence selectivity of PNAs. In terms of DNA/RNA binding affinity, γ-PNAs are the most potent. PNA can be synthesized by Fmoc- or Boc-solid phase peptide synthesis. While Fmoc-and Boc-protected monomers bearing each of the four canonical nucleobases are commercially available, PNA monomers bearing modified nucleobases, backbone or ligands are not; and must be synthesized in the laboratory instead. Suitable reactions have been reported for preparation of modified nucleobases and coupling of these nucleobase acetic acids to the PNA backbone.

Figure II.3 shows a generic PNA oligomer that includes examples of all types of modifications incorporated in PNA in our lab. The hydroxypyridone and 8-hydroxyquinoline ligand-containing monomers are used to create alternative basepairs or base triplets when included in complementary positions in PNA duplexes or triplexes, respectively. $[Ru(Bpy)_3]^{2+}$ and Ferrocene (Fc) are introduced in PNA because they are redox active and the former complex has also useful luminescence properties. Cysteine and cysteamine have been introduced in the PNA to provide points of attachments to the Au surface.

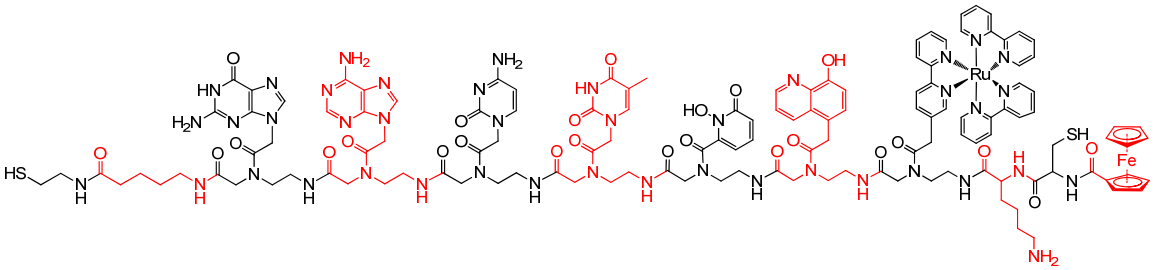

Figure II.3 Generic PNA oligomer that includes A, G, C, and T nucleobases, hydroxypyridone and 8-hydroxyquinoline ligand-containing monomers, inorganic $[Ru(Bpy)_3]^{2+}$-containing PNA monomer and terminal ferrocene complexes, Lysine and cysteine aminoacids, and a terminal cysteamine unit.

In our lab, research is focused on the uses of modified PNA oligomers for several applications. To serve these aims, synthesis of different small organic molecules is required. In this chapter, in addition to synthesis of PNA monomers, synthesis of ligands and some linkers that I have synthesized are discussed (Figure II.4). PNA monomers and thiol linker were synthesized by modified published procedures.[17, 31-32] Amino acid monomers were prepared by SPPS methadology. Acetic acids of pyrene, C2-amino uracil and bipydridine were coupled on the resin. Boc derivative of C2-amino uracil acetic acid was synthesiszed for the first time with a moderate yield upon modification of the published procedure.[33] Bpy and Tpy acetic acids were also prepared by published procedures. [34-37]

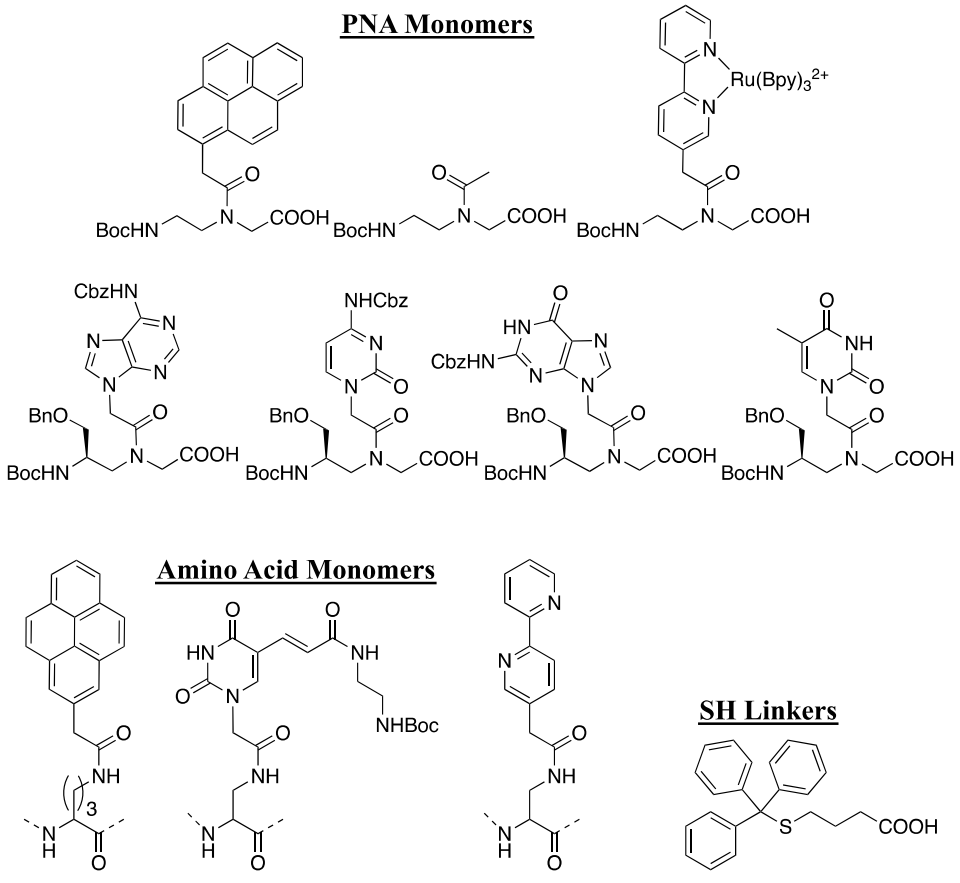

Figure II.4 Structures of the small molecules that were used in research described in the thesis to study the properties of PNA/PNA and PNA/DNA duplexes.

II.2. Results

II.2.1. Synthesis of Boc-(2-(2-benzyloxyethoxy)ethyl)-L-serine-Ψ[CH_2N]Gly-OEt 12

Mitsunobu reaction is one of the synthetic procedures published to synthesize γ-modified PNA monomers. Ly et al. have synthesized Boc-protected $^{R\text{-}MP}$γPNA (R-MP, miniPEG) monomer by the Mitsunobu procedure shown in Scheme II.5. [15] R-MP is a relatively small hydrophilic group improving PNA oligomers' solubility properties. We attempted to synthesize R-MP modified PNA monomers following the procedure described by Ly et al. In our hands, first 6 steps of the reactions outlined in

Scheme II.**5** were successfully produced. However, compound **12** could not be obtained pure which prevented completion of the last two steps. Diffuculty of purifying compound **12** was most likely due to the hydrophilicity of the MP group. Here we only described the reactions steps upto compound **12**.

The Boc-protected L-serine **5** was alkylated with ((2-(2-iodoethoxy)ethoxy)methyl)benzene **4.** Slow addition of **5** into a vigorously stirred, chilled solution of DMF containing sodium hydride, followed by addition of ((2-(2-iodoethoxy)ethoxy)methyl)benzene **4** afforded compound **6**. The transformation of the carboxylic acid functional group of **6** to alcohol is necessary in order to prevent the racemization in the subsequent reaction steps. This is achieved by activation of the alkylated product **6** with butylchloroformate in DME followed by reduction with sodium borohydride to yield serinol **10**. In order to obtain **11**, Compound **10** was coupled using the Mitsunobu reaction to N-[(2,4-dinitrophenyl)sulfonyl]glycine ethyl acetate **9**, that was prepared according to the published procedure.[38] Removal of the (2,4-

dinitrophenyl)sulfonyl group of **11** with a mild base n-propylamine in DCM yielded compound **12**.

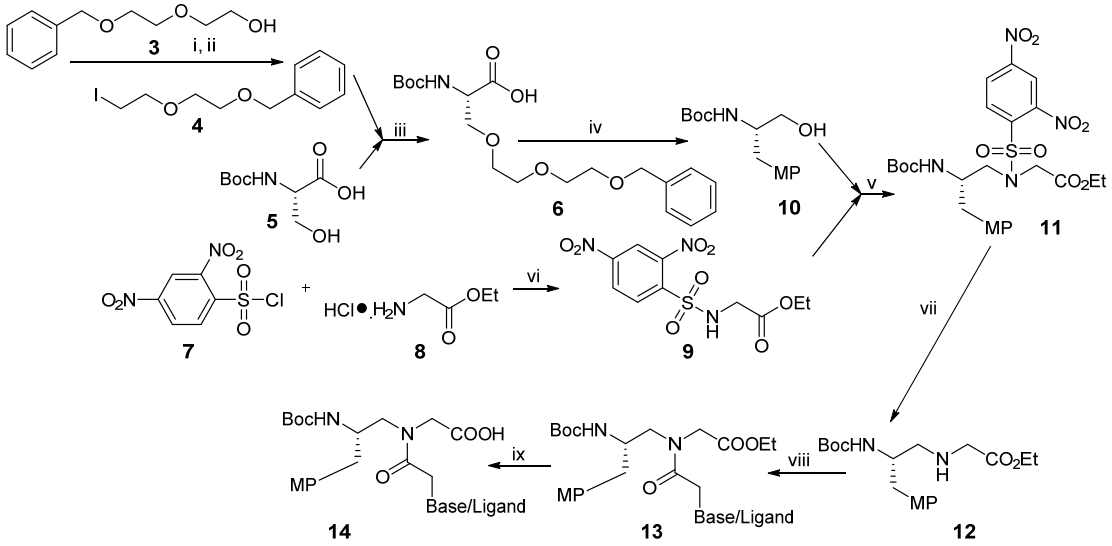

Scheme II.5 Synthesis of Boc-(2-(2-benzyloxyethoxy)ethyl)-L-serine-Ψ[CH_2N]Gly-OEt i) MsCl, Et_3N, DCM, 0°C to rt, 12 h, quantitative yield ii) NaI, Acetone, reflux, 2 h, 95% iii) NaH, DMF, 0°C, 6 h, 60%, iv) Butylchloroformate, NMM, DME, $NaBH_4$, 0°C to rt, 1 h, 71% v) DIAD, TPP, THF, 0°C to rt, 12 h, 66% vi) Pyridine, DCM, rt, 12 h, 63% vii) n-$PrNH_2$, DCM, rt, 30 mi, 74% viii) L-COOH, coupling, ix) 2M NaOH/THF(1:1), 0°C, 45 min.

II.2.2. Synthesis of ^{L}S-γPNA Monomers

Due to the difficulty of the purification of the miniPEG functionalized PNA monomers, we have decided to make serine modified γ-PNA monomers which was less hydrophilic compared to miniPEG moiety. Boc-protected ^{L}S-γPNA monomers were synthesized according to the procedures described by Ly group outlined in Scheme II.6.[17] In this procedure γ-serine aminoethylglycine backbone was constructed by using reductive amination as a key step. Prior to amidation of the Boc-protected L-serine **15** using *N,O*-dimethylhydroxylamine hydrochloride, carboxylic end of compound **15** was activated to a mixed anhydride with the drop-wise addition of isobutyl chloroformate at -

15 °C. Reduction of the Weinrab amide **17** using $LiAlH_4$ gave the corresponding aldehyde **18**. Direct reductive amination of the aldehyde involves formation of imine with the addition of glycine ethyl ester hydrochloride in the presence of DIPEA followed by reduction of this intermediate using $Na(OAc)_3BH$ to give intermediate **19**. Four γ-modified PNA monomers **21a-d** were synthesized based on coupling of the related carboxymethylnucleobases to the Boc-protected ester of γ-modified aminoethyl glycine backbone **19** in the presence of DCC and DhbtOH in DMF, followed by hydrolysis of the resulting esters with sodium hydroxide.

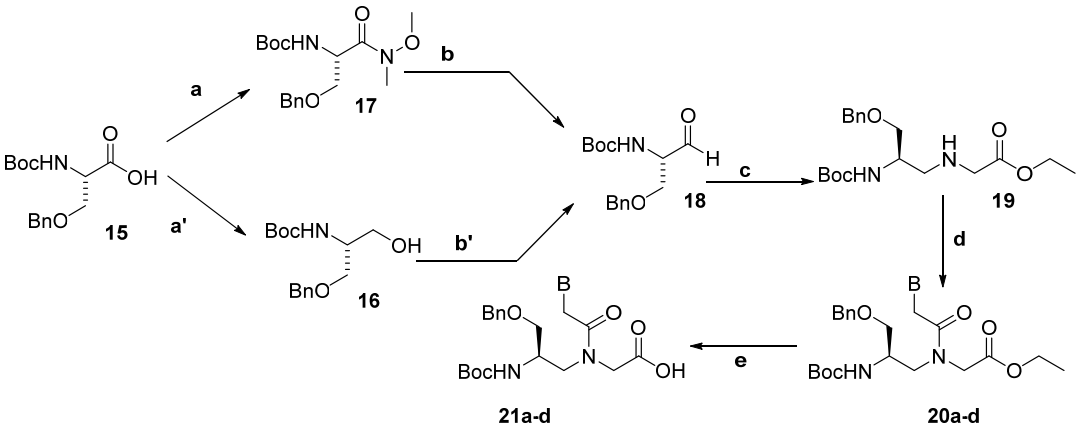

Scheme II.6 Synthesis of γ-serine modified PNA monomers. (a) NMM, $ClCO_2iBu$,$CH_3NHOCH_3 \cdot HCl$, CH_2Cl_2, rt, 14 h , 89%, (b) $LiAlH_4$, THF, 0 °C , 1 h, 86%, (a′) NMM, $ClCO_2$i-Bu, DME, $NaBH_4$, qtv. Yield (b′)DMSO, $(COCl)_2$, Et_3N, DCM, N_2, -78°C, 1.5 h 95%(c) ethyl ester glycine, MeOH, 4 °C, 4 h, then AcOH, $NaBH(OAC)_3$, 30 min., 40%, (d) carboxymethylnucleobase (B: A, G, C, T), DCC, DhbtOH, DMF, 40°C, 24 h, 39-63% (e) NaOH/THF (1:1), 30 min., 0°C. 76-96%.

In order to increase the reaction yield, the first two steps and the last step that is hydrolysis have been modified. Instead of amidation of the Boc-protected L-serine **15** using *N,O*-dimethylhydroxylamine hydrochloride, the carboxylic end of compound **15** was reduced to its alcohol derivative **16** in the presence of *i*-buthylchloroformate (IBCF), *N*-methyl morpholine (NMP), and sodium borohydride. Next, **16** was converted to

aldehyde **18** via Swern oxidation using oxalyl chloride, dimethylsulsoxide, and triethyl amine. The reaction yield was almost quantitative. Based on this result, we conclude that the Swern oxidation provides better quality product than $LiAlH_4$ reduction; another advantage of this oxidation is that it does not require the use of the expensive reagent *N,O*-dimethylhydroxylamine hydrochloride.

II.2.3. Synthesis of Thymine 5-C2 Amino Linker 25

The thymine 5-C2 amino linker was synthesized using a modified published procedure (Scheme II.7).[33] Commercially available iodouracil **22** was alkylated at N1 with ethyl α-bromoacetate in the presence of potassium carbonate in anhydrous DMF under nitrogen at room temperature for 24 h to give ethyl ester **23** in quantitative yield. The iodo group of **23** was exchanged with an acryloyl group via Heck reaction with acrylic acid to give the carboxylic acid **24** in 60% yield. Next, the carboxylic acid **24** was activated with HATU in the presence of DIEA in anhydrous DMF and was coupled to Boc-protected etylenediamine. The hydrolysis of the resulting ethyl ester to carboxylic acid using LiOH led to the final product **25** in 75% yield over last two steps.

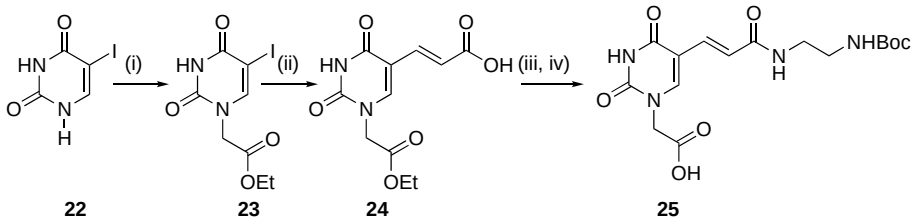

Scheme II.7 Synthesis of of Thymine 5-C2 Amino Linker: K_2CO_3, DMF, α-bromo ethyl acetate, DMF, 0 ^oC to rt, 24 h, qtv yield, (ii) $Pd(OAc)_2$, Bu_4NBr, DMF/DIE/H_2O, acrylic acid, 80-90 ^oC, 16 h 60%, (iii) $BocNH(CH_2)_2NH_2.HCl$, HATU, DIEA, DMF, 0 ^oC to rt, 12 h (iv) LiOH, THF, 0 ^oC to rt, 12 h, 75%.

II.2.4. Synthesis of Tpy-COOH

In order to incorporate a tridentate metal binding unit into a PNA 2-([3,2':6',3"-terpyridin]-4'-yl)acetic acid **30** was synthesized using a previously reported procedure (Scheme II.8).[36-37] **30** was synthesized using Kröhnke reaction of 2-Pyridacylpyridinium iodide **31** with α,β-saturated ketone **28**.

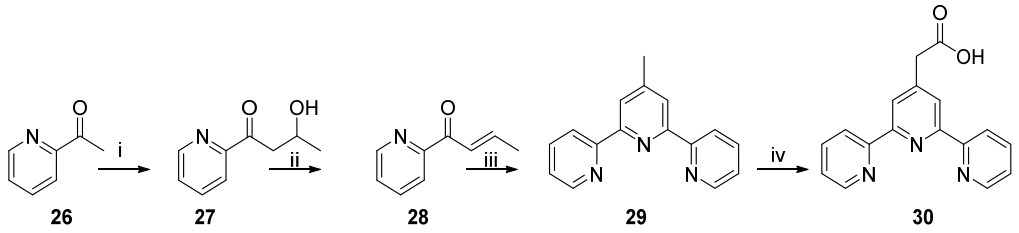

Scheme II.8 Synthesis of 2-([3,2':6',3"-terpyridin]-4'-yl)acetic acid (i) LDA, acetaldehyde, THF, -15°C, 47%; (ii) Methanesulfonyl chloride, Et_3N, in DCM, -30°C, 64% (iii) 2-Pyridacylpyridinium iodide **31**, CH_3COONH_4, DCM, reflux, 70% (iv) MeLi, 2,2,6,6-tetramethylpiperidine, CO_2, THF, -10°C 40%.

The formation of the enolate of 2-acetylpyridine **26** by treatment with LDA followed by addition to acetaldehyde at low temperature gave the aldole product 3-hydroxy-1-(pyridin-2-yl)butan-1-one **27** in 47% yield.

Dehydration of the aldol **27** by methanesulfonyl chloride in the presence of triethylamine at -30^{o}C gave the enone (E)-1-(pyridin-2-yl)but-2-en-1-one **28**, which was then allowed to react with pyridacylpyridinium iodide **31** and ammonium acetate in DCM to give 4'-methyl-3,2':6',3"-terpyridine **29**. Carboxylation of 4'-methyl-3,2':6',3"-terpyridine **5**, by treatment with methyl lithium, 2,2,6,6-tetramethyl piperidine CO_2 at low temperature in THF gave **30** with a 40% yield.

II.2.5. Synthesis of 2-([2,2'-bipyridin]-5-yl)acetic acid

The starting material for the synthesis of Bipy acetic acid is 2-acetylpyridine **26.**[34-35] Refluxing **26** in pyridine with iodine to provide 2-pyridacylpyridinim iodide **31**,

the cyclization of which allowed the formation of 4-methyl-2,2'-bipyridine **32**. 4-methyl-2,2'-bipyridine **32** is the key reagent in obtaining the acetic acid derivative of bipyridine. Carboxylation of **32** in the presence of carbon dioxide and LDA provided the desired product **33** with a yield of 82% Scheme II.9.

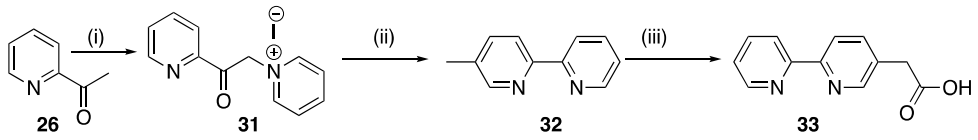

Scheme II.9 Synthesis of Bpy-CH_2COOH (i) I_2, pyridine, reflux for 3 h, 75% (ii) Formamide, NH_4Ac, reflux for 6 h in methacrolein, 76% (iii) LDA, THF, CO_2 (g) or CO_2(s), 4 h, -78^oC to rt.

II.2.6. Synthesis of Pyrene Monomer

Pyrene can be used as a fluorescent marker that makes possible the measurement of distances between or within biomolecules. Pyrene can be inserted in PNA oligomers either as part of a PNA monomer or as side chain of an amino acid.[31, 39]

The synthesis of the pyrene monomer ester is outlined in Scheme II.10. First, commercially available 1-pyrene acetic acid was activated using the coupling reagents DCC and DhBtOH. Aeg backbone was added to the solution of the activated 1-pyrene acetic acid to give the desired pyrene PNA monomer **36**.

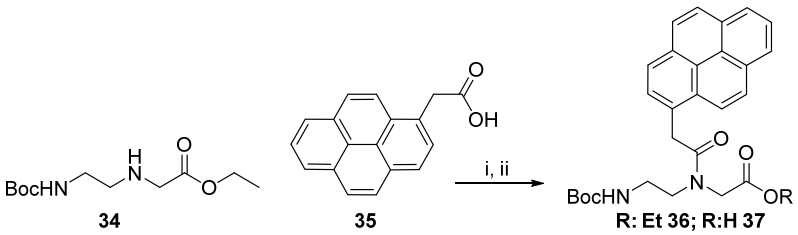

Scheme II.10 Synthesis of Pyrene monomer ester: (i) DhBtOH, DCC, DMF, rt to 50 ^oC, 24 h, 79% (ii) 2 N NaOH, THF, 0 ^oC to rt, 3 h, 82%.

After obtaining compound **36**, hydrolysis of this compound was performed in the presence of 2 N NaOH in THF to afford compound **37**.

II.2.7. Synthesis of the [Ru(Bpy)$_3$] PNA Monomer

Boc-protected Ru-bpy monomer was synthesized according to the procedure described by Kise et al. (Scheme II.11).[40]

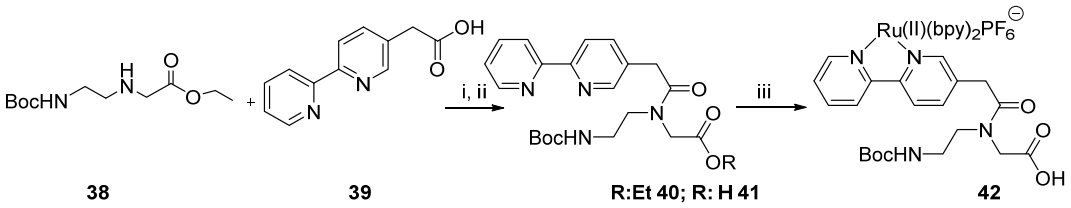

Scheme II.11 Sythesis of Ru-Bpy monomer: (i) DCC, HOBt, DMF, 0^{o}C to rt (ii) 2M NaOH/THF (1:1) 0^{o}C, (iii) cis-Ru(bpy)$_2$Cl$_2$, 70% EtOH, on, reflux

II.2.8. Synthesis of 4-(Tritylthio)Butyric acid

Compound **45** was prepared for use in PNA oligomers that contain an N-end propyl thiol using a published procedure (Scheme II.12).[41] S-alkylation of commercially available trityl mercaptan **43** with 4-bromo butyric acid **44** in the presence of NaH in DMF gave compound **45** in high yield (91%).

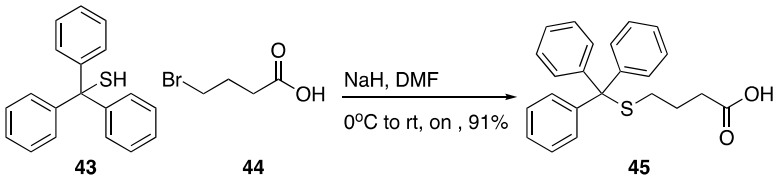

Scheme II.12 Synthesis of 4-(tritylthio)butyric acid **45** through S-alkylation of trityl mercaptan **43.**

II.3. Conclusions

Seven PNA monomers with different features were prepared. They were used in research described in the thesis to study the properties of PNA/PNA and PNA/DNA

duplexes such as helical sense (γ-modified monomers) and fluorescence (pyrene). Acetic acids of Tpy and Bpy ligands, which are used in the synthesis of PNA monomers were prepared to insert these fragments into peptide nucleic acids through solid phase peptide synthesis strategy. A new derivative of acetic acid of C2-amino uracil was prepared. Propylthiol linkers were made in high yields and used to prepare N-end thiol modified peptide nucleic acids.

II.4. Materials and Methods

All reagents were purchased from commercial suppliers and used as received. NMR spectra were recorded on a Bruker Avance™ -300 MHz Spectrometer. Low-resolution mass spectra were recorded on a Thermo LCQ ESI/APCI Ion Trap mass spectrometer using an electrospray ionization source. HPLC was performed on Waters 600 Controller and Pump. Absorbance was measured with a Waters 2996 Photodiode Array Detector. Characterization of the oligomers was performed by MALDI-TOF mass spectrometry on an Applied Biosystems Voyager Biospectrometry Workstation with Delayed Extraction. Column purifications were performed using silica gel flash chromatography unless mentioned otherwise. All reactions were performed under ambient atmosphere unless otherwise noted. Anaerobic reactions were performed in Schlenk tubes. These reactions were deoxygenated by performing five vacuum-backfill cycles with N_2 and were run under a constant purge of N_2. Dichloromethane were dried over 4Å molecular sieves, before use. Acetaldehyde was treated with $NaHCO_3$ and distilled from CaH_2. Tetrahydrofuran (THF) was distilled over Na and benzophenone. Diisopropylethylamine and triethylamine were distilled from CaH_2 and stored over

molecular sieves. Acetylpyridine and 2,2,6,6-tetramethylpiperidine were distilled over CaH_2.

II.4.1. Mini-PEG Modified Monomer Synthesis

((2-(2-iodoethoxy)ethoxy)methyl)benzene **4**: To a stirred solution of of 2-(2-(benzyloxy)ethoxy)ethanol **3** (20.1 g, 51.3 mmol) in 400 mL of DCM at 0 ^{o}C, triethylamine (18.7 mL, 133.4 mmol) was slowly added under nitrogen atmosphere and this mixture was stirred at 0 ^{o}C for 15 min. To this mixture, methanesulfonyl chloride (11.3 mL, 143.6 mmol) was added and after stirring for 30 min 0 ^{o}C, a white precipitate was formed. Reaction mixture was slowly warmed up to room temperature and continued to stir for overnight. The reaction mixture was washed with water (3 x 150 mL). The combined organic layers were dried over anhydrous Na_2SO_4. The solvent was evaporated under reduced pressure to afford and the oily residue (46.6 g, 152.3 mmol). Yield; quantitative.

To a stirred solution of 2-(2-(benzyloxy)ethoxy)ethyl methanesulfonate (product obtained from the first step) in acetone (350 mL) was added sodium iodide (76.9 g, 513.1 mmol) and refluxed for 2 h. The reaction mixture was filtered through celite. The filtrate concentrated under reduced pressure and the remaining dark brown oil was dissolved in hexane. The solution was washed with 5% Na_2SO_3 and aqueous layer extracted with hexane (4 x 200 mL). The combined organic layers were dried over anhydrous Na_2SO_4. The solvent was evaporated under reduced pressure, and the oily residue was purified by column chromatography using EtOAc/Hexane (20:80) as an eluent to afford a yellow liquid **4** (29 9 g, 97.7 mmol). Yield; 95%. ^{1}H NMR (300 MHz,

$CDCl_3$): δ 3.29 (t, *J* = 6.2, 2 H), 3.69 (m, 4 H), 3.79 (t, 2 H), 4.61 (s, 2 H), 7.38-7.27 (m, 5 H).

Boc-(2-(2-benzyloxyyethoxy)ethyl)-L-serine **6**: To a stirred, ice-cold (0 ^oC) solution of NaH (60% suspended in mineral oil, 1.7 g, 42.6 mmol) in dry DMF (80 mL) under an inert atmosphere was added Boc-L-Ser-OH **5** (4.0 g, 19.6 mmol) in DMF (30 mL) dropwise over a period of 3 h. To this mixture, while still in the ice bath, was added ((2-(2-iodoethoxy)ethoxy)methyl)benzene **4** (6.4 mL, 42.6 mmol) at once. The ice bath was then removed, and the reaction was allowed to gradually warm to room temperature and stirred for another 3 h. The reaction mixture was quenched with H_2O (100 mL) at 0 ^oC. The solvents (DMF and water) were evaporated under reduced pressure at room temperature. Water (20 mL) was added to the crude residue and acidified with 5% HCl to pH≈3 at 0 ^oC. The aqueous layers were extracted with ethyl acetate (5 x100 mL) and dried over Na_2SO_4. The solvent was evaporated under reduced pressure, and the oily residue was purified by column chromatography to afford a colorless liquid **6** (4.56 g, 11.9 mmol). Yield; 60%. ESI-MS calcd for $C_{19}H_{29}NNaO_7$ $(M+Na)^+$ 406 found: 406.

Boc-(2-(2-benzyloxyethoxy)ethyl)-L-serinol **10**: To a stirred solution of Boc-(2-(2-benzyloxyethoxy)ethyl)-L-serine **6** (4.6 g, 11.8 mmol) in 22.5 mL of DME in an ice bath was added NMM (1.3 mL, 11.8 mmol) dropwise under an inert atmosphere, followed by isobutyl chloroformate (1.6 mL, 12.3 mmol). The reaction mixture was stirred at the same temperature for another 0.5 h. The cold solution was filtered, and the precipitate was washed with DME (2 x10 mL). To the combined filtrate stirred in an ice bath was added $NaBH_4$ (0.67 g, 17.7 mmol in 10 mL water) slowly. A strong bubbliness occurred. The aqueous layer was extracted using ethyl acetate (3 x 150 mL), and the combined

organic layers were washed with brine and dried over Na_2SO_4. The solvent was evaporated under reduced pressure, and the oily residue was purified by column chromatography to give a colorless liquid **10** (2.9 g, 10.9 mmol). Yield; 71% ESI-MS calcd for $C_{19}H_{31}NNaO_6$ $(M+Na)^+$ 392 found: 392.

Boc-(2-(2-benzyloxyethoxy)ethyl)-L-serine-Ψ[CH2N(o,p-diNBS)]Gly-OEt **11**: To a stirred, cold solution of o,p-diNBS-Gly-OEt **9** (5.0 g, 15.1 mmol), triphenylphosphine (4.1 g, 15.1 mmol), and compound **10** (2.8 g, 7.5 mmol) in dried THF (28 mL) under an inert atmosphere was added DIAD (2.96 mL, 15.1 mmol) dropwise over a period of 0.5 h. The reaction mixture was allowed to warm to room temperature and then stirred overnight. The solvent was evaporated, and the oily residue was purified by column chromatography to afford a yellow oil **11** (3.4 g, 4.9 mmol). Yield; 66% ESI-MS calcd for $C_{29}H_{40}N_4NaO_{13}S$ $(M+Na)^+$ 707 found: 707.

Methyl *N*-(*o*,*p*-dinitrophenyl sulfonyl)-glycinate **9**: To a stirred solution of glycine ester **8** (5.0 g, 35.8 mmol) in dichloromethane (20 mL) was added 2,4-dinitrobenzenesulphonyl chloride **7** (9.6 g, 35.8 mmol) at room temperature. Pyridine (5.8 mL, 71.6 mmol) was added to the reaction mixture over a 15 min span and stirred at ambient temperature for another 0.5 h. The organic layer was washed several times with water, followed by brine and dried over anhydrous Na_2SO_4. The solvent was evaporated under reduced pressure to dryness, and the crude product was purified by column chromatography and dried to give a yellow solid **9** (7.5 g, 22.5 mmol). Yield 63%. ^{1}H NMR ($CDCl_3$) δ 1.21 (t, 6 Hz, 3 H), 4.09-4.02 (m, 4 H), 8.32 (d, J = 8.5 Hz, 1 H), 8.55 (dd, J = 8.5 and 2.3 Hz, 1 H), 8.77 (d, J = 2.3 Hz, 1 H).

Boc-(2-(2-benzyloxyethoxy)ethyl)-L-serine-Ψ[CH2N]Gly-OEt **12**: To a stirred solution of **11** (3.4 g, 4.9 mmol) in dichloromethane (34 mL) was added n-propylamine (8.2 mL, 100.0 mmol) under an inert atmosphere. The reaction mixture was stirred at room temperature for another 20 min. The solvent was evaporated, and the crude mixture was purified by column chromatography to afford yellow oil **12** (1.7 g, 3.4 mmol). Yield; 74%. ESI-MS calcd for $C_{23}H_{38}N_2O_7$ $(M+H)^+$ 455 found: 455.

II.4.2. Serine Modified Monomer Synthesis

N-*tert*-butyloxycarbonyl-*O*-benzyl serine-weinrebamide **17**: To a stirred solution of **15** (10 g, 33.8 mmol) in anhydrous DCM (200 mL) was added NMM (8.2 mL, 74.4 mmol) at -15 °C (dried ice/MeOH) under argon atmosphere. Isobutyl chloroformate (4.9 mL 18.8 mmol) was added drop-wise. After stirring for 15 min, *N,O*-dimethylhydroxylamine hydrochloride (3.3 g, 33.8 mmol) was added and the stirring was continued for 14 h at room temperature. The solution was washed with 0.2 M $KHSO_4$ (120 mL) and the aqueous layer extracted with DCM (3 x 100 mL). The combined organic phases were dried (Na_2SO_4) and the solvent was removed under reduced pressure. The residue was purified by silica gel flash chromatography to afford 10.18 g (89%) of **17** as colorless solid. R_f = 0.5 (Hex:EtOAc =2:3) ^{1}H NMR (300 MHz, $CDCl_3$) 7.29 (5 H, m), 5.42 (1 H, s), 4.88 (1 H, s), 4.53 (2 H, *J*= 12.2 Hz), 3.71 (3 H, s), 3.67 (2 H, dd, *J* = 9.5 and 4.8 Hz), 3.21 (3 H, s), 1.44 (9 H, s). ESI-MS (m/z): Mass calculated for $C_{17}H_{26}N_2O_5$ 338.18, found 361.20 (338.18 + Na^+).

tert-Butyl (R)-(1-(benzyloxy)-3-hydroxypropan-2-yl)carbamate **16**: To a stirred solution of O-benzyl-N-(tert-butoxycarbonyl)-L-serine **15** (5 g, 16.93 mmol), in DME (50 mL) were added NMM (1.88 g, 18.62 mmo) added at -15 ^{o}C and stirred for 20 min. under N_2

atmosphere. *i*-Buthylchloroformate (2.54 g, 18.62 mmol) was added and the reaction was stirred at -15 ^{o}C for 30 min. Next, the precipitate was removed by filtration and washed with DME (2x 20 mL) and then filtrate and washings combined in a 500 ml flask and cooled down in a ice-salt bath. A solution of $NaBH_4$ (965 mg in 8.46 mL H_20) was added to reaction mixture at once, producing a strong evolution of gas, followed by water (423 mL) immediately afterwards. After stirring for 30 min. extracted with EtOAc (3x50 mL). The combined organic layers were washed with brine and dried over anhydrous Na_2SO_4. The solvent was removed under reduced pressure and the residue was purified by silica gel chromatography (40:60 EtOAc/Hex) to afford 5.36 g (qtv yield) of **16** as a white solid. Mass calcd for $C_{15}H_{23}NO_4$ 281.6, found 304 (M+Na).

N-tert-butyloxycarbonyl-*O*-benzyl serinal **18** (by reduction): A stirred solution of **17** (10.18 g, 30.12 mmol) in dry THF (265 mL) was cooled to 0 °C under argon atmosphere. Lithium aluminum hydride (2.2 g, 57.89 mmol) was added in portions and after 1 h, 0.2 M $KHSO_4$ (30 mL) was added. The organic compounds were extracted with diethyl ether (3 x 50 mL). The combined organic layers were washed with 1 M HCl (3 x 50 mL), brine (3 x 50 mL) and dried over Na_2SO_4. The solvent was removed under reduced pressure to afford 7.24 g (86%) of **18** as yellow oil, which was used in the next step without further purification.

N-tert-butyloxycarbonyl-*O*-benzyl serinal **18** (by oxidation): To a stirred solution of oxalyl chloride in dry DCM (10 mL) was slowly added DMSO (1.11 g, 14.24 mmol) at -78 ^{o}C. After stirring for 30 min, compound **16** (1.00 g, 3.56 mmol) in dry DCM (5 mL) was added and the reaction was stirred for 90 min at -78 ^{o}C. Then, Et_3N (2.16 g, 21.36 mmol) was added to reaction mixture and stirring continued for another 30 min. Reaction

mixture quenched with saturated NH_4Cl and extracted with DCM (3x 50 mL), The combined organic layers were washed with brine and dried over anhydrous Na_2SO_4. The solvent was removed under reduced pressure to afford 1.03 g of **18** as a yellow oil, which was used in the next step without further purification.

N-tert-butyloxycarbonyl-1-(O-benzyloxymethyl)–aminoethylglycine ethyl ester **19**: A stirred solution of **18** (0.52 g, 1.84 mmol) in dry MeOH (15 mL) was cooled to 0 °C under nitrogen atmosphere. In a separate round bottom flask, glycine ethyl ester hydrochloride (0.54 g, 3.86 mmol) was dissolved in MeOH (5 mL) and DIPEA (0.67 mL, 3.86 mmol). The flasks were then mixed and stirred at 4 °C for 4 h at which point acetic acid (0.3 mL, 5.7 mmol) was added, followed by $Na(OAc)_3BH$ (0.61 g, 2.87 mmol) and the solution was allowed to stir for another 30 min. 10% $NaHCO_3$ (50 mL) was then added to the solution and extracted with EtOAc (3 x 30 mL). The combined organic layers were washed with brine and dried (Na_2SO_4).The solvent was evaporated under reduced pressure and the residue was purified by flash silica gel chromatography to afford 0.27 g (40%) of **19** as viscous liquid. R_f = 0.38 (Hex:EtOAc = 2:3). ^1H NMR (300 MHz, $CDCl_3$) 7.31 (5 H, m), 5.10 (1 H, s), 4.52 (2 H, s), 4.18 (2 H, q, *J*= 7.2 Hz), 3.82 (1 H, m), 3.61 (1 H, dd, *J*= 9.4 Hz and 3.7 Hz), 3.52 (1 H, dd, *J*= 9.4 Hz and 4.9 Hz), 3.4 (2H, *J*= 17.3 Hz), 2.87 (1 H, dd, *J*= 12.2 Hz and 5.9 Hz), 2.77 (1 H, dd, J= 12.2 Hz and 5.7 Hz), 1.44 (*9* H, s), 1.27 (3 H, t, *J*= 7.2Hz). ESI-MS (m/z): Mass calcd for $C_{19}H_{30}N_2O_5$ 366.45, found 367.10.

Boc-(BzlOCH2)-T-OEt **20a**: To a stirred solution of thymine acetic acid (0.30 g, 1.63 mmol) in dry DMF (5 mL) were added DCC (0.34 g, 1.36 mmol) and DhbtOH (0.27 g, 1.63 mmol) under argon atmosphere. The stirring was continued for 1 h at room

temperature. Compound **19** (0.5g, 1.36 mmol) in dry DMF (5 mL) was added and the reaction was stirred at 50 °C for 24 h. Following evaporation of the solvent, the residue was partitioned between EtOAc (25 mL) and saturated $NaHCO_3$ (25 mL). The organic layer was washed with 10 % $KHSO_4$ (3 x 50 mL), 10 % $NaHCO_3$ (3 x 50 mL), brine (100 mL) and dried over Na_2SO_4. The solvent was removed under reduced pressure and purified by flash silica gel chromatography to afford 0.46 g (63 %) of **20** as pale yellow powder. R_f = 0.4 (Hex:EtOAc = 1:9). ^{1}H NMR (300 MHz, CDCl3) 8.17 (1 H, s), 7.32 (5 H, m), 7.01& 6.86 (1 H, q, *J*=1.2 Hz), 5.20 & 5.09 (1 H, s,), 4.58 (2 H, s), 4.4-4.7 (2 H, m), 4.16 (4 H, m), 3.97 & 3.91 (2H, s), 3.80 (1 H, m), 3.65-3.45 (2 H, m), 1.90 (3 H, d, *J* =1.2 Hz), 1.43 (9H, s), 1.33-1.20 (3H, t, *J*=7.1 Hz). ESI/MS (m/z): Mass calculated for $C_{26}H_{36}N_4O_8$ 531.58, found 555.20 (532.01+Na^+).

Boc-(BzlOCH2)-GCbz–OH **20b**: Guanine monomer synthesis was performed using the same procedure outlined above for thymine monomer. ESI/MS (m/z): Mass calculated for $C_{34}H_{41}N_7O_9$ 691.74, found 692.20.

Boc-(BzlOCH2)-CCbz–OH **20c**: Cytosine monomer synthesis was performed using the same procedure outlined above. ESI-MS (m/z): Mass calculated for $C_{33}H_{41}N_5O_9$ 651.72, found 674.20 (651.72+Na^+).

Boc-(BzlOCH2)-ACbz–OH **20d**: Adenine monomer synthesis was performed using the same procedure outlined above. ESI-MS (m/z): Mass calculated for C_{34} $H_{41}N_7$ O_8 675.34, found 676.20.

Boc-(BzlOCH2)-T-OH **21a**: To a solution of 5a (1.3 g, 2.46 mmol) in THF (20 mL) was added drop-wise 1 N lithium hydroxide (20 mL) at 0 ^{o}C. After stirring for 30 minute at the same temperature, water (100 mL) was added and extracted with ethyl acetate (3x 75

mL). The aqueous layer was acidified with 1 M HCl to pH ≅4 at 0 ^{o}C and then extracted with ethyl acetate (4x 100 mL). Organic layers were combined and dried over anhydrous Na_2SO_4. The solvent was removed under reduced pressure to afford 0.3270 g (80%) of **6a** as pale yellow powder. ^{1}H NMR (300 MHz, CDCl3) 8.06 (1 H, s), 7.35 (5 H, m), 7.12 & 6.90 (1 H, m), 5.20 (1 H, s), 4.60 (2 H, s), 4.50 (2 H, m), 4.16 (2 H, m), 3.97 (2 H, m), 3.80 (1 H, m), 3.57 (2 H, m), 1.90 (3 H, m), 1.43 (9 H, s). ESI/MS (m/z): Mass calculated for $C_{24}H_{32}N_4O_8$ 504.54, found 527.13 (504.54+Na^+).

Boc-(BzlOCH$_2$)-G-OH **21b**: Guanine monomer synthesis was performed using the same procedure outlined above for thymine monomer. ESI/MS (m/z): Mass calculated for $C_{32}H_{37}N_7O_9$ 663.69, found 686.3 (663.3+Na^+).

Boc-(BzlOCH$_2$)-C-OH **21c**: Cytosine monomer synthesis was performed using the same procedure outlined above for thymine monomer. ESI/MS (m/z): Mass calculated for $C_{31}H_{37}N_5O_9$ 623.66, found 646.3, (623.66+Na^+).

Boc-(BzlOCH$_2$)-A-OH **21d**: Adenine monomer synthesis was performed using the same procedure outlined above for thymine monomer. ESI/MS (m/z): Mass calculated for $C_{32}H_{37}N7O_8$ 647.69, found 648.27, (647.69+H^+).

II.4.3. Synthesis of Thymine 5-C2 Amino Linker

Ethyl 2-(5-iodo-2,4-dioxo-3,4-dihydropyrimidin-1(2H)-yl)acetate **23**: To a suspension of iodouracil **22** (1.9 g, 5 mmol) and anhydrous K_2CO_3 (0.76 g, 55 mmol) in anhydrous DMF (17.5 mL) at 0 °C in an oven dried round bottom flask , ethyl bromoacetate (0.83 g, 5 mmol) in anhydrous DMF (2.5 mL) was slowly added via syringe under a nitrogen atmosphere. After addition, the resulting reaction mixture was warmed up to rt gradually

and vigorously stirred for 24 h. Reaction completion checked by TLC (5% DCM/MeOH). The byproduct precipitate of KBr salt was filtered under vacuum and washed with 2 mL of DMF. The solvent was evaporated under vacuum, and diluted with EtOAc (20 mL) and washed with water (3 × 100 mL). The aqueous phase was back extracted with EtOAc (3 × 100 mL). Combined organic layers dried over Na_2SO4, and concentrated to 10 mL on rotovap. To this solution a few drops of hexane was added and as a result a pale yellow solid formed. The solid was then filtered over vacuum and washed with water and cold diethyl ether. Yielding product **23** (1.7 g, 5.2 mmol, qtv yield) was dried over vacuum and used for the next step without further purification. ^{1}H NMR (500 MHz, DMSO-d_6) δ (ppm): 11.8 (1 H, s), 8.2 (1 H, s), 4.5 (2 H, s), 4.2 (2 H, q, J= 7.1 Hz), 1.2 (3 H, t, J = 7.1 Hz); ^{13}C NMR (500 MHz, DMSO-d_6) δ (ppm) 168.4, 161.4, 151.1, 150.5, 68.8, 61.9, 49.2, 14.4. ESI-HRMS (positive ion mode) calcd for $C_8H_9IN_2O$ 324.07; found 324.96.

(E)-3-(1-(2-ethoxy-2-oxoethyl)-2,4-dioxo-1,2,3,4-tetrahydropyrimidin-5-yl)acrylic acid **24**: To a clean, dry 100 mL round-bottom flask was added ethyl 2-(5-iodo-2,4-dioxo-3,4-dihydropyrimidin-1(2H)-yl)acetate **23** (1.0 g, 3.1 mmol) and N-tetrabutylammonium bromide (1.2 g, 3.7 mmol), and dissolved in anhydrous DMF (13 mL). The flask was evacuated and kept under nitrogen atmosphere. Then, the catalyst, $Pd(OAc)_2$ (0.21 g, 0.94 mmol), was added under nitrogen. A mixture of DMF/H_2O/DIEA (10:10:10 mL) was added via syringe, and the reaction was evacuated (freed of any oxygen gas) and kept with stirring at rt under nitrogen for 10 minutes. Last, acrylic acid (2.16 g, 30 mmol) in dry DMF (10 mL) was slowly added to the reaction mixture via a stainless steel syringe under nitrogen. The reaction mixture was then heated to 80-90 °C in an oil bath for 16 h.

The reaction mixture turned black for the first few hours, and then palladium particles precipitated while the solution turned yellow. The black particles were filtered under vacuum, and the DMF was evaporated under vacuum at 45 ^{o}C. The reaction mixture was then dissolved with water (5 mL) and extracted with diethyl ether (5×50 mL). The organics were combined, dried over Na_2SO_4, and evaporated to give the crude product as yellow oil. The product was then precipitated by adding a few drops of hexane in an ice bath. The pale yellow powder **24** (0.5 g, 1.9 mmol, 60 %) was collected by vacuum filtration in a sintered glass funnel and dried under vacuum. ^{1}H NMR (500 MHz, DMSO-$d_{6)}$ δ (ppm): 12.2 (1 H, s); 11.8 (1 H, s), 8.2 (1 H, s), 7.2 (2 H, d, *J*= 15.9 Hz), 6.7 (2 H, d, *J*= 15.9 Hz), 4.6 (2 H, s), 4.2 (2 H, q, *J*= 7.1 Hz), 1.2 (3 H, t, *J*= 7.1 Hz); ^{13}C NMR (500 MHz, DMSO-$d_{6)}$ δ (ppm) 168.3, 162.9, 150.4, 149.0, 137.0, 118.6, 108.5, 61.8, 49.6, 14.5. ESI-HRMS (negative ion mode) calcd for $C_{11}H_{12}N_2O6$ 268.23; found 267.04.

(E)-2-(5-(3-((2-((tert-butoxycarbonyl)amino)ethyl)amino)-3-oxoprop-1-en-1-yl)-2,4-dioxo-3,4-dihydropyrimidin-1(2H)-yl)acetic acid **25**: To a stirred solution of (E)-3-(1-(2-ethoxy-2-oxoethyl)-2,4-dioxo-1,2,3,4-tetrahydropyrimidin-5-yl)acrylic acid **24** (0.70 g, 2.6 mmol) in anhydrous DMF (10 mL) were added DIEA (0.74 g, 5.7 mmol) HATU(1.18 g, 3.12 mmol) under nitrogen atmosphere. Reaction mixture was stirred at 0 ^{o}C for 30 min. Then, hydrochloric acid salt of tert-butyl (2-aminoethyl) carbamate (0.43 g, 2.2 mmol) in dry DMF (2 mL) was slowly added to the reaction mixture via a stainless steel syringe under nitrogen. The reaction mixture was warmed up to rt and stirred for 12 h. The reaction completion was checked by TLC. The DMF was evaporated at 45 ^{o}C under vacuum. The crude product was dissolved in water and extracted with ethyl acetate (5x 100 mL). The organics were combined, dried over Na_2SO_4, and evaporated to give the

crude product as yellow oil. The product obtained used for the next step without further purification.

To a stirred solution of crude product obtained from earlier step ethyl (E)-2-(5-(3-((2-((tert-butoxycarbonyl)amino)ethyl)amino)-3-oxoprop-1-en-1-yl)-2,4-dioxo-3,4-dihydropyrimidin-1(2H)-yl)acetate (0.57 g, 1.90 mmol) in THF (8 mL) was added dropwise LiOH (0.39 g) in 8 mL H_2O at 0 ^{O}C. After stirring 30 min at the same temperature, reaction mixture was warmed up to rt and was stirred overnight. Then, water (2.5 mL) added and pH was adjusted to 4 at which point precipitate was formed. The precipitate was filtered and washed over hexane (3x5 mL) and (3x5 mL) diethyl ether, respectively. The product **25** obtained dried under vacuum (0.54g, 1.42 mmol, 75%). ^{1}H NMR (500 MHz, DMSO-d_6) δ (ppm): 11.5 (1 H, s), 8.1 (1 H, t, *J*= 5.8 Hz), 8.0 (1 H, s), 7.0 (1 H, d, *J*= 15.5 Hz), 6.9 (1 H, d, *J*= 15.4 Hz), 6.8 (1 H, t, *J*= 5.0 Hz), 4.2 (2 H, s), 3.0 (2 H, t, *J*= 6.3 Hz), 3.2 (2 H, d, *J*= 6.2 Hz), 1.4 (9 H, s). ^{13}C NMR (500 MHz, DMSO-d_6) δ (ppm) 169.6, 166.3, 162.8, 156.1, 150.4, 149.2, 132.4, 121.4, 108.3, 78.1, 50.4, 40.3, 39.3, 28.7. ESI-MS (positive ion mode) calcd for $C_{16}H_{22}N_4O_7$ 382.3; found 382.7.

II.4.4. Ligand Synthesis

3-Hydroxy-1-pyridin-2-yl-butan-1-one **27**: To a solution of LDA prepared from dry diisopropylamine (17.5 mL, 125.0 mmol) and n-BuLi (2.5 M, 50 mL, 125.0 mmol) in dry THF (250 mL) cooled at -15°C was added dropwise 2-acetylpyridine **26** (9.3 mL, 83.0 mmol). The resulting solution was stirred at -15^{o}C for 2 h. Acetaldehyde (9.3 mL, 166.0 mmol) was added dropwise and the reaction mixture was stirred for 0.5h at -15 ^{o}C followed by the addition of a saturated solution of NH_4Cl. The organic phase was

collected, and the aqueous phase extracted with Et_2O (3 x 100 mL). The combined organic layers were dried over anhydrous Na_2SO_4. The solvent was evaporated under reduced pressure to dryness. The crude product was purified by column chromatography using EtOAc-hexane to afford yellow oil **27** (6.5 g, 39.3 mmol). Yield; 47%. ^{1}H NMR (300 MHz , $CDCl_3$) δ (ppm): 8.59-8.62 (1 H, m), 7.95-8.03 (1 H, m), 7.76-7.85 (1 H, m), 7.41-7.49 (1 H, m), 4.26-4.38 (1 H, m), 3.16-3.41 (2 H, m), 1.25 (3 H, d, J = 6.2 Hz).

1-Pyridine-2-yl-but-2-en-1-one **28**: To a stirred solution of compound **27** (6.55 g, 39.7 mmol) in DCM (350 mL) was added triethylamine (16.6 mL, 118.9 mmol) at -30°C. Methanesulfonyl chloride (3.7 mL, 47.58 mmol) was added dropwise to this reaction mixture. The solution was allowed to reach ambient temperature overnight. The dark solution was filtered. The solvent was evaporated under reduced pressure. The crude product was purified by column chromatography using EtOAc-hexane to afford a yellow liquid **28** (3.8 g, 25.5 mmol)**.** Yield; 64%. ^{1}H NMR (300 MHz , $CDCl_3$) δ (ppm): 8.59-8.62 (1 H, m), 8.09-8.16 (1 H, m), 7.81-7.89 (1 H, m), 7.56-7.66 (1 H, m), 7.43-7.51 (1 H, m), 7.18-7.33 (1 H, m), 2.04 (3 H, dd, J = 7.0 and 1.5 Hz).

4'-methyl-3,2':6',3''-terpyridine **29**: To a stirred solution of a mixture of 1-Pyridine-2-yl-bet-2-en-1-one **28** (0.94 g, 6.4 mmol in MeOH (19 mL) were added 2-pridylacylpriydinium iodide **31** (2.09 g, 6.4 mmol) and ammonium acetate (10.09 g, 138 mmol). The reaction mixture was refluxed for 6 h. The solvent was evaporated under reduced pressure and the solid residue was purified by column chromatography using Al_2O_3 as absorbent and EtOAc/Hexane (40:60) as an eluent to afford a yellow solid **29** (0.7 g, 2.7 mmol)**.** Yield; 70%. ^{1}H- NMR (300MHz, $CDCl_3$) δ (ppm): 8.72-8.74 (2 H, m), 8.63-8.72 (2 H, m), 8.33 (2 H, s), 7.85-7.91 (2 H, m), 7.33-7.39 (2 H, m), 2.56 (3 H, s).

2-Pyridacylpyridinium iodide **31**: To a stirred solution of 2-acetylpyridine **26** (5.0 g, 41.3 mmol) in pyridine (50 mL) was added iodine (12.6 g, 49.5 mmol) and refluxed for 3 h. The reaction mixture was cooled down to room temperature slowly. The black precipitate was filtered and washed with cold pyridine. The product was obtained as a black solid **31** (10.1 g, 30.9 mmol) Yield; 75%. ^{1}H NMR (300 MHz , $CDCl_3$): δ 6.53 (2 H, s), 7.80-7.89 (1 H, m), 8.04-8.19 (2 H, m), 8.24-8.35 (2 H, m), 7.69-7.79 (1 H, m), 8.83-8.91 (1 H, m), 8.99-9.08 (2 H, m).

2-([3,2':6',3''-terpyridin]-4'-yl)acetic acid **30**: An oven-dried flask was purged and refilled 3x with N_2, after which tetrahydrofuran (25 mL) was added. While the solvent was stirred at -15 C, 2,2,6,6-tetramethyl piperidine (0.77 mL, 4.4 mmol) and methyl lithium (2.5 mL, 3.9 mmol) were added and the solution stirred for 15 min. A deaerated solution of 4'-methyl-3,2':6',3''-terpyridine **29** (0.87 g, 3.5 mmol) dissolved in a minimal amount of THF was added and stirred for 30 min. CO_2 (g) was then bubbled into the reaction for 1 h. The resulting solid was collected and dissolved in 1 M HCl (20 mL). Ethanol (30 mL) was added to the solution, and the solvent volume was reduced via flash evaporation until a brown solid began to precipitate. After cooling in the freezer overnight, a brown solid was collected (0.4 g, 1.4 mmol). Yield; 40%. ^{1}H- NMR (300 MHz, in D_2O) δ (ppm): 8.5 (2 H, d), 8.0 (2 H, d), 7.8 (2 H, t), 7.75 (2 H, s), 7.4 (2 H, t), 3.6 (2 H, s).

2-([2,2'-bipyridin]-5-yl)acetic acid **33** (using CO_2 gas):

(a) Me-Bpy in THF (b) After addition of 1st drop of LDA (c) After addition of all BuLi (d) After stirring 2h (e) After adding CO2 gas (f, g) Product obtained after work up

5-methyl-2,2'-bipyridine **32** (500 mg; 2.94 mmol) was dissolved in 17 mL of dry THF, and cooled to -78°C under nitrogen. To this solution, 2.1 mL of 1.5 M LDA in cyclohexane (3.23 mmol) was added dropwise with stirring, and the reaction mixture was vigorously stirred at -78°C for 2h. After that, anhydrous CO_2 (ultrahigh purity) was bubbled through the dark brown solution. 4 mL of THF were added to compensate for the solvent that was "distilled" by the N_2 and CO_2 flow. Gradually, the solution became yellowish. This reaction mixture was left to slowly warm up to rt, and stirred for another 2 h. To the resulting yellow solution, 1 mL of H_2O was added and stirred at r.t. for 15 min. The solvent was evaporated to dryness, and the product was extracted with 1 N NaOH. Then, the pH of the extract was adjusted to 5 after dropwise addition of 3 M HCl. BpyCH_2COOH was then extracted with EtOAc. The organic layer was dried over anhydrous Na_2SO_4. EtOAc was removed *in vacuo* to give a yellowish solid (0.6 g). ^{1}H NMR (300 MHz, DMSO-d_6) δ (ppm): 7.44-8.68 (7 H, m), 3.73 (2 H, s).

2-([2,2'-bipyridin]-5-yl)acetic acid **33** (using CO_2 solid): 5-methyl-2,2'-bipyridine **32** (500 mg; 2.94 mmol) was dissolved in 17 mL of dry THF, and cooled to -78°C under nitrogen. To this solution, 2.1 mL of 1.5 M LDA in cyclohexane (3.23 mmol) was added dropwise with stirring, and the reaction mixture was vigorously stirred at -78°C for 2 h. After that, solid CO_2 (crashed into sand-size particles) was added to the dark brown solution. To release the extra-pressure, a balloon containing small amount of dry N_2 was inserted using a needle into the septum. Upon carbon dioxide addition, the color of the solution changed from brown to yellow, and then to white. The stirring was continued for 1 h, then the mixture was allowed to reach slowly the ambient temperature. To the resulting white suspension, 1 mL of H_2O was added and stirred at rt for 15 min. The

solvent was evaporated to dryness, and the product was dissolved with 1 N NaOH. And this aqueous solution was extracted with EtOAc to remove the unreacted starting material **32**. Then, the pH of the aqueous solution was adjusted to 5 after dropwise addition of 3 M HCl. $BpyCH_2COOH$ was then extracted with EtOAc. The organic layer was dried over anhydrous Na_2SO_4. EtOAc was removed *in vacuo* to give a yellowish solid. In this batch, most of the product remained in the aqueous layer. Therefore, H_2O was evaporated *in vacuo*, and the carboxylic acid extracted with DMF. 0.52 g of the solid product obtained. ^{1}H NMR (300 MHz, DMSO-d_6) δ (ppm): 7.44-8.68 (7 H, m), 3.73 (2 H, s).

Synthesis of Pyrene Monomer Ester **36**: To a stirred solution of 1-pyrene acetic acid **35** (0.5 g, 1.92 mmol) in dry DMF (45 mL) were added DCC (0.39 g, 1.92 mmol) and DhbtOH (0.31 g, 1.92 mmol) under nitrogen atmosphere. The stirring was continued for 1 h at room temperature. Compound **34** (0.39 g, 1.6 mmol) in dry DMF (5 mL) was added and the reaction was stirred at 50 ^{o} C for 24 h. Following evaporation of the solvent, the residue was partitioned between EtOAc (100 mL) and saturated $NaHCO_3$ (100 mL). The organic layer was washed with 10 % KHSO4 (3 x 50 mL), 10% NaHCO3 (3 x 50 mL), brine (100 mL) and dried over Na_2SO4. The solvent was removed under reduced pressure and purified by flash silica gel chromatography to afford 0.61 g (79%) of **36** as pale brown solid. ESI-MS (positive ion mode) calcd for $C_{29}H_{32}N_2O_5$ 488.58; found 511.3.

Synthesis of Pyrene Monomer **37**: To a solution of **36** (0.05 g, 0.1 mmol) in THF (0.5 mL) was added drop-wise 2 N NaOH (2.5 mL) at 0 ^{o}C and stirred at this temperature for 30 min. Raction mixture gradually was brought to room temperature and stirred for another 2 h. Then, reaction miture was stirred at concentrated under reduced pressure

and water (10 mL) was added and the pH was adjusted to 4. Aqueous solution was extracted with EtOAc (3X20 mL) and combined organic layers dried over Na_2SO_4. Dried organic layer was concentrated under reduced pressure to give desired product as a yellow solid **37** (0.091 g, 91%). ESI-MS (positive ion mode) calcd for $C_{27}H28N_2O_5$ 460.53; found 483.1.

Ethyl2-(2-([2,2'-bipyridin]-5-yl)-N-(2-((tert-butoxycarbonyl)amino)ethyl)acetamido)-acetate **40**: HOBt (604 mg, 4.07 mmol) and 2-([2,2'-bipyridin]-5-yl)acetic acid **39** were added to a solution of aeg **38** in anhydrous DMF (20 mL). DCC (1.005 g, 4.87 mmol) was added to stirred solution at 0 ^oC, reaction mixture was stirred at 0 ^oC for 1 h. Then, the reaction mixture was allowed to warm to room temperature and stirred overnight. After completion of the reaction, solvent was removed under reduced pressure to dryness. Then, oily residue dissolved in EtOAc (100 mL) and washed with $NaHCO_3$ and brine, respectively. Organic layer was dried over anhydrous Na_2SO_4. Solvent was removed under reduced pressure to dryness and product was purified by silica gel column chromatography using EtOAc:Hexane (50:50) and a yellow solid **40** was obtained (1.3 g product, 80%).

2-(2-([2,2'-Bipyridin]-5-yl)-N-(2-((tert-butoxycarbonyl)amino)ethyl)acetamido)acetic acid **41**: 2M NaOH (50 mL) was added to a stirred solution of ethyl 2-(2-([2,2'-bipyridin]-5-yl)-N-(2-((tert-butoxycarbonyl)amino)ethyl)acetamido)acetate **40** over a period of 15 min in THF (50 mL). After 30 min, reaction mixture was diluted and with water (200 mL) and washed with EtOAc (3 x 100 mL). Aqueous layer was acidified with 1 M HCl to pH≈ 4 at 0^oC. Then, aq. layer was extracted with EtOAc (4 x 150 mL). The

combined organic layers were dried over anhydrous Na_2SO_4 and removed under reduced pressure to dryness. No purification was needed. (1.1 g, 90%).

Synthesis of Ruthenium Monomer **42**: All manipulations were carried out under conditions of low light. Boc-protected bipyridine monomer **41** (1.00 g, 2.41mmol) was suspended in a 70% ethanol (100 mL) solution. To this solution was added cis-dichlorobis(2,2'-bipyridine)ruthenium(II) (1.20 g, 2.30 mmol). The reaction mixture was refluxed for 8 h. During the reaction, the color changed from dark purple to dark orange. After the reaction, the mixture was cooled to room temperature. The solvent was removed under reduced pressure, and the residue was set aside overnight. The compound was purified by column chromatography using CM-sepharose resin, with an ammonium chloride step gradient. A light yellow band was removed with 0.01 M NH_4Cl, a broad, orange band was eluted with 0.1 M NH_4Cl, and a red-orange band was eluted with 1 M NH_4Cl. A purple band remained on the column, most likely unreacted dichlorobis(2,2'-bipyridine)ruthenium(II). The desired product eluted at 0.1 M NH_4Cl and was precipitated out of solution by addition of saturated ammonium hexafluorophosphate. The precipitate was filtered and washed several times with water and ether. A hard, crusty orange residue remained (1.39 g).

Synthesis of 4-(Tritylthio)Butyric acid **45**: Trityl mercaptan **43** (1) 93.3 g, 11.97 mmol) was added stepwise to a suspension of NaH (1.05 g, 26.33 mmol) in 10 mL DMF under a nitrogen atmosphere at 0 ^{o}C. After completion of the addition, the reaction mixture was stirred for 30 min. A solution of a 4-bromo butyric acid **44** in 15 mL DMF was added slowly. After addition was completed, the reaction mixture was stirred for 30 min., and temperature was gradually increased to room temperature and reaction mixture stirred for

overnight. Then, 200 mL chloroform was added to the reaction mixture and the reaction mixture was washed with 4x(100 mL) $NaHSO_4$ and 4x(100 mL) H_2O. The organic layer was evaporated and the remaining oil was precipitated by addition of distilled water and solid product was collected by suction filtration. The crude powder then stirred in petroleum ether for a few minutes. The solid was collected by filtration to give a white powder **45** (3.95 g, 10.91 mmol, 91%). ^{1}H NMR (300 MHz, $CDCl_3$) δ(ppm) 7.5-7.2(15 H, m), 2.30 (2 H, t, *J*= 7.2 Hz), 2.2 (2 H, t, *J*=7.2 Hz), 1.67 (2 H, quint, *J*=7.2 Hz); ^{13}C NMR (500 MHz, DMSO-d_6) δ (ppm) 173.7, 140.2, 125.0, 123.2, 121.9, 62.0, 28.2, 26.6, 18.9. ESI-MS (positive ion mode) calcd for $C_{23}H_{22}O_2S$ $[M+H]^+$ 362; found 362.

II.5. References

1. Nilsson, B. L.; Soellner, M. B.; Raines, R. T., Chemical synthesis of proteins. *Annu. Rev. Biophys. Biomol. Struct.* **2005,** *34*, 91.
2. Gupta, P.; Muse, O.; Rozners, E., Recognition of Double-Stranded RNA by Guanidine-Modified Peptide Nucleic Acids. *Biochemistry* **2012,** *51* (1), 63-73.
3. Nielsen, P. E.; Haaima, G.; Lohse, A.; Buchardt, O., Peptide nucleic acids (PNAs) containing thymine monomers derived from chiral amino acids: hybridization and solubility properties of d-lysine PNA. *Angew. Chem. Int. Ed. (English)* **1996,** *35* (17), 1939-1942.
4. Püschl, A.; Sforza, S.; Haaima, G.; Dahl, O.; Nielsen, P. E., Peptide nucleic acids (PNAs) with a functional backbone. *Tetrahedron Lett.* **1998,** *39* (26), 4707-4710.
5. Corradini, R.; Sforza, S.; Dossena, A.; Palla, G.; Rocchi, R.; Filira, F.; Nastri, F.; Marchelli, R., Epimerization of peptide nucleic acids analogs during solid-phase synthesis: optimization of the coupling conditions for increasing the optical purity. *J. Chem. Soc., Perkin Trans. 1* **2001,** (20), 2690-2696.
6. Tedeschi, T.; Corradini, R.; Marchelli, R.; Pushl, A.; Nielsen, P. E., Racemization of chiral PNAs during solid-phase synthesis: effect of the coupling conditions on enantiomeric purity. *Tetrahedron: Asymmetry* **2002,** *13* (15), 1629-1636.
7. Richter, L. S.; Zuckermann, R. N., Synthesis of peptide nucleic acids (PNA) by submonomer solid-phase synthesis. *Bioorg. Med. Chem. Lett.* **1995,** *5* (11), 1159-1162.
8. Viirre, R. D.; Hudson, R. H., Optimization of a solid-phase synthesis of a PNA monomer. *Org. Lett.* **2001,** *3* (24), 3931-3934.
9. Dueholm, K. L.; Petersen, K. H.; Jensen, D. K.; Egholm, M.; Nielsen, P. E.; Buchardt, O., Peptide nucleic acid (PNA) with a chiral backbone based on alanine. *Bioorg. Med. Chem. Lett.* **1994,** *4* (8), 1077-1080.
10. Sforza, S.; Haaima, G.; Marchelli, R.; Nielsen, P. E., Chiral peptide nucleic acids (PNAs): helix handedness and DNA recognition. *Eur. J. Org. Chem.* **1999,** *1999* (1), 197-204.
11. Sugiyama, T.; Imamura, Y.; Demizu, Y.; Kurihara, M.; Takano, M.; Kittaka, A., β-PNA: Peptide nucleic acid (PNA) with a chiral center at the β-position of the PNA backbone. *Bioorg. Med. Chem. Lett.* **2011,** *21* (24), 7317-7320.
12. Tedeschi, T.; Sforza, S.; Corradini, R.; Marchelli, R., Synthesis of new chiral PNAs bearing a dipeptide-mimic monomer with two lysine-derived stereogenic centres. *Tetrahedron Lett.* **2005,** *46* (48), 8395-8399.
13. Falkiewicz, B.; Kołodziejczyk, A. S.; Liberek, B.; Wiśniewski, K., Synthesis of achiral and chiral peptide nucleic acid (PNA) monomers using Mitsunobu reaction. *Tetrahedron* **2001,** *57* (37), 7909-7917.
14. Sahu, B.; Chenna, V.; Lathrop, K. L.; Thomas, S. M.; Zon, G.; Livak, K. J.; Ly, D. H., Synthesis of conformationally preorganized and cell-permeable guanidine-based γ-peptide nucleic acids (γGPNAs). *J. Org. Chem.* **2009,** *74* (4), 1509-1516.
15. Sahu, B.; Sacui, I.; Rapireddy, S.; Zanotti, K. J.; Bahal, R.; Armitage, B. A.; Ly, D. H., Synthesis and characterization of conformationally preorganized,(R)-diethylene glycol-containing γ-peptide nucleic acids with superior hybridization properties and water solubility. *J. Org. Chem.* **2011,** *76* (14), 5614-5627.

16. Crawford, M. J.; Rapireddy, S.; Bahal, R.; Sacui, I.; Ly, D. H., Effect of steric constraint at the γ-backbone position on the conformations and hybridization properties of PNAs. *J Nucleic Acids* **2011,** *2011*.
17. Dragulescu-Andrasi, A.; Rapireddy, S.; Frezza, B. M.; Gayathri, C.; Gil, R. R.; Ly, D. H., A Simple γ-Backbone Modification Preorganizes Peptide Nucleic Acid into a Helical Structure. *J. Am. Chem. Soc.* **2006,** *128* (31), 10258-10267.
18. Ellipilli, S.; Ganesh, K. N., Fluorous Peptide Nucleic Acids: PNA Analogues with Fluorine in Backbone (γ-CF2-apg-PNA) Enhance Cellular Uptake. *J. Org. Chem.* **2015,** *80* (18), 9185-9191.
19. Smart, B. E., Fluorine substituent effects (on bioactivity). *J. Fluorine Chem.* **2001,** *109* (1), 3-11.
20. Doi, Y.; Katafuchi, A.; Fujiwara, Y.; Hitomi, K.; Tainer, J. A.; Ide, H.; Iwai, S., Synthesis and characterization of oligonucleotides containing 2′-fluorinated thymidine glycol as inhibitors of the endonuclease III reaction. *Nucleic Acids Res.* **2006,** *34* (5), 1540-1551.
21. Dolain, C.; Patwa, A.; Godeau, G.; Barthélémy, P., Nucleic acid based fluorinated derivatives: new tools for biomedical applications. *Appl. Sci.* **2012,** *2* (2), 245-259.
22. Rozners, E., Recent Advances in Chemical Modification of Peptide Nucleic Acids. *J Nucleic Acids* **2012,** *2012*, 8.
23. Sugiyama, T.; Kittaka, A., Chiral peptide nucleic acids with a substituent in the N-(2-aminoethy) glycine backbone. *Molecules* **2012,** *18* (1), 287-310.
24. De Costa, N. T. S.; Heemstra, J. M., Evaluating the effect of ionic strength on duplex stability for PNA having negatively or positively charged side chains. *PloS One* **2013,** *8* (3), e58670.
25. Avitabile, C.; Moggio, L.; Malgieri, G.; Capasso, D.; Di Gaetano, S.; Saviano, M.; Pedone, C.; Romanelli, A., γ Sulphate PNA (PNA S): highly selective DNA binding molecule showing promising antigene activity. *PloS One* **2012,** *7* (5), e35774.
26. Suparpprom, C.; Srisuwannaket, C.; Sangvanich, P.; Vilaivan, T., Synthesis and oligodeoxynucleotide binding properties of pyrrolidinyl peptide nucleic acids bearing prolyl-2-aminocyclopentanecarboxylic acid (ACPC) backbones. *Tetrahedron Lett.* **2005,** *46* (16), 2833-2837.
27. Vilaivan, T.; Srisuwannaket, C., Hybridization of pyrrolidinyl peptide nucleic acids and DNA: Selectivity, base-pairing specificity, and direction of binding. *Org. Lett.* **2006,** *8* (9), 1897-1900.
28. Mansawat, W.; Vilaivan, C.; Balázs, Á.; Aitken, D. J.; Vilaivan, T., Pyrrolidinyl peptide nucleic acid homologues: effect of ring size on hybridization properties. *Org. Lett.* **2012,** *14* (6), 1440-1443.
29. Bagmare, S.; Varada, M.; Banerjee, A.; Kumar, V. A., Synthesis of all four nucleoside-based β-amino acids as protected precursors for the synthesis of polyamide-DNA with alternating α-amino acid and nucleoside-β-amino acids. *Tetrahedron* **2013,** *69* (3), 1210-1216.
30. Banerjee, A.; Bagmare, S.; Varada, M.; Kumar, V. A., Glycine-Linked Nucleoside-β-Amino Acids: Polyamide Analogues of Nucleic Acids. *Bioconjug. Chem.* **2015,** *26* (8), 1737-1742.

31. Manicardi, A.; Guidi, L.; Ghidini, A.; Corradini, R., Pyrene-modified PNAs: Stacking interactions and selective excimer emission in PNA2DNA triplexes. *Beilstein J. Org. Chem.* **2014,** *10* (1), 1495-1503.
32. Tedeschi, T.; Tonelli, A.; Sforza, S.; Corradini, R.; Marchelli, R., A pyrenyl-PNA probe for DNA and RNA recognition: Fluorescence and UV absorption studies. *Artif DNA PNA XNA* **2010,** *1* (2), 83-89.
33. Oquare, B. Y.; Taylor, J.-S., Synthesis of Peptide Nucleic Acid FRET Probes via an Orthogonally Protected Building Block for Post-Synthetic Labeling of Peptide Nucleic Acids at the 5-Position of Uracil. *Bioconjug. Chem.* **2008,** *19* (11), 2196-2204.
34. Beyeler, A.; Belser, P.; Cola, L. D., Rhenium Complexes with a Photochemically Variable Anthracene Subunit: A Molecular Switch. *Angew. Chem. Int. Ed.* **1997,** *36* (24), 2779-2781.
35. Dey, S.; Jäschke, A., Tuning the Stereoselectivity of a DNA-Catalyzed Michael Addition through Covalent Modification. *Angew. Chem. Int. Ed.* **2015,** *54* (38), 11279-11282.
36. Coppock, M. B.; Kapelewski, M. T.; Youm, H. W.; Levine, L. A.; Miller, J. R.; Myers, C. P.; Williams, M. E., CuII Cross-Linked Antiparallel Dipeptide Duplexes Using Heterofunctional Ligand-Substituted Aminoethylglycine. *Inorg. Chem.* **2010,** *49* (11), 5126-5133.
37. Wolpher, H.; Sinha, S.; Pan, J.; Johansson, A.; Lundqvist, M. J.; Persson, P.; Lomoth, R.; Bergquist, J.; Sun, L.; Sundström, V., Synthesis and electron transfer studies of ruthenium-terpyridine-based dyads attached to nanostructured TiO2. *Inorg. Chem.* **2007,** *46* (3), 638-651.
38. Fukuyama, T.; Cheung, M.; Jow, C.-K.; Hidai, Y.; Kan, T., 2,4-Dinitrobenzenesulfonamides: A simple and practical method for the preparation of a variety of secondary amines and diamines. *Tetrahedron Lett.* **1997,** *38* (33), 5831-5834.
39. Sacui, I.; Hsieh, W.-C.; Manna, A.; Sahu, B.; Ly, D. H., Gamma peptide nucleic acids: as orthogonal nucleic acid recognition codes for organizing molecular self-assembly. *J. Am. Chem. Soc.* **2015,** *137* (26), 8603-8610.
40. Kise, K. J.; Bowler, B. E., A ruthenium (II) tris (bipyridyl) amino acid: synthesis and direct incorporation into an α-helical peptide by solid-phase synthesis. *Inorg. Chem.* **2002,** *41* (2), 379-386.
41. Qvit, N.; Reuveni, H.; Gazal, S.; Zundelevich, A.; Blum, G.; Niv, M. Y.; Feldstein, A.; Meushar, S.; Shalev, D. E.; Friedler, A., Synthesis of a novel macrocyclic library: discovery of an IGF-1R inhibitor. *J. Comb. Chem.* **2008,** *10* (2), 256-266.

CHAPTER III. SPIN FILTERS BASED ON SELF ASSEMBLED γ-MODIFIED PEPTIDE NUCLEIC ACIDS

This chapter presents the results of collaborative work with the groups of Prof. Ron Naaman from the Weizmann Institute of Science, Rehovot, Israel and Prof. Helmut Zacharias from Physics Institute, WWU Muenster, Germany. My role was to synthesize and characterize peptide nucleic acid monomers and oligomers. Self-assembled monolayers (SAMs) preparation and characterizations were done by Nirit Kantor and Francesco Tassinari (Naaman Group). Spin effect by Mott polarimeter was measured by Paul Moellers (Zacharias Group).

III.1. Introduction

In 1996, the US Defense Advanced Research Projects Agency announced a new research program in spin transport electronics for which it coined the term of spintronics.[1] In contrast to electronics, which is built on the use of the charge properties of the electron, spintronics is built on the electron's spin.[1] Electronics is based on electron flow through electrical circuits that include components with nonlinear behavior such as diodes or transistors. The nonlinear behavior makes possible the amplification of small electric signals and the construction of switches useful for information storage. Spintronics is based on the control of spin orientation or polarization of electrons and the associated magnetic properties of the materials containing the electrons. The key points to create a spintronic device are the ability to "write" the spin polarization of electrons, i.e. create a population of electrons in which most electrons have the same spin orientation, and to "read" the electron polarization by measuring a property that depends on the relative orientation of the spin. Metal-based spintronic devices have very high

sensitivity to small magnetic fields, can function as spin polarizers and spin valves, and have widely been used as read/write heads in computer hard drives.[2]

Research is currently under way on spintronic devices based on a range of materials including semiconductors but many simple questions regarding combination of semiconductors with other materials to generate feasible spintronic technology are still to be clearly answered. For example, whether or how placing a semiconductor in contact with another material would impede spin transport across the interface is yet to be well defined.[2] On the other hand, it has been shown that inorganic semiconductors can be easier integrated with current electronic devices. Intense work has also focused on organic spintronics, where organic molecules are used within spin-specific devices. The organic material is generally used as an intermediate that transfers the spin without changing the spin orientation or magnitude.[3] The ability to use a self-assembled molecular layer as a spin filter provides greater energy efficiency and smaller device size.[3]

For many years, organic molecules have not been considered good candidates for spintronic devices because they could not be applied as spin filters at room temperature.[4] However, in a 2011 study by Gohler et al.,[5] dsDNA was used a spin filter to polarize electrons ejected from surfaces coated with a self-assembled dsDNA at room temperature. The spin orientation of the transmitted electrons was measured using a Mott polarimeter. Unpolarized electrons were ejected from the gold substrate using linearly polarized light. Most of the electrons transmitted through the DNA monolayer were polarized with their spin aligned antiparallel to their velocity. The spin polarization was independent of the polarization of the incident light but depended on the length of the

DNA and its organization in the monolayer. Specifically, Gohler et al. showed that the absolute value of electron spin polarization increases with the increasing length of the dsDNA from 26-bp, to 40-bp, to 50-bp, and on to 78-bp. These DNAs contained 2.6; 4; 5 and 7.8, helical turns, respectively.

Typically, DNA adopts a right-handed B-DNA structure so it can be used to obtain only one type of spin filter, i.e. for spin electrons. My research is aimed at verifying that the spin filter properties of DNA are common for other chiral nucleic acids and to obtain spin filters for spin down electrons as well as "switchable" spin filters.

This chapter describes the result of spin polarization of PNA homo-duplexes. The short-term goal was to obtain spin filters based on PNA. The long-term goal is to create "switchable" spin filters, which can undergo transitions between spin up and spin down polarization in response to external input. The project makes use of SAMs containing PNA duplexes with thiol linkers cysteamine (Cya), Cysteine (Cys) or propyl thiol (PT). Solid state devices were prepared to measure the magnetoresistance. Mott polarimeter was used to measure the spin polarization.

III.2. Research Design

Previous experimental and theoretical studies of room-temperature spin filters showed a correlation between the number of helical turns and the spin polarization effect. Given that PNA duplexes can have more than 20 bases/turn, we chose to examine 20 base-pair duplexes.[6] The synthesis of long PNA strands is time consuming and relatively low yield, and thus costly. Hence, we decided to use a template method in which two short 10-base PNA single strands (yellow and blue in Figure III.1). The 20-bp duplex can be formally seen as the stitching of two 10-base pair duplexes.

(a) (b) (c)

Figure III.1 Types of duplexes based on the 20-mer PNA or DNA template with **(a**) two complementary 10-mer PNAs, or **(b)** and **(c)** one single 10-mer PNA.

We chose the sequence of nucleobases of the 20-bp duplex by stitching of 10-bp gamma PNA duplexes reported by Ly et al., such that we could use the characterization data reported by Ly et al. in the analysis of the 20-bp duplexes. The sequence of the two 10-bp PNA duplexes of Ly and of our 20-bp duplex is shown in the first two lines of the Table III.1.

Ly et al. have synthesized both DNA/DNA and DNA/PNA 10-bp duplexes with the sequences shown in the Table III.1. As expected, the melting temperature of the PNA/PNA duplexes is significantly larger than that of the DNA/PNA ones which is larger than that of the DNA/DNA duplexes. γPNAs have a simple backbone modification at the γ-position of N-(2-aminoethyl) glycine unit. CD spectra of γ-Me-PNA and γ-Ser-PNA (number of chiral centers varied around 1 to 10) showed biphasic exciton coupling pattern characteristic of a right-handed helix. CD intensity of ss γPNAs with different number of γ-modifications was similar to one another, in both shape and amplitude in the nucleobase region.

Table III.1 Melting temperatures (T_m) of duplexes

No	Sequence*	Type of Duplex	T_m/°C	Ref
1	GAC CAC AGA T	DNA/DNA	39	[7]
2	CTG GTG TCT A	DNA/PNA	59	[7]
		DNA/γ-Me-PNA	90	[7]
3	AGT TTG TAC G	DNA/DNA	27	IDT
4	TCA AAC ATG C	DNA/γ-Ser-PNA	63	[8]
5	GAC CAC AGA T TCA AAC ATG C	DNA/DNA	52	
6	CTG GTG TCT A AGT TTG TAC G			IDT

* The sequences of the upper strands are written in 5'-3'/N-C order & we have estimated the melting temperature T_m = 52°C of the 20-bp DNA/DNA duplex using OligoAnalyzer database on IDT website.

γ-Serine PNA monomers have been incorporated in the 10-base PNA single strands to ensure a preferred handedness for the PNA homo-duplexes. These PNA monomers were synthesized as described in Chapter II. Cysteamine (Cya), Cysteine (Cys) or propylthiol (PT), which contain thiol groups, were introduced in the PNA oligomers that were used in the formation of self-assembled monolayers on Au surfaces. Pyrene has been used to probe the proximity of different PNA strands because pi-stacked pyrene dimers show a characteristic excimer. The pyrene has been introduced in the PNA oligomers by attaching a carboxylic acid of the pyrene to the amino group on the side chain of a lysine placed in the PNA oligomer.

Table III.2 shows the sequences of all duplexes prepared for the studies presented in this chapter. The 20-base template strand is termed PNA1 or DNA1; PNA2 and DNA2 are the 20-base strands complementary to PNA1 and DNA1. PNA1 contained 3 Lysines to ensure the solubility of this relatively long strand. The two short 10-base PNAs complementary to the first and second halves of PNA1 are termed PNA3 and PNA4, respectively. We varied the position of the terminal Lys (at the C-end and N-end) of PNA3 to check if the placement of Lys in PNA3 and PNA4 affects the stability of the

20-bp PNA duplex. PNA3 and PNA4 have been prepared in the aeg form and in the gamma-serine form, γPNA3$_{C\text{-}Lys}$ and γPNA4$_{C\text{-}Lys}$, respectively, by incorporation of three γ-modified PNA monomers. Both PNA3 and PNA4 have also been prepared with a pyrene.

Table III.2 Sequence of oligonucleotides[a]

	PNA Sequence
PNA1$_{C\text{-}Lys}$	H-CGT ACA AAC TTA GAC ACC AG Lys_3-NH_2
PNA1$_{N\text{-}Cys}$	H-Cys-CGT ACA AAC TTA GAC ACC AG Lys_3-NH_2
PNA1$_{N\text{-}Cya}$	H-Cya-CGT ACA AAC TTA GAC ACC AG Lys_3-NH_2
PNA1$_{C\text{-}Lys(pyr)}$	H-Lys_2 CGT ACA AAC T TAG ACA CCA G Lys Lys(*pyr*)NH_2
PNA2	H-CTG GTG TCT A AGT TTG TAC G Lys_3-NH_2
PNA3$_{N\text{-}Lys}$	H-Lys-CTG GTG TCT A-NH_2
γPNA3$_{N\text{-}Dap(Fc)}$	Fc(Dap)-CTG GTG TCT A-Lys-NH_2
γPNA3$_{C\text{-}Lys}$	H-CTG GTG TCT A-Lys-NH_2
PNA3$_{C\text{-}Lys(pyr)}$	H-Lys CTG GTG TCT A Lys(*pyr*)-NH_2
PNA3$_{N\text{-}Lys(pyr)}$	H-Lys Lys(*pyr*)CTG GTG TCT A NH_2
PNA4$_{C\text{-}SH+N\text{-}Ac}$	Ac-AGT TTG TAC G-$(CH_2)_3SH$
γPNA4$_{C\text{-}Lys}$	H-AGT TTG TAC G-Lys-NH_2
γPNA4$_{N\text{-}Lys(pyr)}$	H-(*pyr*)Lys AGT TTG TAC G Lys-NH_2
PNA4$_{C\text{-}Lys(pyr)}$	H-AGT TTG TAC G Lys(*pyr*)LysNH_2
	DNA Sequence
DNA1$_{5'\text{-}3'}$	CGT ACA AAC T TAG ACA CCA G
DNA1$_{3'\text{-}5'}$	CGT ACA AAC T TAG ACA CCA G
DNA2$_{5'\text{-}3'}$	CTG GTG TCT A AGT TTG TAC G
DNA1$_{5'(pyr)/3'(pyr)}$	(*pyr*)CGT ACA AAC T TAG ACA CCA G(*Pyr*)
DNA3$_{5'(pyr)}$	(*pyr*)CTG GTG TCT A
DNA4$_{3'(pyr)}$	AGT TTG TAC G(*Pyr*)

[a] Underlined letters indicate S-serine γ-backbone modification

III.3. Results

III.3.1. Thermal Stability of Homo- and Hetero-Duplexes

UV absorption of the duplexes P(D)NA1/PNA3/γPNA4 and P(D)NA(1)/PNA3 or γPNA4 were recorded between 220-350 nm. UV absorption spectra of the homo- or hetero-duplexes at 90°C and 15°C show that absorbance of duplexes at 260 nm decreased with the decreasing temperature, which is characteristic of the formation of nucleic acid structures by hybridization (Figure III.2).

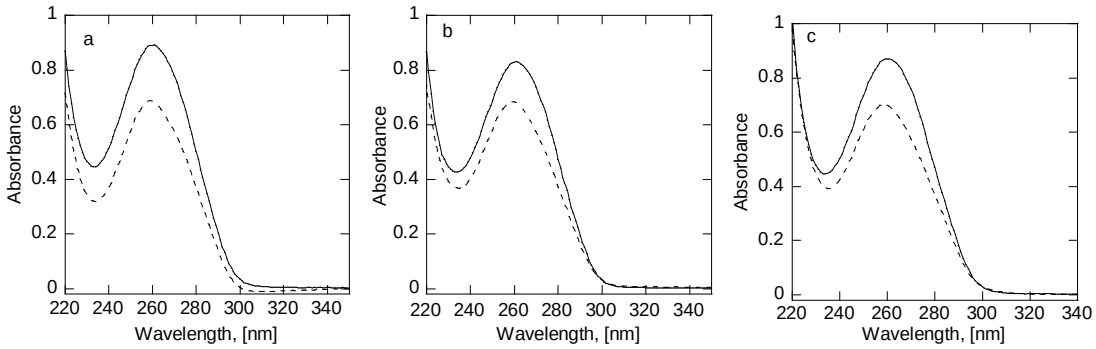

Figure III.2 UV-vis spectra recorded at 90°C (solid line) and 15°C (dashed line) for (a) $PNA1_{C\text{-}Lys}/PNA3_{C\text{-}Lys}/\gamma PNA4_{C\text{-}Lys}$ (b) $PNA1_{C\text{-}Lys}/PNA3_{C\text{-}Lys}$ (c) $PNA1_{C\text{-}Lys}/\gamma PNA4_{C\text{-}Lys}$.

Two types of UV-melting experiments were performed. In the first type, hybridization of the 20-base $PNA1_{C\text{-}Lys}$ or DNA template with both complementary 10-base strands PNA3-PNA4 was studied; in this experiment, it is possible to form the stitched 20-bp duplex. In the second type, the template $PNA1_{C\text{-}Lys}$ or DNA1 was hybridized with only one of the two complementary 10-base PNA oligomers (PNA3 or PNA4); in this case, one half of the template forms a 10-base pair duplex and the second half of the template acts as an overhang. Figure III.4 - Figure III.5 show UV melting profiles. The melting temperatures of stitched homo-PNA/PNA and hetero-PNA/DNA duplexes are shown in Table III.3.

The UV melting curves recorded for PNA1/PNA3/γPNA4 and DNA1/PNA3/γPNA4 duplexes show no evidence for multiple transitions; they show a transition more cooperative than that of the template with one of the two 10-mer strands. (Figure III.4 - Figure III.5). Figure III.3a shows that for a 20-base pair duplex the melting temperature determined from the maximum of the first derivative of the melting curve (88 ^{o}C) and that determined from the simulation of the melting curve using the formula M1+M2/(1+exp((M3-M0)/M4)); M1=0.1; M2=17; M3=71; M4=5 (87 ^{o}C) coincide. Panels b and c of Figure III.3 also show that the same coincidence occurs for the melting temperatures of the stitched duplexes (black curves, T_m= 71, 72^{o}C), but not for the 10-base pair duplexes that contain a 20-base template and only one 10-base strand (red and blue curves). This analysis supports the idea that stitched 20-base duplexes are formed from the 20-base pair DNA1 or PNA1 template strand with the short 10-base PNA3 and PNA4 strands.

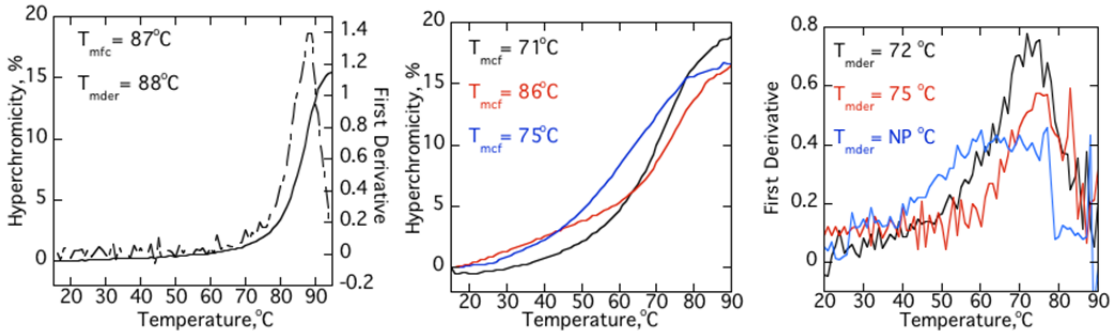

Figure III.3 (a) UV-melting profiles and first derivatives of melting profiles of PNA1$_{C\text{-}Lys}$/DNA2 (b) first derivatives of melting profiles of PNA1$_{C\text{-}Lys}$/PNA3$_{C\text{-}Lys}$/γPNA4$_{C\text{-}Lys}$ (black line); PNA1$_{C\text{-}Lys}$/PNA3$_{C\text{-}Lys}$ (red line); PNA1$_{C\text{-}Lys}$/γPNA4$_{C\text{-}Lys}$ (blue line); (c) UV-melting profiles of PNA1$_{C\text{-}Lys}$/PNA3$_{C\text{-}Lys}$/γPNA4$_{C\text{-}Lys}$ (black line); PNA1$_{C\text{-}Lys}$/PNA3$_{C\text{-}Lys}$ (red line); PNA1$_{C\text{-}Lys}$/γPNA4$_{C\text{-}Lys}$ (blue line).

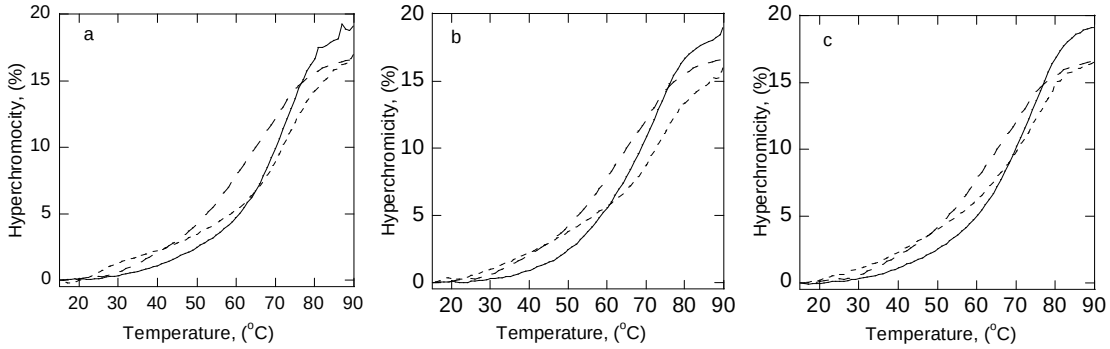

Figure III.4 UV-melting profiles of PNA/PNA homo-duplexes (a) $PNA1_{C\text{-}Lys}/PNA3_{C\text{-}Lys}/\gamma PNA4_{C\text{-}Lys}$; $PNA1_{C\text{-}Lys}/PNA3_{C\text{-}Lys}$; $PNA1_{C\text{-}Lys}/\gamma PNA4_{C\text{-}Lys}$ (b) $PNA1_{C\text{-}Lys}/PNA3_{N\text{-}Lys}/\gamma PNA4_{C\text{-}Lys}$; $PNA1_{C\text{-}Lys}/PNA3_{N\text{-}Lys}$; $PNA1_{C\text{-}Lys}/\gamma PNA4_{C\text{-}Lys}$(c) $PNA1_{C\text{-}Lys}/\gamma PNA3_{C\text{-}Lys}/\gamma PNA4_{C\text{-}Lys}$; $PNA1_{C\text{-}Lys}/\gamma PNA3_{C\text{-}Lys}$; $PNA1_{C\text{-}Lys}/\gamma PNA4_{C\text{-}Lys}$ duplexes. The curves for solutions that contain three PNAs are represented by solid lines; The curves for $PNA1_{C\text{-}Lys}/\gamma PNA4_{C\text{-}Lys}$ are shown by dashed lines. The curves for $PNA1_{C\text{-}Lys}/PNA3_{C\text{-}Lys}$; $PNA1_{C\text{-}Lys}/PNA3_{N\text{-}Lys}$, and $PNA1_{C\text{-}Lys}/\gamma PNA3_{C\text{-}Lys}$ are shown as dotted lines. Samples contained stoichiometric amounts of oligonucleotides at 3 μM strand concentration. Only heating curves are shown.

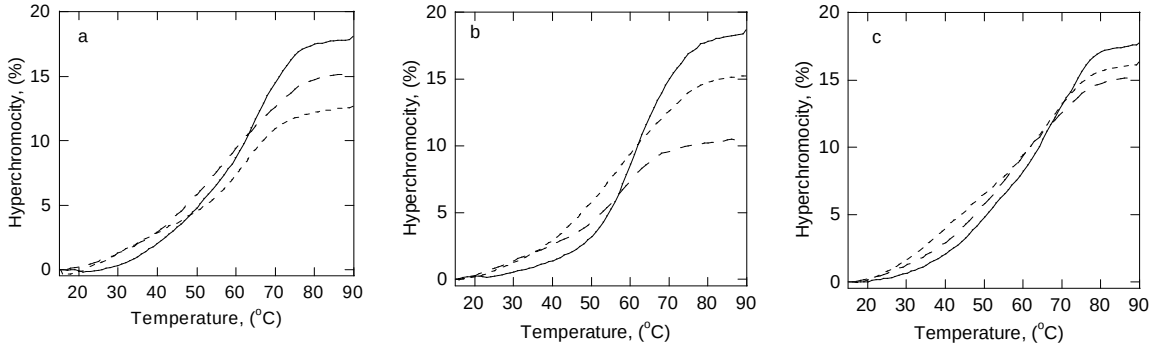

Figure III.5 UV-melting profiles of antiparallel DNA/PNA hetero-duplexes (a) $DNA1/PNA3_{C\text{-}Lys}/\gamma PNA4_{C\text{-}Lys}$; $DNA1/PNA3_{C\text{-}Lys}$; $DNA1/\gamma PNA4_{C\text{-}Lys}$ (b) $DNA1/PNA3_{N\text{-}Lys}/\gamma PNA4_{C\text{-}Lys}$; $DNA1/PNA3_{N\text{-}Lys}$; $DNA1/\gamma PNA4_{C\text{-}Lys}$ (c) $DNA1/\gamma PNA3_{C\text{-}Lys}/\gamma PNA4_{C\text{-}Lys}$; $DNA1/\gamma PNA3_{C\text{-}Lys}$; $DNA1/\gamma PNA4_{C\text{-}Lys}$ duplexes. The curves for solutions that contain three PNAs are represented by solid lines; The curves for $DNA1/\gamma PNA4_{C\text{-}Lys}$ are shown by dashed lines. The curves for $DNA1/PNA3_{C\text{-}Lys}$; $DNA1/PNA3_{N\text{-}Lys}$, and $DNA1/\gamma PNA3_{C\text{-}Lys}$ are shown as dotted lines. Samples contained stoichiometric amounts of oligonucleotides at 3 μM strand concentration. Only heating curves are shown.

Table III.3 Summary of Thermal Stabilities for Stitched PNA/PNA Homo-duplexes(T_m[^{o}C]) and Stitched DNA/PNA Antiparallel Hetero-duplexes (T_m[^{o}C])

Homo- PNA/PNA Duplex	**T_m[^{o}C]**	**Hetero- DNA/PNA Duplex**	**T_m[^{o}C]**
		DNA2/PNA1	>90
$PNA1_{C\text{-}Lys}/PNA3_{C\text{-}Lys}/\gamma PNA4_{C\text{-}Lys}$	71	$DNA1/PNA3_{C\text{-}Lys}/\gamma PNA4_{C\text{-}Lys}$	63
$PNA1_{C\text{-}Lys}/PNA3_{N\text{-}Lys}/\gamma PNA4_{C\text{-}Lys}$	68	$DNA1/PNA3_{N\text{-}Lys}/\gamma PNA4_{C\text{-}Lys}$	61
$PNA1_{C\text{-}Lys}/\gamma PNA3_{C\text{-}Lys}/\gamma PNA4_{C\text{-}Lys}$	72	$DNA1/\gamma PNA3_{C\text{-}Lys}/\gamma PNA4_{C\text{-}Lys}$	63
$PNA1_{C\text{-}Lys}/PNA3_{C\text{-}Lys}$	75	$DNA1/PNA3_{C\text{-}Lys}$	61
$PNA1_{C\text{-}Lys}/PNA3_{N\text{-}Lys}$	77	$DNA1/PNA3_{N\text{-}Lys}$	57
$PNA1_{C\text{-}Lys}/\gamma PNA3_{C\text{-}Lys}$	76	$DNA1/\gamma PNA3_{C\text{-}Lys}$	61
$PNA1_{C\text{-}Lys}/\gamma PNA4_{C\text{-}Lys}$	64	$DNA1/\gamma PNA4_{C\text{-}Lys}$	60

T_m are known within 2 ^{o}C. T_m were obtained from the curve-fitting data or estimated from the first derivative of the melting curves. The $T_{m's}$ are average of at least two experiments.

The T_ms of 10-base pair hetero-duplexes of DNA1 with PNA3 or of DNA1 with PNA4 (57-61 ^{o}C) are similar to each other and only slightly lower than that of the stitched 20-base pair duplex that contains DNA1 and both PNA3 and PNA4 (61-63 ^{o}C). The melting temperature of the non-stitched, 20-base duplex $PNA1_{C\text{-}Lys}$/DNA2 (>90 ^{o}C) is much higher than that of the stitched 20-base pair duplex that contains DNA1 and both PNA3 and PNA4 (61-63 ^{o}C). These results suggest that the stitching has a negative consequence on the stability of the 20-base pair PNA/DNA hetero-duplex.

The T_m of the 10-base pair homoduplex made of PNA1 with PNA3 (75-77 ^{o}C) is higher than that of the duplex formed by PNA1 with PNA4 (64 ^{o}C). The T_m of the stitched 20-base pair PNA duplex PNA1/PNA3/PNA4 (70 ^{o}C) is close to the average of the T_ms of the two 10 base pair ones. This observation suggests that the two halves of the stitched, 20-base pair PNA duplex affect each others' thermal stability. The melting temperature of the PNA1/PNA3/γPNA4 duplexes is higher than that of

DNA1/PNA3/γPNA4, which is in agreement with previous reports on the similar relative stability of PNA/PNA and PNA/DNA duplexes.[9]

The stitched duplexes that contained three or six gamma serine monomers had T_m nearly identical to that of the corresponding aeg stitched duplexes (Table III.3). This result is in contrast to previous studies, which have shown that gamma serine modification stabilizes PNA/DNA duplexes by 2-4 ^oC for each modified monomer included in the duplex PNA.[8, 10] Most likely, the stabilization effect of gamma serine modification is compensated by the destabilization effect of the stitching.

III.3.2. Chirality of the homo-and hetero-duplexes

γ-serine modified PNA monomers were used to make right-handed PNA oligomers. The right handedness of the homo-duplexes (PNA/PNA) and hetero-duplexes (PNA/DNA) was confirmed by CD spectra. Figure III.6 through Figure III.7 show the CD spectra for homo-PNA/PNA and PNA/DNA hetero-duplexes. Consistent with the literature findings, the spectra show distinct exciton coupling patterns with minima at 242 and 280 nm and maxima at 260 nm characteristic right-handed helix structure.

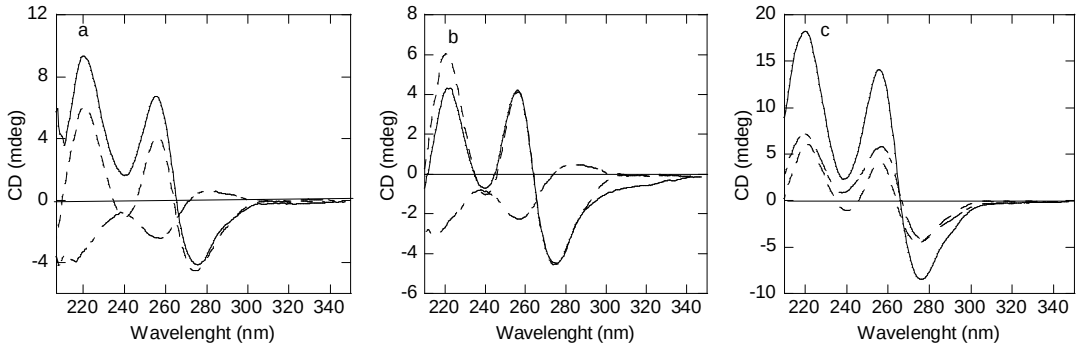

Figure III.6 CD spectra of PNA/PNA homo-duplexes (a) $PNA1_{C\text{-}Lys}/PNA3_{C\text{-}Lys}/\gamma PNA4_{C\text{-}Lys}$; $PNA1_{C\text{-}Lys}/PNA3_{C\text{-}Lys}$; $PNA1_{C\text{-}Lys}/\gamma PNA4_{C\text{-}Lys}$ (b) $PNA1_{C\text{-}Lys}/PNA3_{N\text{-}Lys}/\gamma PNA4_{C\text{-}Lys}$; $PNA1_{C\text{-}Lys}/PNA3_{N\text{-}Lys}$; $PNA1_{C\text{-}Lys}/\gamma PNA4_{C\text{-}Lys}$(c) $PNA1_{C\text{-}Lys}/\gamma PNA3_{C\text{-}Lys}/\gamma PNA4_{C\text{-}Lys}$; $PNA1_{C\text{-}Lys}/\gamma PNA3_{C\text{-}Lys}$; $PNA1_{C\text{-}Lys}/\gamma PNA4_{C\text{-}Lys}$ duplexes. The curves for solutions that contain three PNAs are represented by solid lines; The curves for $PNA1_{C\text{-}Lys}/\gamma PNA4_{C\text{-}Lys}$ are shown by dashed lines. The curves for $PNA1_{C\text{-}Lys}/PNA3_{C\text{-}Lys}$; $PNA1_{C\text{-}Lys}/PNA3_{N\text{-}Lys}$, and $PNA1_{C\text{-}Lys}/\gamma PNA3_{C\text{-}Lys}$ are shown as dotted lines. Samples containing stoichiometric amounts of oligonucleotides at 3 μM strand concentration were prepared in 10 mM NaPi buffer.

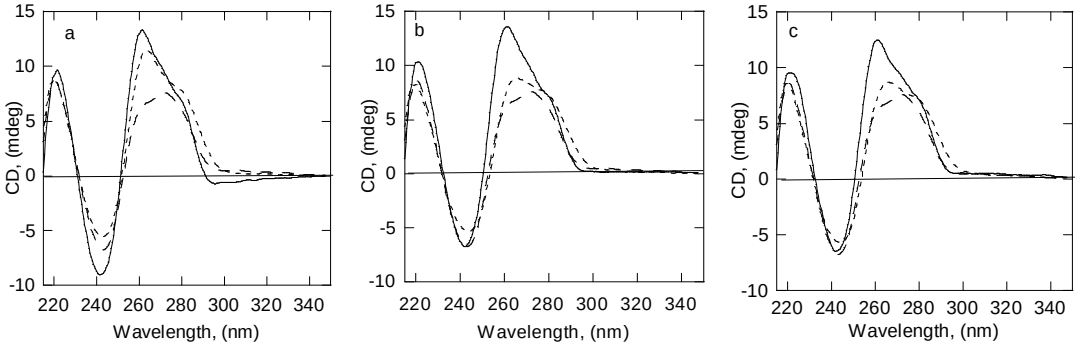

Figure III.7 CD spectra of PNA/DNA antiparallel hetero-duplexes (a) $DNA1/PNA3_{C\text{-}Lys}/\gamma PNA4_{C\text{-}Lys}$; $DNA1/PNA3_{C\text{-}Lys}$; $DNA1/\gamma PNA4_{C\text{-}Lys}$ (b) $DNA1/PNA3_{N\text{-}Lys}/\gamma PNA4_{C\text{-}Lys}$; $DNA1/PNA3_{N\text{-}Lys}$; $DNA1/\gamma PNA4_{C\text{-}Lys}$ (c) $DNA1/\gamma PNA3_{C\text{-}Lys}/\gamma PNA4_{C\text{-}Lys}$; $DNA1/\gamma PNA3_{C\text{-}Lys}$; $DNA1/\gamma PNA4_{C\text{-}Lys}$ duplexes. The curves for solutions that contain three PNAs are represented by solid lines; The curves for $DNA1/\gamma PNA4_{C\text{-}Lys}$ are shown by dashed lines. The curves for $DNA1/PNA3_{C\text{-}Lys}$; $DNA1/PNA3_{N\text{-}Lys}$, and $DNA1/\gamma PNA3_{C\text{-}Lys}$ are shown as dotted lines. Samples containing stoichiometric amounts of oligonucleotides at 3 μM strand concentration were prepared in 10 mM NaPi buffer.

The single strand $PNA1_{C\text{-}Lys}$ shows no CD signal. The single strands $\gamma PNA3_{C\text{-}Lys}$ and $\gamma PNA4_{C\text{-}Lys}$ showed weaker signals compared to the ds-γPNAs, indicative of a right-handed structure.[6a, 8, 10-11]

The duplexes formed between $PNA1_{C\text{-}Lys}/PNA3_{C\text{-}Lys}$; $PNA1_{C\text{-}Lys}/PNA3_{N\text{-}Lys}$ adopted a left-handed helix due to lack of any γ-modified PNA oligomer. In the presence of a γ-modified PNA oligomer $\gamma PNA3_{C\text{-}Lys}$ or $\gamma PNA4_{C\text{-}Lys}$, the PNA duplexes adopted a right-handed helical structure. Upon hybridization of $PNA1_{C\text{-}Lys}$ to $\gamma PNA3_{C\text{-}Lys}$ and $\gamma PNA4_{C\text{-}Lys}$, the intensity of the CD signal increased since the total number of γ-modified monomers was increased. The PNA/DNA hetero-duplexes with aeg or gamma PNA, adopted a right-handed helical structure, which suggests that the conformation of the hetero-duplexes is governed by the DNA component, which is in agreement with previous published reports.[8-9]

CD experiments confirmed that a right-handed helical structure is formed in the presence of a γ-modified PNA oligomer (Figure III.6). The intensity of the CD signal increased with the increasing number of the γ-modification in a hybridized duplex. The most significant change occurred in the 200-230 nm regions for stitched PNA/PNA homo-duplexes, with an increase in the amplitude of the 210 band which is corresponding to the n-π* transition of the amides in the backbone.[8] The increase in CD signal in the spectrum could be attributed to the variation in the backbone conformation, reflecting the helical twist of the oligomers. As the number of the modified backbone units and the paired bases increase, the helical twist of the oligomer becomes more prominent. CD experiments proved that each complementary half of the PNA or DNA templates, PNA3 or γPNA4**,** fully hybridized with template strands when they existed in the same solution. $PNA1_{C\text{-}Lys}$ and $PNA3_{C\text{-}Lys}$ as well as $PNA1_{C\text{-}Lys}$ and $PNA3_{N\text{-}Lys}$ formed left-handed helices, which is due to the chiral induction effect of L-Lys.[12] $PNA1_{C\text{-}Lys}$ and $\gamma PNA3_{C\text{-}Lys}$

as well as PNA1$_{C\text{-}Lys}$ and γPNA4$_{C\text{-}Lys}$ formed right-handed helices due to presence of γ-modified monomers in PNA3 and PNA4.

III.3.3. Stitching Studies Using Pyrene-Modified Monomers

Two possible pathways can be used to incorporate pyrene in PNA oligomers. In one approach, 1-pyrene acetic acid, which is commercially available, can be attached to the side chain of a lysine incorporated in PNA during the solid phase synthesis of the PNA oligomer. In another approach, a pyrene-containing PNA monomer can be prepared in the reaction between aminoethyl-glycine and 1-pyrene acetic acid in solution. From a synthetic point of view the first method is preferable because the purification of the product PNA is simple. The caveat is that the flexibility of the Lysine side chain could diminish the formation of a pyrene pair and the observation of an excimer. Consequently, we synthesized a 9-mer peptide that included two adjacent pyrenes on lysine side chains (Figure III.8). The peptide also contained an AIB amino acid, which can increase the solubility of peptides[13] to compensate for the possible decrease in solubility due to the presence in the same peptide of two hydrophobic pyrenes. A strong pyrene excimer emission at ~480 nm and weaker monomer emission at ~400 nm have been observed following excitation at 345 nm (Figure III.10 (c)). This result confirmed that the pyrene excimer can form despite the flexibility of the alkane side chain of the lysine. Therefore, pyrenes were inserted in PNA strands on the lysine side chain.

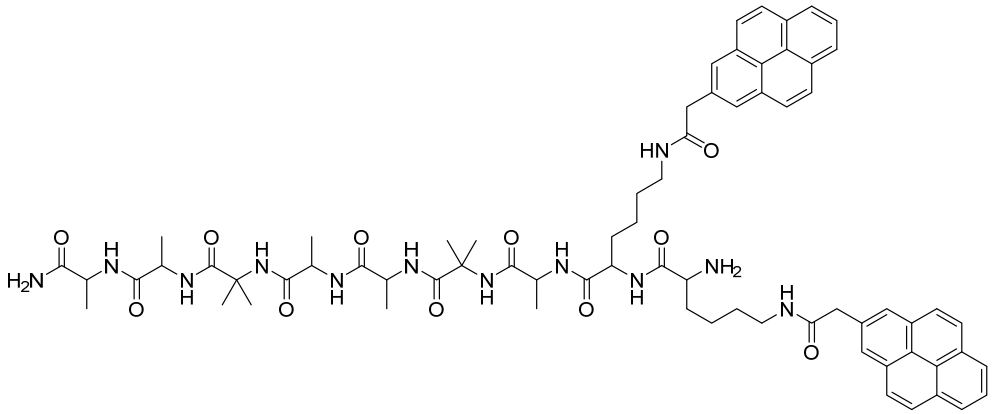

Figure III.8 9-mer peptide containing two adjacent pyrenes

The concomitant hybridization of the 10-base PNA oligomers on the 20-base nucleic acid template was evaluated using the fact that pyrene dimers form a characteristic excimer. For this study, I synthesized a non-modified 20-base PNA with a C-end pyrene modification ($PNA1_{C\text{-}Lys(pyr)}$) and four pyrene-containing 10-bp PNA oligomers $PNA3_{C\text{-}Lys(pyr)}$, $PNA3_{N\text{-}Lys(pyr)}$, $\gamma PNA4_{N\text{-}Lys(pyr)}$, $PNA4_{C\text{-}Lys(pyr)}$. A γ-modified version of one of these 10-base oligomers ($\gamma PNA4_{C\text{-}Lys}$) was also prepared. The sequences of these PNAs are listed in Table III.2.

The relative position of the pyrenes in the 20-bp duplexes is shown in Figure III.9. In case A, two adjacent pyrene are situated in the middle of the duplex, each on one of the two 10-base PNA oligomers, and form a central dimer of pyrenes; in cases B and C, pairs of adjacent pyrenes are terminal, from pyrenes situated in complementary positions on the 20-base template and one of the two 10-base oligomers. For the 20-bp PNA duplexes that contain terminal pyrene pairs (B and C in Figure III.9), we have measured the fluorescence of solutions containing the three ss PNAs, PNA1, PNA3 and PNA4, after they were slowly annealed from 90 ^{o}C to 20 ^{o}C (Sample 1). In the second set of fluorescence experiments, we first annealed solutions comprising a 20-base strand and only one 10-base PNA strand, i.e. samples B2 and C2 made of PNA1 and PNA3 and of

B3 and C3 made of PNA1 and PNA4. The goal was to use the relative intensity of the monomer and excimer of pyrene PL_{400}/PL_{480} ratio to verify the hybridization of PNA3 and PNA4 to PNA1.

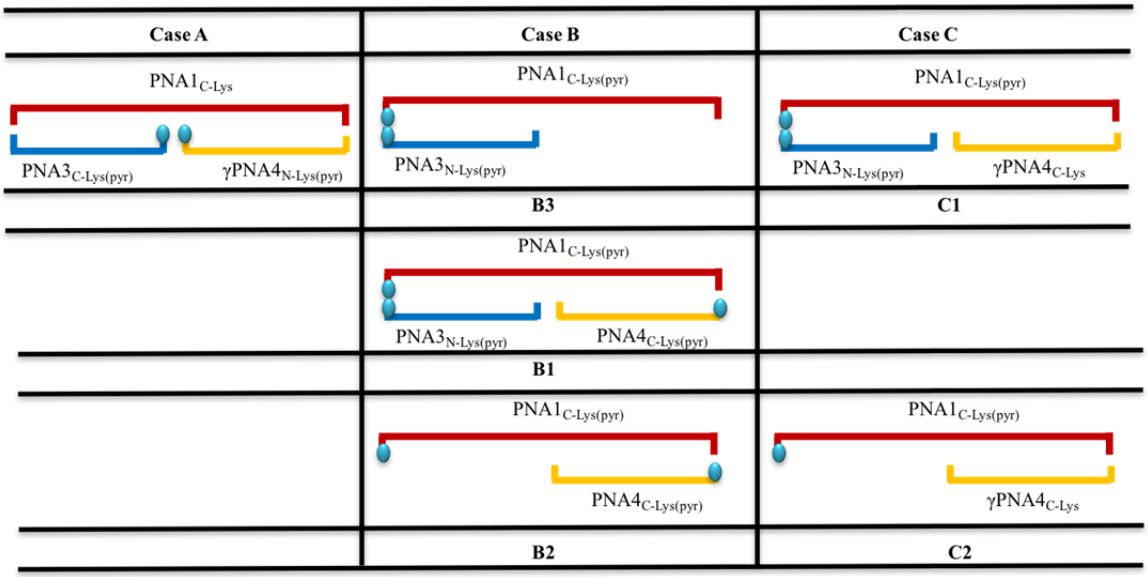

Figure III.9 Cases A-C of pyrene modified stitched duplexes

Table III.4 Summary of T_m, ratio of the photoluminescence at 400 nm (monomer) to the photoluminescence at 480 nm (excimer), and helical sense for Cases B and C. (PL_{400}/PL_{480} and T_m are averages of at least 2 measurements)

Sample	Duplex ID	PL_{400}/PL_{480}	M/E[&]	T_m	Helical Sense
B1	$PNA1_{C\text{-}Lys(pyr)}/PNA3_{C\text{-}Lys(pyr)}/PNA4_{N\text{-}Lys(pyr)}$	0.64	1/1	71	R
B2	$PNA1_{C\text{-}Lys(pyr)}/PNA4_{N\text{-}Lys(pyr)}$	142.8	2/0	69	R
B3*	$PNA1_{C\text{-}Lys(pyr)}/PNA3_{C\text{-}Lys(pyr)}$	1.72	0/1	75	R
C1	$PNA1_{C\text{-}Lys(pyr)}/PNA3_{C\text{-}Lys(pyr)}/\gamma PNA4_{C\text{-}Lys}$	0.55	0/1	70	R
C2	$PNA1_{C\text{-}Lys(pyr)}/\gamma PNA4_{C\text{-}Lys}$	45.7	1/0	65	R

*B3 = C3
[&]M/E: Monomer / Excimer

The duplex formed in case A showed a sigmoidal melting curve with a melting temperature T_m= 77 ^oC (Figure III.10), which is slightly higher than that of the duplex with the same sequence that didn't contain pyrene. This difference suggests that the

pyrene acts as overhang exerts a stabilization effect. Excitation at 345 nm of the duplex $PNA1_{C\text{-}Lys}/PNA3_{C\text{-}Lys(pyr)}/\gamma PNA4_{N\text{-}Lys(pyr)}$ (Case A) led to no excimer emission at 480 nm (Figure III.10 (c)). This observation may be due to either a steric constraint that prevents the formation of a pi-staked pair by the pyrenes or to a quenching effect exerted by the nucleobase situated near the two pyrenes, possibly the thymine.[14]

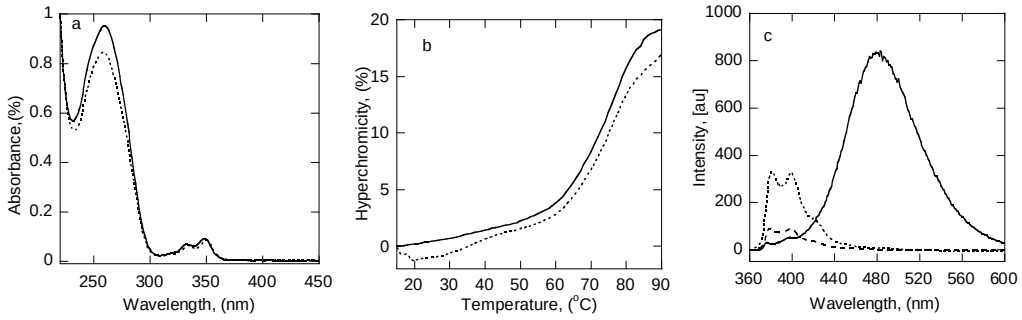

Figure III.10 Absorption spectra and melting curve for a 3 μM solution of $PNA1_{C\text{-}Lys}/PNA3_{C\text{-}Lys(pyr)}/\gamma PNA4_{N\text{-}Lys(pyr)}$ prepared in 10 mM NaPi. (a)UV-absorbance at 90 and 15 °C (solid line and dotted line, respectively) and (b) UV-absorption profile at 260 nm for both the heating and cooling (solid line and dotted line, respectively) (c) OD-corrected fluorescence spectra for solutions that contained 9 mer peptide (solid line); $PNA1_{C\text{-}Lys/}PNA3_{C\text{-}Lys(pyr)}/\gamma PNA43_{N\text{-}Lys(pyr)}$ (dotted line); single strand $PNA3_{C\text{-}Lys(pyr)}$ (dashed line).

Figure III.11 and Figure III.12 show UV-melting profiles, CD spectra and OD-corrected fluorescence spectra of the 20-mer PNA duplexes that contain terminal pairs of pyrenes, Cases B and C in Figure III.9 show the PL_{400}/PL_{480} ratio, melting temperature and handedness of the three samples for Cases B and C.

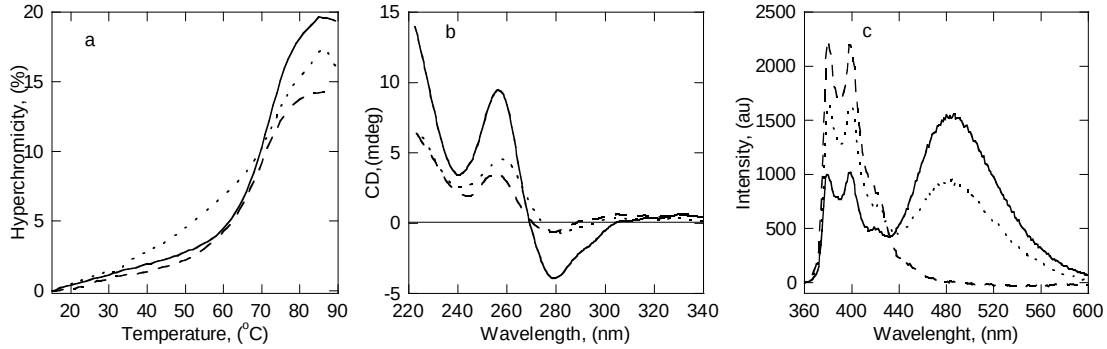

Figure III.11 (a) UV-melting profile, (b) CD spectra, and (c) OD corrected fluorescence spectra for solutions that contain three PNAs, specifically $PNA1_{C\text{-}Lys(pyr)}$/$PNA4_{N\text{-}Lys(pyr)}$/$PNA3_{C\text{-}Lys(pyr)}$, solid lines or two PNAs, specifically $PNA1_{C\text{-}Lys(pyr)}$/$PNA4_{N\text{-}Lys(pyr)}$ dashed lines and $PNA1_{C\text{-}Lys(pyr)}$/$PNA3_{C\text{-}Lys(pyr)}$, dotted lines. 3 μM strand concentration were prepared in 10 mM NaPi.

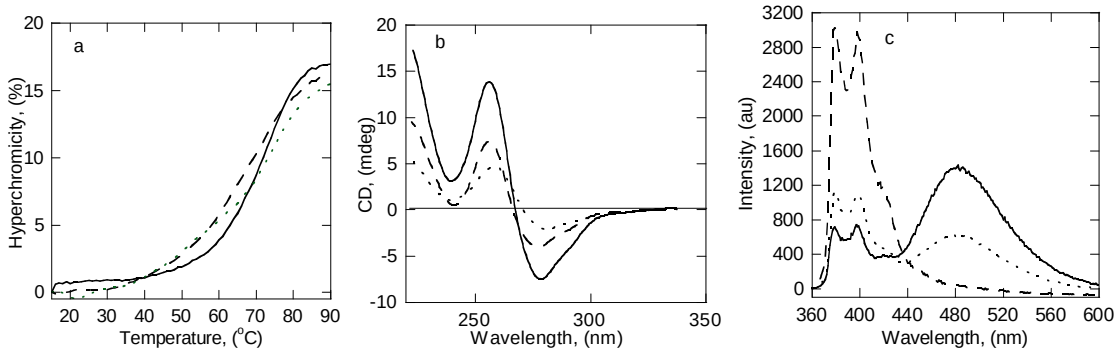

Figure III.12 3 μM strand concentration were prepared in 10 mM NaPi Fluorescence results for two experiments involving the stitched pyrene modified PNA homo-duplexes. The curves for solutions that contain three PNAs are represented by solid lines; The curves for $PNA1_{C\text{-}Lys(pyr)}$/γ$PNA4_{C\text{-}Lys}$ are shown by dashed lines. The curves for $PNA1_{C\text{-}Lys(pyr)}$/ $PNA3_{C\text{-}Lys(pyr)}$ are shown as dotted lines.

Based on the number of pairs of adjacent pyrenes and of isolated pyrenes in the duplexes, one would expect that (i) the PL_{400}/PL_{480} decreases in the order B2>B1>B3, C2>C1~C3, and possibly (ii) the PL_{400}/PL_{480} for B3 and C1 are similar.

The experimental results show that:

- ✓ B2 and C2 show only monomer emission; they have the largest PL_{400}/PL_{480}.

- ✓ The duplexes B1, C1 and B3, which are expected to contain a pair of pyrenes situated in complementary positions, specifically at the N-end of the 10-base PNA3 and C-end of 20-base PNA1 template, have relatively low PL_{400}/PL_{480} values.
- ✓ In the latter category, the duplexes that also contain the 10-base PNA4, B1 and C1, have the lower PL_{400}/PL_{480} values than that which does not, B3. This result could be rationalized if when PNA3 is hybridized to PNA1 but PNA4 is not, the single stranded portion of PNA1 could bend back and make possible partial quenching of the excimer emission of the pair of the pyrenes in complementary positions on PNA1 and PNA3.

These results support the idea that a 20-base pair duplex of two, stitched 10-base pair duplexes and that the properties of each 10 base half vary as a function of the presence or absence of the single stranded PNA on the opposite half.

The effect of the pyrene on the PNAs thermal stability depends on its position in the duplexes. Incorporation of pyrene at the end of the stitched PNA duplexes (PNA1/PNA3/PNA4) did not affect the melting temperature of the duplexes ($\Delta T_m < 71$ ^oC) (Case B and Case C in Figure III.9), in contrast to previous observation of an increase in the thermal stability by overhang pyrenes,[8, 14a] This difference may be due to the compensation of a potential increase in stabilization by the pyrene by a destabilization due to stitching. The melting temperature of the duplex that contained two pyrenes in the center of the stitched duplex (Case A in Figure III.9) was greater by $\Delta T_m \sim 5\text{-}6$ ^oC than that that if duplexes that contained the pyrenes at terminal positions or stitched PNAs with gamma modifications.

We examined the fluorescence properties of PNA duplexes that contained either centrally or terminal pyrene. In these duplexes, the pyrene environment is different. We can rationalize the differences between the fluorescence properties of internally- and terminally-pyrene-modified duplexes by the different environments in which the pyrene resides.[15], [16] Oxidative electron transfer from guanine makes this base the strongest quencher while cytosine, and to a lesser degree, thymine are moderately strong quenchers via reductive electron transfer to the nucleobase.[17] Adenine is a weak quencher.

Our results could be further investigated and explained by MD simulations. We could also measure the fluorescence of an internally labelled duplex as in Case A eliminating the adenines nearby the pyrenes to reduce the steric clash. This way we could know better quenching effect caused by the thymines.

III.3.4. Characterization of Self Assembled Monolayers (SAM)

Gold surfaces coated with self-assembled monolayers (SAMs) with attached dsPNA were characterized by two commonly used technique: ellipsometry and PM-IRRAS.

Ellipsometry

Ellipsometry was utilized to determine the film thickness. The ellipsometric thickness of the stitched dsPNA ($PNA1_{N\text{-}Cya/}$ $\gamma PNA3_{C\text{-}Lys}/\gamma PNA4_{C\text{-}Lys}$) SAMS on Au surface was 34.75 Å and 46.96 Å after incubation for 1.5 h and 60 h, respectively The calculated length of dsPNA was 68 Å (20x3.4 Å); the length of the base pair rise has been estimated by adding 3.4 Å for the base pairs[18] in the duplex. The difference between the measured thickness of the SAM and the calculated length of a dsPNA may be due to the

tilting of the molecules with respect to the surface normal similar to the coexistence of a mixture of "standing-up" and "lying-down" molecules as shown by Paul.[18] The "standing-up" molecules were taken as perpendicular to the surface, and the "lying-down" molecules were assumed to be parallel to the Au surface. The average thickness was calculated by means of a weighted sum of the thicknesses for the "lying-down" and the "standing-up" molecules. The percentage of each phase was determined by equating the ellipsometric thickness to the average thickness. The percentage of the "lying-down" phase was found to be 69.2% and 43.9% after incubation for 1.5 h and 60 h, respectively.

Atomic force microscopy could be also used to determine the thickness of SAMs formed. This way we could compare the results obtained by AFM and ellipsometry for characterization of SAMs.

PM-IRRAS

Polarization modulation infrared reflection absorption spectroscopy (PM-IRRAS) was used to investigate the quality of the SAMs and their packing (Figure III.13). In order to record a PM-IRRAS spectrum of a molecule, the dipole transition moment of the absorbed molecules must have a component orientated along the surface normal to absorb the IR incident radiation. PM-IRRAS has been used to characterize the molecules' orientation on surfaces since, only the parallel component of the incident radiation is adsorbed by the adsorbed molecules on the metal substrate due to the surface selection rule and the absorption of the parallel component of the incident radiation is directly proportional to the film thickness when the film is thin enough (<10nm). [19]

PM-IRRAS spectra of SAMs composed of stitched PNA homo-duplexes $PNA1_{N\text{-}Cya}/\gamma PNA3_{C\text{-}Lys}/\gamma PNA4_{C\text{-}Lys}$ and $PNA4_{(C\text{-}SH)+(N\text{-}Ac)}/PNA1_{(C\text{-}Lys)}/\gamma PNA3_{(C\text{-}Lys)+(N\text{-}Dap(Fc)}$ on Au are given in Figure III.13.

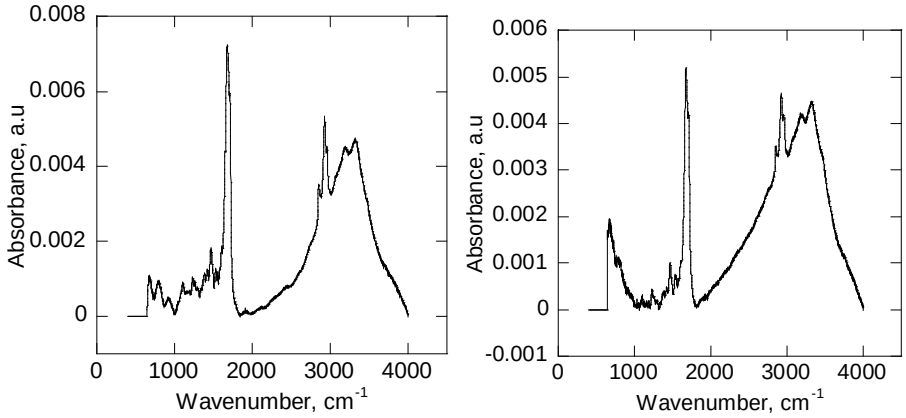

Figure III.13 PM-IRRAS spectra of (a) $PNA1_{N\text{-}Cya}/\gamma PNA3_{C\text{-}Lys}/\gamma PNA4_{C\text{-}Lys}$ monolayers on Au (b) $PNA4_{(C\text{-}SH)+(N\text{-}Ac)}/PNA1_{(C\text{-}Lys)}/\gamma PNA3_{(C\text{-}Lys)+(N\text{-}Dap(Fc)}$ PNA-Fc monolayer on Au. The carbonyl stretching bands at 1750 to 1540 cm^{-1} includes bands characteristic for pure T and G- 1716, pure C -1648, pure A-1639. Absence of S-H at 2550 cm^{-1}**.**

Table III.5 Wavenumbers and spectral assignments of selected IR bands in nucleic acids

Assignment	**Stretching/In Plane Vibrations**	**Wavenumber, cm^{-1}**
CH_2	asymmetric	2931-2928
	symmetric	2864-2852
(C=O) -thymine & guanine	bending	1716
(C=O) -cytosine	bending	1648
(C=O) -adenine	bending	1639
C-C& C=N adenine & cytosine	in plane	1550
(C=O) Amide I	symmetric	1650
(N-H) Amide II	symmetric	1540

Wavenumbers and spectral assignments of selected IR bands in nucleic acids are given in Table III.5. The region from 3000 to 2830 cm^{-1} corresponds to CH_2 asymmetric and symmetric stretching modes. The CH_2 groups are present in the molecular backbone of the PNA and in the spacer group. The appearance of both asymmetric and symmetric

stretching in our spectra, at 2931-2928 and 2864-2852 cm^{-1}, respectively, means that the chain is oriented with respect to the surface in such a way that allows both vibrations to be dipole active.

The region from 1750 to 1540 cm^{-1} is mainly dominated by the infrared features of the nucleobases. [20] The presence of these bands in our spectra means that it is possible to distinguish the in-plane ring vibrations, which could suggest that not all the nucleic bases that protrude from the PNA backbone lie parallel to the surface.[21] Other vibrations that appear in the same region are related to amide group: Amide I and Amide II. Frequencies of amide vibrations are difficult to identify because they are mixed with the nucleic base absorptions and present very low intensity.

It is well-known that the strong S-Au interactions are promoted by the SH group,[22] so that the lack of S-H feature at 2550 cm^{-1} in the spectra indicates that the sulfur atom is the anchoring point for the formation of PNA-SAMs.[23]

III.3.5. Spin Filter Measurements

Magnetoresistance Measurements with a Solid State Device

Magnetoresistance was measured with a solid state device as described by Mondal et al. (Figure III.14a).[4, 24] When there is no external magnetic field, the domains in the nickel are oriented mostly in plane such that the net magnetization is zero and the spin polarized electrons injected by the chiral film into Ni get scattered from the differently oriented domains. Therefore, the resistance of the device at zero field is the same independent on the magnitude and sign of the field before it was nulled. This feature confirms the strong in-plane magnetic anisotropy of the Ni film. The density of states for a specific spin in the Ni, near the Fermi level, depends on the sign of the applied

magnetic field. Therefore, the device shows either higher or lower magnetoresistance depending on the direction of the field. When the external magnetic field is tuned up from zero, more domains in the Ni are magnetized in the field direction and hence the magnetoresistance either increases or decreases depending on the spin alignment of the electrons conducted (namely, depending on the handedness of the chiral medium) and on the direction of the external field.[4, 24]

MR device is made with SAM composed of a thin gold film (120 nm thickness) on top of which a stitched PNA duplex ($PNA1_{(C\text{-}Lys)}$/γ$PNA3_{(C\text{-}Lys)}$/$PNA4_{(C\text{-}SH)+(N\text{-}Ac)}$) was absorbed by dipping. An Al_2O_3 film of 2 nm thickness is grown on top of the SAM by atomic layer deposition (ALD) to act as an efficient tunnel barrier for the spin injection.[25] A 120 nm Ni layer was deposited on the Al_2O_3 layer in order to analyze the spin injection efficiency. The magnetoresistance (MR) of the device was measured as a function of an external magnetic field, when the field was applied parallel to the current through the PNA film (perpendicular to the Ni film/sample plane). The MR is reported as a percentage; namely, MR 1⁄4 [R(H)-R(H 1⁄4 0)]/R(H 1⁄4 0) 100%, where R(H) is the measured in-field resistance and R(H 1⁄4 0) is the zero-field resistance.

The chiral SAM/Al_2O_3 tunneling barrier polarizes the spin distribution of transmitted electrons and it is probed by magnetic field dependence of the resistivity through the Ni layer.

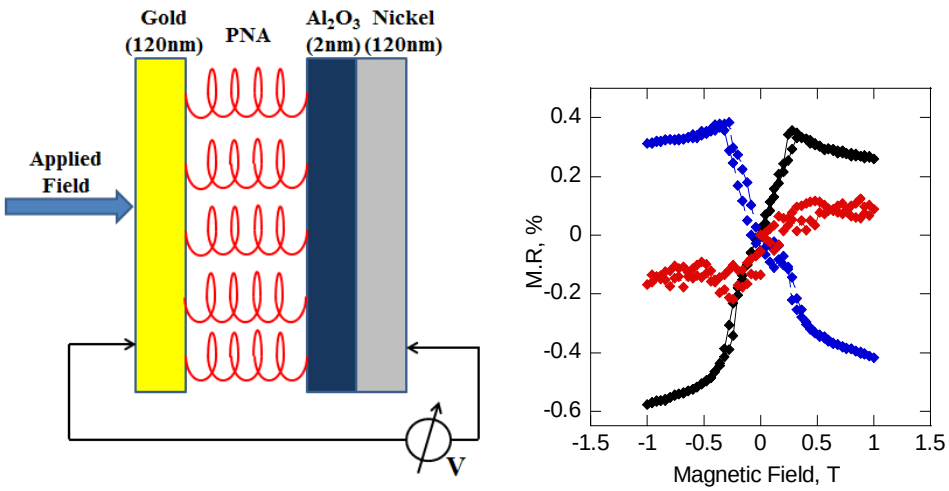

(a) (b)

Figure III.14 (a) Schematic representation of Au/SAM/Al_2O_3/Ni device. 2-nm-thick chiral Al_2O_3 deposited on top of SAM of peptide nucleic acids on a gold surface (b) MR, % was measured at 300^o K. Red diamond curve: Blank; black and blue diamond curves have been measured for two different samples prepared in the same way. The blank was a device having structure Au/Al_2O_3/Ni, which is the same as that with PNA samples but without the PNA monolayer.

Two devices that contained SAMs of PNA and were built in the same way showed opposite sign of the magnetoresistance suggesting that they have different chirality in the device (Figure III.14b). One possible explanation for this surprising finding is related to the fact that the SAM of PNA is subject to high temperature during the building of the device. Next, we provide details of the device construction pertinent to this issue.

One of the main problems in building vertical devices using SAMs was the possibility of pinholes: the top electrode might penetrate the organic layer through these gaps and create shorts. The electron conduction would then happen preferentially through these pathways instead of the organic molecules. To prevent this, the most common technique is to evaporate a thin insulating layer on top of the monolayer to close the pinholes. This strategy was used in our experiments using Al_2O_3, since the possibility of

using (ALD) for its deposition is well known and very reliable. Unfortunately, the ALD deposition of Al_2O_3 revealed itself as the crucial point of the device fabrication: the PNA monolayer could not withstand the high temperature necessary to form a continuous 2nm thick layer of the oxide. Deposition technique was adjusted, going for e-beam evaporation to try to circumvent the temperature problem, but a good electrical insulating layer could not be obtained due to the relatively high roughness of the oxide layers produced with this strategy. To solve this problem, material will be changed and a thin layer of MgO will be evaporated. In our preliminary experiments, it was seen that the e-beam evaporation of MgO gave a smooth, continuous film, even for small thicknesses. This might allow us to solve the problem of pinholes while avoiding the PNA monolayer denaturation..

Mott Polarimeter Measurements

A compact, conventional Mott-type electron polarimeter was used to determine the spin polarization of the photoelectrons at room temperature. Self-assembled dsPNA ($PNA1_{C\text{-}Lys}/PNA3_{N\text{-}Lys}/PNA4_{C\text{-}SH+N\text{-}Ac}$) and dsγPNA ($PNA1_{C\text{-}Lys}/\gamma PNA3_{N\text{-}Lys}/PNA4_{C\text{-}SH+N\text{-}Ac}$) monolayers were prepared according to standard procedures by depositing dsPNA or dsγPNA, which was thiolated on the C-end of one of the PNA strands on a clean gold substrate (Si/Titanium 8 nm/Gold 120 nm).

The histograms Figure III.15 and Figure III.16 show the number of measurements for which a specific spin polarization value was obtained for ds-γPNA and ds-aeg-PNA. Each figure show two separate measurement performed on the same sample (left and right halves) for repeatability. The distribution width is due to the statistical nature of the scattering process and depends on e.g. the integration time per measurement.

Measurements were done alternately on the actual sample and a reference sample, which consisted of either molybdenum or polycrystalline gold. Molybdenum does not emit spin-polarized photoelectrons, independent of the polarization of the incident laser light. Therefore, this distribution defines the point of zero spin polarization. When a polyAu reference was used, the lower plot was again separated into the different polarizations and the linear polarization served as a reference as shown in the lower half of the plots in Figure III.15 and Figure III.16.

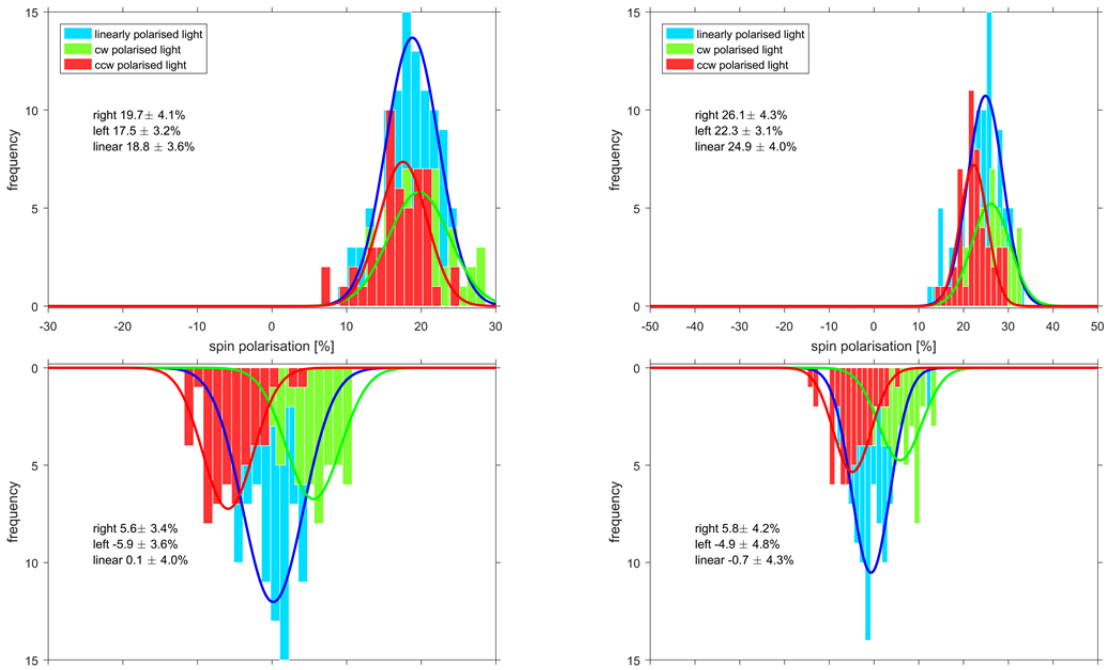

Figure III.15 The photoelectron polarization as measured for electrons ejected from poly(Au)-coated substrate with a monolayer of ds-γPNA duplex $PNA1_{C\text{-}Lys}$/$\gamma PNA3_{N\text{-}Lys}$/$PNA4_{C\text{-}SH+N\text{-}Ac}$/poly-Au. For the cw polarized light, the electron polarization is (26.1±4.3)(green); for the linearly polarized light, the electron polarization is (24.9±4.0) (blue); for the ccw polarized light, the electron polarization is (22.3±3.1)(red).

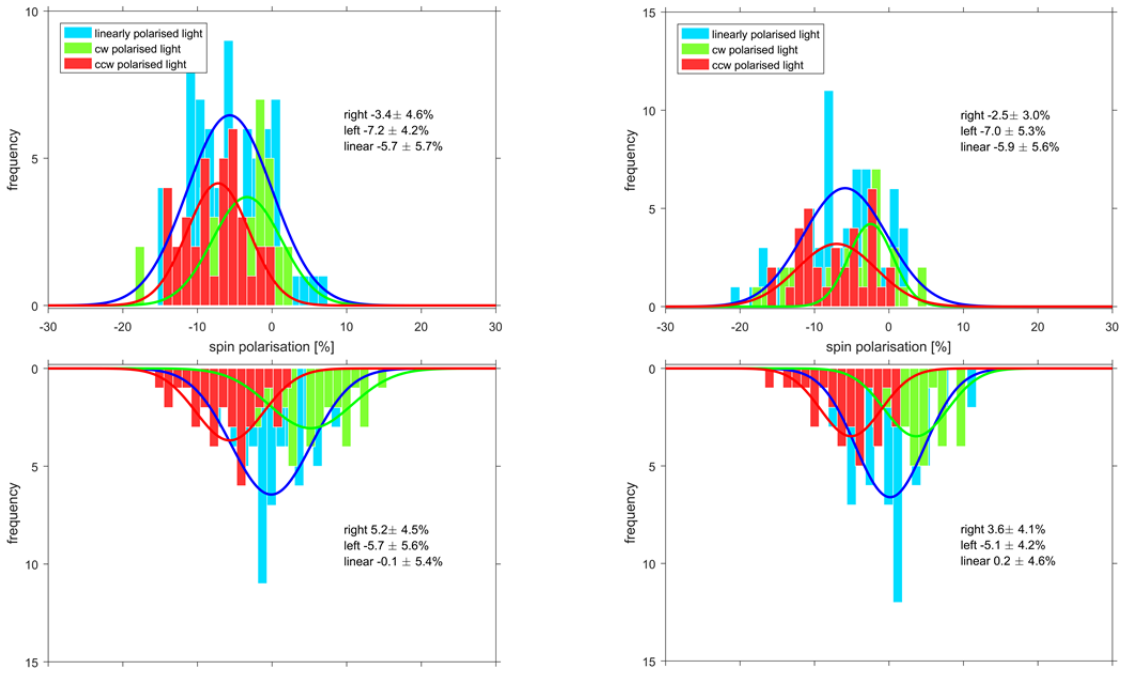

Figure III.16 The photoelectron polarization as measured for electrons ejected from poly(Au)-coated substrate with a monolayer of ds-aeg-PNA duplex $PNA1_{C\text{-}Lys}/PNA3_{N\text{-}Lys}/PNA4_{C\text{-}SH+N\text{-}Ac}$/poly-Au. For the cw polarized light, the electron polarization is (-3.4±4.6) (green); for the linearly polarized light, the electron polarization is (-5.7±3.6) (blue); for the ccw polarized light, the electron polarization is (-7.2±4.2)(red).

The spin polarizations of the electrons from the same Au(111) single crystal, emitted through a self-assembled monolayer of 20-bp modified and non-modified PNA duplexes, were measured for excitation with clockwise (cw) and counterclockwise (ccw) circularly polarized light, and linearly polarized light. Spin polarized electrons with average polarizations of (26.1±4.3); (22.3±3.1) and (24.9±4.0), respectively, were observed for dsγPNA ($PNA1_{C\text{-}Lys}/\gamma PNA3_{N\text{-}Lys}/PNA4_{C\text{-}SH+N\text{-}Ac}$). Spin polarized electrons with average polarizations of (-3.4±4.6); (-7.2±4.2) and (-5.7±3.6)), respectively, were observed for dsPNA ($PNA1_{C\text{-}Lys}/PNA3_{N\text{-}Lys}/PNA4_{C\text{-}SH+N\text{-}Ac}$).

The opposite sign of polarization for ds-γPNA and dsPNA is attributed to the different handedness of the two duplexes. Indeed, CD spectra of the γPNA duplexes show

that it adopts a right-handed helical structure, while non-modified PNA adopts a left-handed helical structure (Figure III.17). We note that there is an apparent correlation between the degree of spin polarization of the PNA and the CD intensity of the duplexes but based on the current level of experimentation and theory, we cannot argue that this is not a fortuitous coincidence.

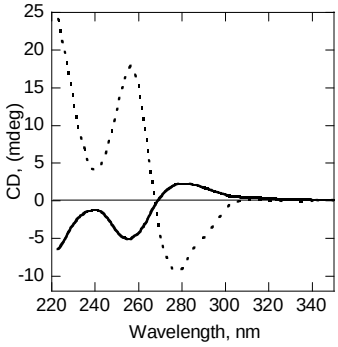

Figure III.17 CD spectra of $PNA1_{C\text{-}Lys}/PNA3_{N\text{-}Lys}/PNA4_{C\text{-}Lys}$ (solid line), $PNA1_{C\text{-}Lys}/\gamma PNA3_{N\text{-}Lys}/PNA4_{C\text{-}SH+N\text{-}Ac}$ (dotted line).

III.4. Conclusions

20-base pair homo-PNA/PNA and hetero-PNA/DNA duplexes could be formed by the hybridization of 10-bp strands onto PNA and DNA template. However, thermal stability of stitched PNA duplexes was found to be lower than ones did not have a nick. Insertion of pyrene in the center of a duplex is increased the $T_{m,}$ whereas insertion of pyrene at the terminals did not make a difference on the T_m. Tm of the duplexes containing only a 20 base template and a 10 base strand could not be determined since a valid denaturation profile could not be obtained. The stitched homo-γPNA/PNA and pyrene-PNA duplexes adopted a right-handed structure.

The intensity of the CD signals of stitched homo-duplexes containing only one 10-bp γPNA was lower when compared to that of the stitched, 20-bp γPNAs duplexes. It

was seen that as the number of the modified backbone units and the paired bases increase, the helical twist of the oligomer became more pronounced. Fluorescence of pyrene fluorophore was found to be strongly correlated to the environment as in described in the literature.[15] Fluorescence experiments with pyrene-containing PNAs supported the successful formation of stitched PNA duplexes. The flexibility of the PNA strand allowed the unfolded portion of PNA strand to bend back and partially quenched the excimer emission of the pyrenes or energy transfer from the monomer on PNA4 to the excimer on PNA1 and PNA3.

For spin polarization measurements samples were designed such that spin polarization could only be measured if the both two 10 base single strands are fully hybridized with the template strand. One of the 10 base strands had gamma modification (γPNA3) allowing the spin polarization to be spin selective and the other 10 base strand ($PNA4_{C\text{-}SH+N\text{-}Ac}$) had the thiol modification to ensure PNAs are attached on the gold monolayer. The room-temperature spin polarizations of SAMs made of stitched γ-modified and non-modified PNA duplexes were approximately +20% and -5%, respectively. The promising spin polarization of γ-PNAs establishes the prospect of using PNA as a room temperature spin filter. Previously, spin polarizations of -35% was reported for 50-bp dsDNA.[5] Currently, spin polarization of duplexes made of two gamma modified 10 base strands with thiol modified 20 base template strand and spin polarization of stitched hetero-PNA/DNA duplexes are under investigation.

III.5. Materials and Methods

DNA was obtained from IDT. Boc/Z and Fmoc/Bhoc PNA monomers were purchased from PolyOrg Inc. and ASM Research Chemicals and used without further

purification. The Boc-protected γ-PNA monomers were synthesized according to slightly changed published procedures (as described in Chapter II). The oligomers were synthesized on MBHA resin. Upon completion of the last monomer coupling, the oligomers were cleaved from the resin (and the protecting groups were simultaneously removed) by immersing the resin in a cocktail containing m-cresol/thioanisole/TFA/TFMSA (150/150/900/300 μL for 100 mg of resin) for 2 h. The crude mixture was eluted and precipitated in ethyl ether, dissolved in water, purified by reversed-phase HPLC using a C18 silica column on a Waters 600 Controller and Pump. Absorbance was measured with a Waters 2996 Photodiode Array Detector. Oligomers were characterized by MALDI-TOF on an Applied Biosystems Voyager Biospectrometry Workstation using R-cyano-4-hydroxycinnamic acid matrix (10 mg/mL in 1:1 water/acetonitrile, 0.1% TFA). The PNA concentrations were determined by UV-vis spectrophotometry assuming $\varepsilon(260)$ =8600, 6600, 13700, and 11700 cm^{-1} M^{-1} for each T, C, A, and G monomer, respectively.[26] Extinction coefficient calculated for pyrene is $\varepsilon(260)$= 12711 and $\varepsilon(345)$= 28319 cm^{-1} M^{-1} (Figure III.18).

Extinction Coefficient for 1-Pyrene Acetic Acid

In order to calculate the concentrations of pyrene modified PNAs, first, extinction coefficient of pyrene acetic acid was found at 90 ^{o}C. A stock solution of pyrene acetic was prepared in MeOH/ACN (1:1) (10 mg in 10.0 mL, 3.84 mM). This solution was diluted to 1.92 mM mixing 500 μL from stock solution with 250 μL AcCN and 250 μL of MeOH. This solution is used to prepare the final solutions with $9.55x10^{-3}$, $1.33x10^{-2}$, $1.71x10^{-2}$, $2.09x10^{-2}$, $2.46x10^{-2}$, $2.84x10^{-2}$ M concentrations. To obtain these

concentrations, six aliquots from the stock were added to 1000 µL H_2O. Volumes of aliquots from the stock was as followed (1x)5µL and (5x)3 µL.

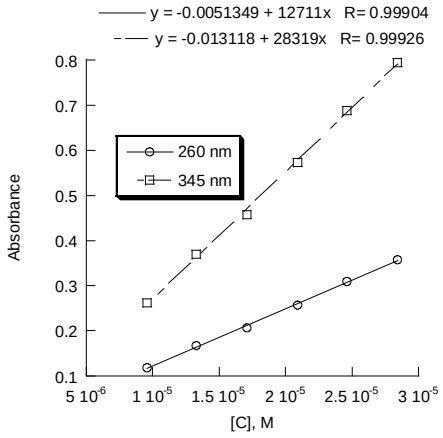

Figure III.18 Linear regression for the evaluation of the extinction coefficient of 1-pyrene acetic acid at 260 nm and 345 nm

Non-Modified, γ- Modified and Ferrocene Modified and Thiol Modified Synthesis

The synthesis of PNA oligomers with C-terminal cysteine, cysteamine and was previously reported.[18, 27] PT containing PNA synthesis was descried in Chapter IV. Briefly, both the non-modified and γ-modified PNA oligomers were synthesized using solid phase peptide synthesis methods with Boc- and Fmoc protection strategies. Ferrocene carboxylic acid (Aldrich) was coupled to the side chain of Dap amino acid similar to insertion of thymidine linker as described in Chapter IV; oligomers were cleaved from the resin using trifluoroacetic acid (TFA) and trifluoromethanesulfonic acid (TFMSA), precipitated in ethyl ether, and dried under nitrogen. Ferrocenecarboxylic acid was purchased from Sigma Aldrich. After cleavage, PNA was precipitated using ethyl ether and was purified by reversed-phase HPLC. PNA oligomers were characterized by MALDI-TOF mass spectrometry. The observed mass of each synthesized PNA agreed

well with the expected mass (Table III.6). PNA solutions were prepared in deionized water, and the PNA concentrations were determined by UV-vis spectrophotometry.

C-End Pyrene Containing Oligomers

To insert the pyrene-lysine moiety on the C end of a PNA as in the case of $PNA1_{C\text{-}Lys(pyr)}$ and $PNA4_{C\text{-}Lys(pyr)}$, Fmoc and Boc strategy used together. MBHA resin was downloaded with Boc-Lys(2-Cl-Z)-OH. Next, Boc group on the Lysine was deprotected by 95% TFA:m-Cresol and coupled with Fmoc-Lys(Boc)-OH. Boc group on the side chain of the lysine was also deprotected by 95% TFA:m-Cresol. Next, side chain of the lysine containing free amine group was coupled with pyrene acetic acid in the presence of HBTU and DIPEA. After capping with 5% acetic anhydride and 6% Lutidine in DMF, Fmoc group from the N-terminus of the lysine was deprotected using 20% Piperidne/DMF. After, introducing the first PNA monomer, for the rest of the steps only Boc-strategy was used. Upon completion of the last monomer coupling, the oligomers were cleaved from the resin (and the protecting groups were simultaneously removed) by immersing the resin in a cocktail containing m-cresol/thioanisole/TFA/TFMSA (150/150/900/300 μL for 100 mg of resin) for 2 h. The crude was purified by reversed-phase HPLC. Fractions collected were characterized by MALDI/TOF mass spectrometry. The observed mass of each synthesized PNA agreed well with the expected mass (Table III.6)

N-End Pyrene Containing Oligomers

We introduced pyrene-lysine on the N end of the $PNA3_{N\text{-}Lys(pyr)}$. In order to make $PNA3_{N\text{-}Lys(pyr)}$, we have started with A monomer downloaded resin and introduced all 10 monomers using Boc- chemistry. After addition of last monomer C, Fmoc-Lys(Boc)-OH

was introduced. First, Boc- on the Lysine side chain was deprotected by 95% TFA:m-Cresol which is followed by coupling of the free amino group with pyrene acetic acid in the presence of HBTU and DIPEA. Next, Fmoc- from the Lysine was deprotected using 20% Piperidne/DMF. After cleavage of the $PNA3_{N\text{-}Lys(pyr)}$ from the resin using the aforementioned cleavage cocktail, crude was purified by reversed-phase analytical HPLC and characterized by MALDI-TOF mass spectrometry. The observed mass of each synthesized PNA agreed well with the expected mass (Table III.6)

Table III.6 Oligomer Sequences and Maldi Data

Oligomer	Oligomer sequence N to C	Cal. MW	Obs. MW
$PNA1_{C\text{-}Lys}$	H-CGT ACA AAC T TAG ACA CCA G Lys_3-NH_2	5783.55	5782.34
$PNA1_{N\text{-}Cys}$	H-Cys-CGT ACA AAC TTA GAC ACC AG Lys_3-NH_2	5886.17	5885.12
$PNA1_{N\text{-}Cya}$	HS-CH_2CH_2CO-CGT ACA AAC TTA GAC ACC AG Lys_3-NH_2	5871.15	5871.02
$PNA1_{C\text{-}Lys(pyr)}$	H-Lys Lys CGT ACA AAC T TAG ACA CCA G Lys Lys*(pyr)*NH_2	6154.93	6155.00
$PNA3_{N\text{-}Lys}$	H-Lys-CTG GTG TCT A-NH_2	2861.83	2861.13
$\gamma PNA3_{N\text{-}Dap(Fc)}$	Fc(Dap)-CTG GTG TCT A-Lys-NH_2	3250.87	3251.46
$\gamma PNA3_{C\text{-}Lys}$	H-CTG GTG TCT A-Lys-NH_2	2951.93	2951.66
$PNA3_{C\text{-}Lys(pyr)}$	H-Lys CTG GTG TCT A Lys(*pyr*)-NH_2	3233.29	3233.74
$PNA3_{N\text{-}Lys(pyr)}$	H-LysLys(*pyr*)CTG GTG TCT A NH_2	3233.29	3233.14
$\gamma PNA4_{N\text{-}Lys(pyr)}$	H-(*pyr*)Lys AGT TTG TAC G Lys-NH_2	3347.54	3347.98
$PNA4_{C\text{-}Lys(pyr)}$	H-AGT TTG TAC G Lys(*pyr*)LysNH_2	3257.03	3257.15
$\gamma PNA4_{C\text{-}Lys}$	H-AG***T*** TT***G*** TA***C*** G-Lys-NH_2	2975.85	2976.64
$PNA4_{C\text{-}SH+N\text{-}Ac}$	Ac-AGT TTG TAC G-$(CH_2)_3$SH	2874.67	2875.25

* Pyr: Pyrene

Variable Temperature UV Spectroscopy

Melting temperature experiments were performed in 10-mm path length quartz cells on a Varian Cary 300 spectrophotometer equipped with a programmable temperature block. PNA stock solutions were prepared in deionized water and were

stored at -18 °C. The PNA solutions for UV and CD experiments were in pH 7.0 10 mM phosphate buffer. The concentration of these solutions was determined by UV absorption at 95 °C using the sum of the published extinction coefficients at 260 nm; ε_{260} of the constituent PNA monomers were taken to be 8600 M^{-1} cm^{-1} for T, 6600 M^{-1} cm^{-1} for C , 13700 M^{-1} cm^{-1} for A, and 11700 M^{-1} cm^{-1} for G.[26, 28]

UV melting curves were recorded in the temperature range 15°C to 95°C. The rate of both cooling and heating was 1°C/min. Prior to the measurement of the melting profiles, the solutions were kept at 15°C for at least 10 min. The melting temperature T_m was taken at the inflection point of the Boltzmann sigmoidal fit function, which assumes a two-state model.

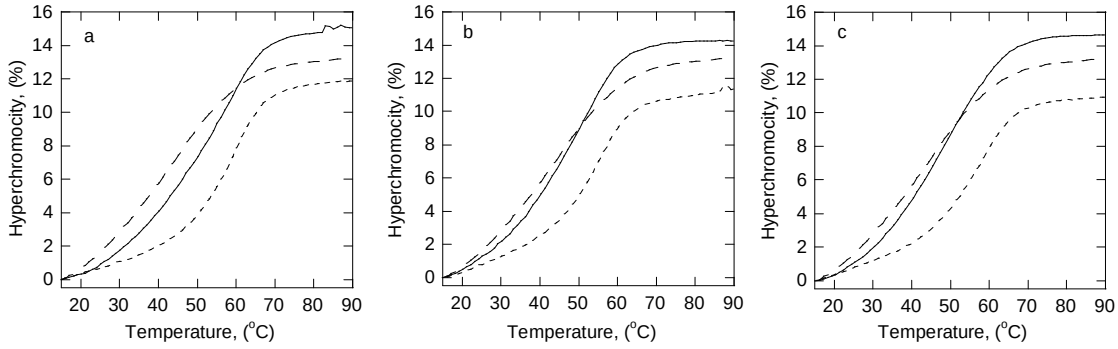

Figure III.19 UV-melting profiles of parallel DNA/PNA hetero-duplexes (a) DNA1/PNA3 $_{C\text{-}Lys}$/γPNA4$_{C\text{-}Lys}$; DNA1/PNA3$_{C\text{-}Lys}$; DNA1/γPNA4$_{C\text{-}Lys}$ (b) DNA1/PNA3$_{N\text{-}Lys}$/γPNA4$_{C\text{-}Lys}$; DNA1/PNA3$_{N\text{-}Lys}$; DNA1/γPNA4$_{C\text{-}Lys}$ (c) DNA1/γPNA3$_{C\text{-}Lys}$/γPNA4$_{C\text{-}Lys}$; DNA1/γPNA3$_{C\text{-}Lys}$; DNA1/γPNA4$_{C\text{-}Lys}$ duplexes. The curves for solutions that contain three PNAs are represented by solid lines; The curves for DNA1- γPNA4$_{C\text{-}Lys}$ are shown by dashed lines. The curves for DNA1/PNA3$_{C\text{-}Lys}$; DNA1/PNA3$_{N\text{-}Lys}$, and DNA1/γPNA3$_{C\text{-}Lys}$ are shown as dotted lines. Samples contained stoichiometric amounts of oligonucleotides at 3 μM strand concentration. Only heating curves are shown.

Table III.7 Summary of Thermal Stabilities for Parallel Stitched DNA/PNA Hetero-duplexes(T_m[^oC])

Hetero- DNA/PNA Duplex	**T_m[^oC] P**
DNA2/PNA1	-
DNA1/PNA3$_{C\text{-}Lys}$/γPNA4$_{C\text{-}Lys}$	50
DNA1/PNA3$_{N\text{-}Lys}$/γPNA4$_{C\text{-}Lys}$	46
DNA1/γPNA3$_{C\text{-}Lys}$/γPNA4$_{C\text{-}Lys}$	46
DNA1/PNA3$_{C\text{-}Lys}$	56
DNA1/PNA3$_{N\text{-}Lys}$	52
DNA1/γPNA3$_{C\text{-}Lys}$	54
DNA1/γPNA4 $_{C\text{-}Lys}$	41

T_m are known within 2 ^oC. T_m were obtained from the curve-fitting data or estimated from the first derivative of the melting curves. The $T_{m's}$ are average of at least two experiments.

We observe a difference between the melting temperature of parallel and antiparallel duplexes of 13-14 ^oC which is in agreement with the previously reported differences of about 13-14 ^oC for 10-bp and 15-bp PNA/DNA heteroduplexes.[9] The T_ms of parallel hetero-duplexes containing overhangs were 2-10 ^oC higher than that of DNA1/PNA3/PNA4, except DNA1/γPNA4 duplex.

CD Spectroscopy

All CD data were recorded at room temperature. All spectra represent an average of at least 10 scans, recorded from 350 to 220 nm at the rate of 50 nm/min. A 1 cm path length cuvette was used, and the temperature was maintained at 20 ^oC. All spectra were processed using KaleidaGraph software, baseline subtracted.

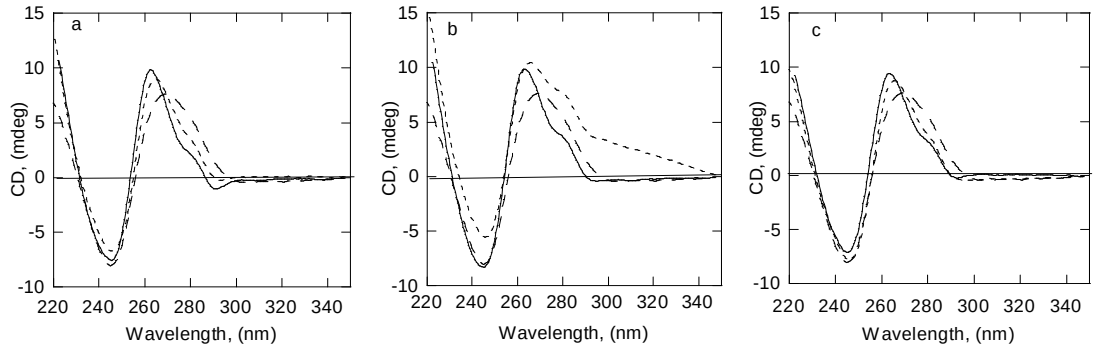

Figure III.20 CD spectra of PNA/DNA parallel hetero-duplexes (a) DNA1/PNA3$_{C\text{-}Lys}$/γPNA4$_{C\text{-}Lys}$; DNA1/PNA3$_{C\text{-}Lys}$; DNA1/γPNA4$_{C\text{-}Lys}$ (b) DNA1/PNA3$_{N\text{-}Lys}$/γPNA4$_{C\text{-}Lys}$; DNA1/PNA3$_{N\text{-}Lys}$; DNA1/γPNA4$_{C\text{-}Lys}$ (c) DNA1/γPNA3$_{C\text{-}Lys}$/γPNA4$_{C\text{-}Lys}$; DNA1/γPNA3$_{C\text{-}Lys}$; DNA1/γPNA4$_{C\text{-}Lys}$ duplexes. The curves for solutions that contain three PNAs are represented by solid lines; The curves for DNA1/γPNA4$_{C\text{-}Lys}$ are shown by dashed lines. The curves for DNA1'/PNA3$_{C\text{-}Lys}$; DNA1/PNA3 $_{N\text{-}Lys}$, and DNA1/γPNA3 $_{C\text{-}Lys}$ are shown as dotted lines. Samples contained stoichiometric amounts of oligonucleotides at 3 μM strand concentration.

The parallel PNA/DNA hetero-duplexes with aeg or gamma PNA adopted a right-handed helical structure.

Fluorescence Spectroscopy

Excitation and emission spectra were obtained using a Cary Eclipse fluorimeter. Emission spectra were recorded with 0.2 ms delay time and 5 ms gate time in the range 360-600 nm with selective irridation at 345 nm (λ_{ex}= 345 nm).

PNA Monolayer Preparation for Characterization

A 20 μM solution of PNA duplex in pH 7.2, 0.4 M potassium phosphate buffer:acetonitrile 1:1 was prepared by mixing the complementary single strand PNA stock solutions in stoichiometric proportions and melting them at 90^{o}C for 10 minutes followed by cooling to 15^{o}C at a rate of 1^{o}C per minute.

After cleaning the work space and glass Petri dish with EtOH, a control humid

environment was prepared in the Petri dish by placing in it clean wipe wet with distilled water. Ni/Au substrates were cleaned by boiling them in acetone for 10 minutes, then in ethanol for 10 minutes, dried with nitrogen and placed in the Petri dish. Au-only substrates underwent an additional UVOX treatment for 10 minutes, followed by 40 minutes of incubation in EtOH. The solution of PNA duplex was applied on the the surfaces for full coverage. This step was done as quickly as possible after washing with EtOH as clean gold is highly reactive in air. Next, the Petri dish was closed with paraffin film and placed in a temperature controlled dark environment for 40 hours at 27^{o}C, followed by rinsing each PNA modified substrate with 0.4 M potassium phosphate buffer at pH=7.2 (2x 2 min), water (2x 30 sec, then 5 secs) and drying under a N_2 flow.

Ellipsometry

SAM thickness was measured using a multiple wavelength ellipsometer (M 2000 V from J. A. Woollam Co., Inc.) at a constant incidence angle of 70^{o} under ambient conditions and was analyzed using commercial software (WVASE32).

Polarization Modulation-Infrared Reflection−Absorption Spectroscopy (PM-IRRAS)

Infrared spectra were recorded in PM-IRRAS mode using a Nicolet 6700 FTIR instrument equipped with a PEM-90 photoelastic modulator (Hinds Instruments, Hillsboro, OR). The incidence angle was 82°.

Fabrication of the Device

Device fabrication was done following the previous procedure by Mondal et al.[24] The device is based on a vertical structure in which the bottom electrode is composed of gold functionalized with the PNA monolayer, on top of which an Al_2O_3 layer is

deposited, followed by a layer of nickel (Figure III.14a). The devices were prepared by photolithography, followed by e-beam evaporation, on a silicon substrate with thermally grown 300 nm SiO_2 (<100>, > 400 Ω cm^{-2}). The 1-μm-wide, 2-mm-long, and 120-nm-thick Au line was evaporated on an 8-nm-thick Cr adhesion layer. An Al_2O_3 layer with a thickness of about 2 nm was deposited on top of the SAM at 100 °C by atomic layer deposition. The top 120-nm-thick, 50-μm-wide Ni line was evaporated without any adhesion layer. 150-nm-thick gold contact pads for wire-bonding were evaporated.

The solid-state device was attached to a sample holder and electrically connected to the measuring units so that electrons will be injected from the Au electrode through the PNA monolayer into the Ni electrode. It was placed in-between the magnetic poles and on a cold finger that could be cooled down to 14 K. A magnetic field up to 1 T could be applied perpendicular to the sample plane by an electromagnet. The temperature of the sample holder was controlled by a PID temperature controller with a temperature stability of 0.3% at 300 K. The resistance of the device was measured at a relative accuracy of more than 10 ppm using a standard four-probe method with cross bridge geometry. Typically, a dc current of 1 mA from a Keithley 6221 current source was passed through the device. The voltage drop across the junction was measured using a Keithley Nanovoltmeter 2182A device.

III.5.1. Sample Preparation for Spin Polarization Measurements

PNA Duplex Preparation and PNA Monolayer *Preparation*

A 20 μM solution of PNA duplex in 20 mM PBS, pH X=7.2 buffer:acetonitrile 1:1 (200 μL) was prepared by mixing the complementary single strand PNA stock

solutions in stoichiometric proportions and melting them at 90°C for 10 minutes followed by cooling to 15°C at a rate of 1°C per minute.

The gold surfaces were prepared by e-beam evaporation on a p-doped, low resistivity silicon (100) wafer. A 8-nm thick titanium film was used as the adhesion layer between the silicon and the gold. The thickness of the gold layer was 120 nm. The surfaces were cleaned by boiling them in acetone for 10 minutes, then in ethanol for 10 minutes, dried with nitrogen and subjected to a UVOX treatment for 10 minutes, followed by 40 minutes in EtOH, then dried with nitrogen and placed in the Petri dish. The surface was then covered with the PNA solution (circa 40 µL) and incubated for 40h at 27 °C in water saturated atmosphere. Afterwards, surface was washed with PBS and water, then dried with N_2.

Experimental Set Up for Mott Polarimeter

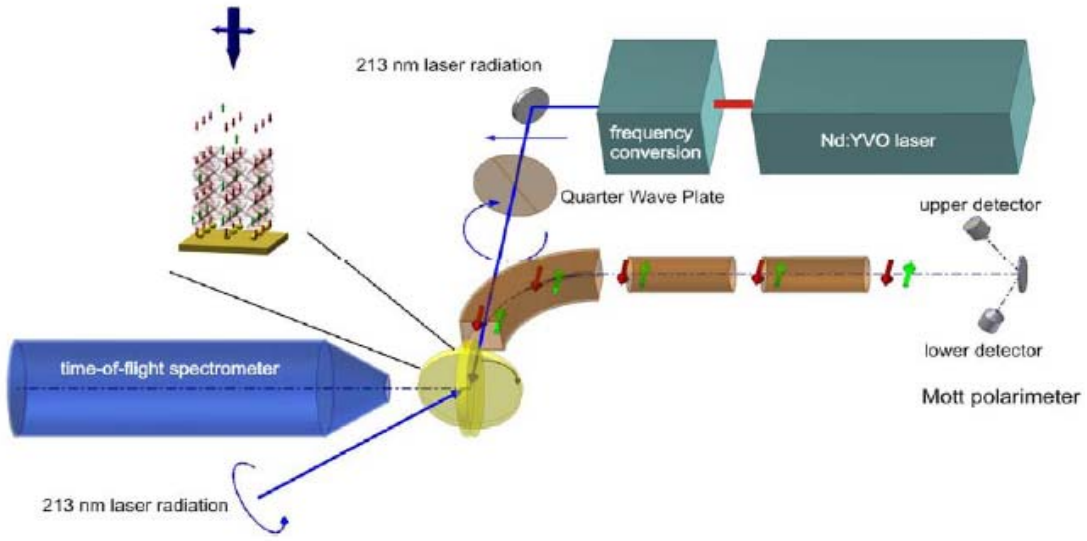

Figure III.21 Scheme of the experiment

A diode-pumped active mode-locked Nd:YVO oscillator operating at 80 MHz is regeneratively amplified (diode-pumped Nd:YVO) at a repetition rate of 20 kHz delivering pulses at 1064 nm of about 1.75 mJ with a pulse duration of about 300 ps. These pulses are frequency doubled in LBO (870 μJ) and quadrupled in BBO (120 μJ). Sum frequency mixing of the 4th harmonic and the fundamental in BBO is used to generate the 5th harmonic at 212.8 nm ($h\nu$ = 5.84 eV) with pulse energies of 5 μJ. Only a very small fraction of this pulse energy is used (about 15 pJ) for photoelectron excitation to prevent sample damage and charging.

Experiments are performed with linearly and with right- and left-circularly polarized light. Since light polarization is very crucial in spin polarized photoemission it has carefully been checked. Even though the laser is linearly polarized a UV calcite polarizer is used to control the linear polarization. A zero-order quarter wave plate (B. Halle Nachfl.) generates circularly polarized light. Circularity is carefully checked by a rotating analyzer (α-BBO, Laser Components). After generation, the polarized light does not path through any optics anymore but the entrance window of the vacuum chamber in order not to distort the polarization. The entrance window is a selected fused silica window (Aachener Quarzglas Technologie) which does not show any birefringence. To exclude tension birefringence a window with 5 mm thickness is used. A possible birefringence has been checked with the chamber both at atmospheric pressure and under vacuum. A distortion of the circularity of the polarization of less than 2% relative change of ellipticity (ratio of major to minor axes of circular polarized light of about 0.96) was measured.

III.6. References

1. Wolf, S. A.; Chtchelkanova, A. Y.; Treger, D. M., Spintronics—A retrospective and perspective. *IBM Journal of Research and Development* **2006,** *50* (1), 101-110.
2. Sarma, S. D., A new class of device based on electron spin, rather than on charge, may yield the next generation of microelectronics. *AmSci* **2001,** *89* (6), 516.
3. Naaman, R.; Waldeck, D. H., Chiral-induced spin selectivity effect. *J. Phys. Chem. Lett.* **2012,** *3* (16), 2178-2187.
4. Mathew, S. P.; Mondal, P. C.; Moshe, H.; Mastai, Y.; Naaman, R., Non-magnetic organic/inorganic spin injector at room temperature. *Appl. Phys. Lett.* **2014,** *105* (24), 242408.
5. Göhler, B.; Hamelbeck, V.; Markus, T.; Kettner, M.; Hanne, G.; Vager, Z.; Naaman, R.; Zacharias, H., Spin selectivity in electron transmission through self-assembled monolayers of double-stranded DNA. *Science* **2011,** *331* (6019), 894-897.
6. (a) He, W.; Crawford, M. J.; Rapireddy, S.; Madrid, M.; Gil, R. R.; Ly, D. H.; Achim, C., The structure of a γ-modified peptide nucleic acid duplex. *Mol. Biosyst.* **2010,** *6* (9), 1619-1629; (b) Petersson, B.; Nielsen, B. B.; Rasmussen, H.; Larsen, I. K.; Gajhede, M.; Nielsen, P. E.; Kastrup, J. S., Crystal Structure of a Partly Self-Complementary Peptide Nucleic Acid (PNA) Oligomer Showing a Duplex− Triplex Network. *J. Am. Chem. Soc.* **2005,** *127* (5), 1424-1430.
7. Rapireddy, S.; He, G.; Roy, S.; Armitage, B. A.; Ly, D. H., Strand invasion of mixed-sequence B-DNA by acridine-linked, γ-peptide nucleic acid (γ-PNA). *J. Am. Chem. Soc.* **2007,** *129* (50), 15596-15600.
8. Dragulescu-Andrasi, A.; Rapireddy, S.; Frezza, B. M.; Gayathri, C.; Gil, R. R.; Ly, D. H., A Simple γ-Backbone Modification Preorganizes Peptide Nucleic Acid into a Helical Structure. *J. Am. Chem. Soc.* **2006,** *128* (31), 10258-10267.
9. Egholm, M.; Buchardt, O.; Christensen, L.; Behrens, C.; Freier, S. M.; Driver, D. A.; Berg, R. H.; Kim, S. K.; Norden, B.; Nielsen, P. E., PNA hybridizes to complementary oligonucleotides obeying the Watson-Crick hydrogen-bonding rules. *Nature* **1993,** *365* (6446), 566.
10. Sahu, B.; Sacui, I.; Rapireddy, S.; Zanotti, K. J.; Bahal, R.; Armitage, B. A.; Ly, D. H., Synthesis and characterization of conformationally preorganized,(R)-diethylene glycol-containing γ-peptide nucleic acids with superior hybridization properties and water solubility. *J. Org. Chem.* **2011,** *76* (14), 5614-5627.
11. Sacui, I.; Hsieh, W.-C.; Manna, A.; Sahu, B.; Ly, D. H., Gamma peptide nucleic acids: as orthogonal nucleic acid recognition codes for organizing molecular self-assembly. *J. Am. Chem. Soc.* **2015,** *137* (26), 8603-8610.
12. Wittung, P.; Eriksson, M.; Lyng, R.; Nielsen, P. E.; Norden, B., Induced Chirality in PNA-PNA Duplexes. *J. Am. Chem. Soc.* **1995,** *117* (41), 10167-10173.
13. Grubišić, S.; Chandramouli, B.; Barone, V.; Brancato, G., Chain length, temperature and solvent effects on the structural properties of α-aminoisobutyric acid homooligopeptides. *PCCP* **2016,** *18* (30), 20389-20398.
14. (a) Boonlua, C.; Ditmangklo, B.; Reenabthue, N.; Suparpprom, C.; Poomsuk, N.; Siriwong, K.; Vilaivan, T., Pyrene-labeled pyrrolidinyl peptide nucleic acid as a hybridization-responsive DNA probe: comparison between internal and terminal labeling. *RSC Advances* **2014,** *4* (17), 8817-8827; (b) Manicardi, A.; Guidi, L.; Ghidini, A.;

Corradini, R., Pyrene-modified PNAs: Stacking interactions and selective excimer emission in PNA2DNA triplexes. *Beilstein J. Org. Chem.* **2014,** *10* (1), 1495-1503.
15. Putnam, F. A.; Fort, T.; Griffiths, R. B., Physical adsorption on patchwise heterogeneous surfaces. 3. Continuous phase transitions of krypton monolayers on (0001) graphite. *J. Phys. Chem.* **1977,** *81* (23), 2171-2176.
16. Umemoto, T.; Hrdlicka, P. J.; Babu, B. R.; Wengel, J., Sensitive SNP Dual-Probe Assays Based on Pyrene-Functionalized 2′-Amino-LNA: Lessons To Be Learned. *ChemBioChem* **2007,** *8* (18), 2240-2248.
17. (a) Seo, Y. J.; Ryu, J. H.; Kim, B. H., Quencher-Free, End-Stacking Oligonucleotides for Probing Single-Base Mismatches in DNA. *Org. Lett.* **2005,** *7* (22), 4931-4933; (b) Østergaard, M. E.; Kumar, P.; Baral, B.; Guenther, D. C.; Anderson, B. A.; Ytreberg, F. M.; Deobald, L.; Paszczynski, A. J.; Sharma, P. K.; Hrdlicka, P. J., C5-Functionalized DNA, LNA, and α-L-LNA: Positional Control of Polarity-Sensitive Fluorophores Leads to Improved SNP-Typing. *Chemistry-A European Journal* **2011,** *17* (11), 3157-3165.
18. Paul, A.; Watson, R. M.; Lund, P.; Xing, Y.; Burke, K.; He, Y.; Borguet, E.; Achim, C.; Waldeck, D. H., Charge Transfer through Single-Stranded Peptide Nucleic Acid Composed of Thymine Nucleotides. *J. Phys. Chem. C* **2008,** *112* (18), 7233-7240.
19. (a) Buffeteau, T.; Desbat, B.; Turlet, J. M., Polarization Modulation FT-IR Spectroscopy of Surfaces and Ultra-Thin Films: Experimental Procedure and Quantitative Analysis. *Appl. Spectrosc.* **1991,** *45* (3), 380-389; (b) Greenler, R. G.; Snider, D. R.; Witt, D.; Sorbello, R. S., The metal-surface selection rule for infrared spectra of molecules adsorbed on small metal particles. *Surf. Sci.* **1982,** *118* (3), 415-428.
20. (a) Wang, Z.; Liu, D.; Dong, S., In-situ FTIR study on adsorption and oxidation of native and thermally denatured calf thymus DNA at glassy carbon electrodes. *Biophys. Chem.* **2001,** *89* (1), 87-94; (b) Yamada, T.; Shirasaka, K.; Takano, A.; Kawai, M., Adsorption of cytosine, thymine, guanine and adenine on Cu(1 1 0) studied by infrared reflection absorption spectroscopy. *Surf. Sci.* **2004,** *561* (2–3), 233-247.
21. Banyay, M.; Sarkar, M.; Gräslund, A., A library of IR bands of nucleic acids in solution. *Biophys. Chem.* **2003,** *104* (2), 477-488.
22. (a) Nuzzo, R. G.; Dubois, L. H.; Allara, D. L., Fundamental studies of microscopic wetting on organic surfaces. 1. Formation and structural characterization of a self-consistent series of polyfunctional organic monolayers. *J. Am. Chem. Soc.* **1990,** *112* (2), 558-569; (b) Nuzzo, R. G.; Zegarski, B. R.; Dubois, L. H., Fundamental studies of the chemisorption of organosulfur compounds on gold(111). Implications for molecular self-assembly on gold surfaces. *J. Am. Chem. Soc.* **1987,** *109* (3), 733-740; (c) Steiner, G.; Möller, H.; Savchuk, O.; Ferse, D.; Adler, H. J.; Salzer, R., Characterisation of ultra-thin polymer films by polarisation modulation FTIR spectroscopy. *J. Mol. Struct.* **2001,** *563–564*, 273-277.
23. (a) Ihs, A.; Liedberg, B., Chemisorption of l-cysteine and 3-mercaptopropionic acid on gold and copper surfaces: An infrared reflection-absorption study. *J. Colloid Interface Sci.* **1991,** *144* (1), 282-292; (b) Manna, A.; Imae, T.; Yogo, T.; Aoi, K.; Okazaki, M., Synthesis of Gold Nanoparticles in a Winsor II Type Microemulsion and Their Characterization. *J. Colloid Interface Sci.* **2002,** *256* (2), 297-303.
24. Mondal, P. C.; Kantor-Uriel, N.; Mathew, S. P.; Tassinari, F.; Fontanesi, C.; Naaman, R., Chiral Conductive Polymers as Spin Filters. *Adv. Mater.* **2015,** *27* (11), 1924-1927.

25. Dankert, A.; Dulal, R. S.; Dash, S. P., Efficient Spin Injection into Silicon and the Role of the Schottky Barrier. *Sci. Rep.* **2013,** *3*, 3196.
26. Nielsen, P. E., *Peptide nucleic acids: protocols and applications*. Garland Science: 2004.
27. Paul, A.; Bezer, S.; Venkatramani, R.; Kocsis, L.; Wierzbinski, E.; Balaeff, A.; Keinan, S.; Beratan, D. N.; Achim, C.; Waldeck, D. H., Role of Nucleobase Energetics and Nucleobase Interactions in Single-Stranded Peptide Nucleic Acid Charge Transfer. *J. Am. Chem. Soc.* **2009,** *131* (18), 6498-6507.
28. Franzini, R. M.; Watson, R. M.; Patra, G. K.; Breece, R. M.; Tierney, D. L.; Hendrich, M. P.; Achim, C., Metal binding to bipyridine-modified PNA. *Inorg. Chem.* **2006,** *45* (24), 9798-9811.

CHAPTER IV. EFFECTS OF THE BACKBONE AND CHEMICAL LINKER ON THE MOLECULAR CONDUCTANCE OF NUCLEIC ACID DUPLEXES

This chapter presents the results of collaborative work with the groups of Prof. David H. Waldeck from University of Pittsburgh and Prof. David Beratan from Duke University. My role was to synthesize and characterize peptide nucleic acid monomers, oligomers and linkers. Self-assembled monolayers (SAMs) preparation and conductance measurements were done by Edward Beall (Waldeck Group). Computation investigations were done by the members of the research group of Prof. David Beratan.

IV.1. Introduction

Charge transfer (CT) is considered one of the most basic and essential chemical reactions. It is common in biological, chemical and physical systems.[1] In biology, CT plays a crucial role in important biological processes responsible for energy transduction such as photosynthesis, respiration and ATP production in mitochondria.[1-3] Although our understanding of charge transfer on the molecular scale and the macroscale[4] is excellent, the understanding of charge transfer on the nanoscale is limited by our ability to easily and reliably create structures that arrange redox-active units near each other in supramolecular systems. Supramolecular scaffolds that effectively and tunably facilitate electron transfer could be used as electron pathways connecting electroactive units over a specific distance or as charge carriers in a molecular device.

The molecular recognition of nucleic acids through Watson-Crick base pairing can be utilized to design and create three-dimensional nanometer scale structures. The π-stacking of nucleobases in DNA provides a conduit for charge transport. Studies of charge transfer in DNA using break junction,[5] scanning tunneling microscopy[6-7] and conductive probe atomic force microscopy (CP-AFM)[8-9] methods have addressed how

the charge transfer properties of dsDNA depend on the nucleobase sequence,[10] the interactions between DNA and its environment (e.g, solvent),[11] mismatches, and structural perturbations and fluctuations of DNA.[12] Previous studies including several from our group and collaborators examined the molecular conductance of both ss and dsDNA and PNA molecules.[7, 13-16] These studies showed that the structural flexibility of nucleic acids has an effect on the electrochemical charge transfer rates.[15, 17-18] Specifically, the electrochemical rate constant for γ-PNA duplexes was found to be a factor 2 smaller than that of aeg-PNA.[15] This difference was attributed to either the fact that aeg-PNA is more flexible than γ-PNA, which leads to either (1) larger energy level broadening of the hole mediating super exchange states, or (2) increased frequency of accessing conformations with the higher electronic couplings. The reduced rate is probably going to emerge from the relative adaptability of the backbones as opposed to from differences in the average nucleobase overlaps that may arise for various helix geometries. γ-PNA has a substituent at the γ-position of the backbone that makes it intrinsically chiral and reduces its conformational freedom.[19] Solution structures obtained by NMR spectroscopy and crystal structures of these nucleic acid duplexes have shown that homo-duplexes of aeg-PNA and γ-PNA adopt a P-helix structure[19-21] whereas DNA homo-duplexes[22] and DNA/PNA hetero-duplexes[23-24] adopt a B-DNA helix structure (Figure IV.1).[20, 25]Examination of the backbone's chemical structure suggest that aeg-PNA is more flexible than γ-PNA, which in turn more flexible than DNA; this interference is supported by NMR studies of these nucleic acids in solution (Table IV.1)[20-21] and by molecular dynamic studies.[12] Thus, a comparison of the single

molecule conductance of these molecules should provide insight into the importance of backbone flexibility on this property.

The reliance of electron exchange rates on structural fluctuations was likewise seen in studies on DNA/LNA hybrids[18] and reported for DNA duplexes at various temperatures.[17] Since the electron exchange rate is specifically identified with the electrical conductance,[16] it appears to be conceivable that such effects can bring about dissimilarities between the single molecule conductance of nucleic acid duplexes.

Table IV.1 Helical parameters of PNA, DNA, RNA homo- and hetero-duplexes[20]

Oligomer	Helical Sense	Disp/Å	Rise/Å	Incl./^{o}	Tilt/^{o}	Twist/^{o}	Bp per/turn
Aeg-PNA	L	7.9(0.7)	3.7(0.1)	-5.0	-0.2	-17.3	21
γ-PNA	R	-9	2.9	11.6	2.1	16.3	22
DNA/PNA	R	0.2	3.2	-10.4	2	28	13
A-DNA	R	-5.3	2.56	12	20	33	11
B-DNA	R	0.0	3.4	2.4	0	36	10

This chapter is intended to study the conductance of the 10-bp and 20-bp PNA and DNA homo-duplexes, the corresponding PNA/DNA hetero-duplexes, and their 'concatenated' duplex analogues. The results presented here correspond to 10-bp homo- and hetero-PNA and DNA duplexes; the study for 20-bp dsPNA and their concatenated analogues are still being performed. A 'concatenated' duplex is comprised of a 20-mer nucleic acid strand and two complementary 10-mer strands that hybridize sequentially on the 20-mer strand. The conductance of the concatenated duplexes is compared to that of the corresponding 20-bp duplexes to determine whether the 'stitching' affects the charge transfer ability of the molecule. The project focused on the investigation of different factors on charge transfer through nucleic acids:

(1) chemical nature of the nucleic acid backbone, i.e. sugar diphosphate (DNA), pseudo peptide (Aeg-PNA), and γ-hydroxymethylene-Aeg (γ-PNA)

(2) the linker that connects the PNA or DNA to the gold surface.

In the long term, the results of this study are relevant for the design of functional, PNA-based scaffolds based on nucleic acids that arrange multiple redox units in three-dimensional space, which function as a redox chain for chemical transformations (as in cellular respiration) or as a logic device (as in molecular electronics).

IV.2. Research Design

Charge transfer studies of the DNA and PNA suggested that PNA enhances the charge-carrying abilities of nucleic acids.[7, 13-15] The limitation of these studies is that the sequence and linkers of the PNA and DNA were different in different studies.[6, 14] Here we planned to compare the properties of PNA, γ–PNA and DNA homo-duplexes and DNA-PNA hetero-duplexes with same sequence. Figure IV.1 shows the chemical nature of the backbone of these nucleic acids and a view of a helical 10-bp duplex of each type.

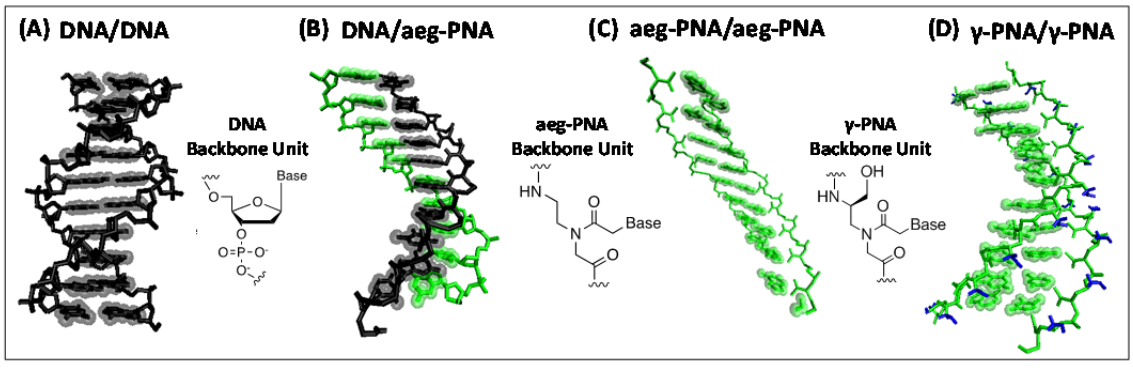

Figure IV.1 Renderings for the four duplexes (A) DNA homo-duplex, (B) DNA /aeg-PNA hetero-duplex, (C) aeg-PNA homo-duplex, and (D) γ-PNA homo-duplex are shown. In each case the sequence is AGTTTGTACG. The insets show the chemical structures for the backbones of DNA, aeg-PNA, and γ-PNA

Scanning tunneling microscope (STM) break junction method with continuous bias modulation was used to measure the single molecule conductance of these duplexes. The study was focused on 10-bp and 20-bp duplexes because of the instability of duplexes below 7 base-pairs (bps) in length. Challenges in the synthesis of long PNAs led us to evaluating the use of 'concatenated' duplexes comprising of a 20-mer strand onto which two complementary 10-mer strands are hybridized to create a 20-bp duplex. We compared the conductance of the concatenated and non-concatenated duplexes to determine the validity and limitations of the stitching approach and this part of the study is still under investigation.

The effect of the chemical linker between the nucleic acid and the electrodes used in STM-BJ was also studied. Molecular structures of the two linkers used in these studies are shown in Figure IV.2. The propylthiol linker can be covalently attached to the N or C end of the nucleic acid strands. The amino thymine linker is covalently connected to a nucleobase.

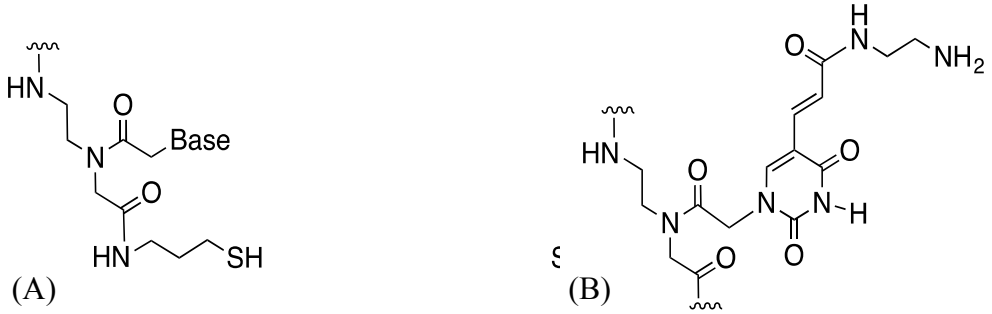

Figure IV.2 Chemical structure of the linkers that connect PNA to the Au surface. Panel A shows the propylthiol that is situated at the C end of the single stranded PNA. Panel B shows the thymine 5-C2 amino linker which can be situated at any position in a single stranded PNA.

Table IV.2 shows the PNA and DNA homo-duplexes and their corresponding PNA/DNA hetero-duplex, and their 'concatenated' duplex analogues that will be

employed in the conductance measurements. The 20-mer duplexes 1, 2, and 3 are chosen with the intent of understanding how hetero-duplexes compare to the homo- varieties of DNA and PNA. In all three 20-mer strands, the sequences were the same to ensure any differences in the measured conductance values could be attributed to the intrinsic ability of the duplex to facilitate charge transfer rather than differences in base pair composition. The 10-bp duplexes 6, 7, and 8 provide a similar comparison. Duplexes 4, 5, 9, and 10 were aimed at evaluating the stitching protocol. Duplexes 4 and 5 were full 20-bp duplexes constructed using the aforementioned stitching technique, while duplexes 9 and 10 were probing the conductance ability of a partially formed 20-bp duplex. This allowed one to distinguish the contribution of the partially formed 20-bp duplex if any exists in the measurements of the full 20-bp duplex. The single PNA strand control was chosen to determine whether unthiolated PNA strands could form the molecular junctions through the free amines.

Table IV.2 The scheme to be employed in the conductance measurements of PNA and DNA homo-duplexes, their corresponding PNA/DNA hetero-duplex, and their 'concatenated' duplex analogues. PNA and DNA strands are shown in blue and black, respectively. The red units are thiol modifications.

20mer+20mer Duplexes		20mer+10mer+10mer Duplexes	
$DNA1_{3'\text{-}SH}$ CGT ACA AAC T TAG ACA CCA G $(CH_2)_3SH$ $DNA2_{3'\text{-}SH}$ $HS(CH_2)_3$ GCA TGT TTG A ATC TGT GGT C	1	$DNA1_{3'\text{-}SH}$ CGT ACA AAC T TAG ACA CCA G $(CH_2)_3SH$ $PNA3_{N\text{-}Lys}$ NH_2-ATC TGT GGT C-Lys-H $PNA4_{N\text{-}Lys+C\text{-}SH}$ $HS(CH_2)_3$ GCA TGT TTG A Lys-H	4
$DNA1_{3'\text{-}SH}$ CGT ACA AAC T TAG ACA CCA G $(CH_2)_3SH$ $PNA2_{N\text{-}Lys+C\text{-}SH}$ $HS(CH_2)_3$ GCA TGT TTG A ATC TGT GGT C Lys-H	2	$DNA1_{3'\text{-}SH}$ CGT ACA AAC T TAG ACA CCA G $(CH_2)_3SH$ $DNA3_{3\text{-}5'}$ ATC TGT GGT C-5′ $DNA4_{3'\text{-}SH}$ $HS(CH_2)_3$ GCA TGT TTG A-5′	5
$PNA1_{N\text{-}Lys+C\text{-}SH}$ H-Lys_3 CGT ACA A ACT TAG ACA CCA G$(CH_2)_3SH$ $PNA2_{N\text{-}Lys+C\text{-}SH}$ $HS(CH_2)_3$ GCA TGT T TGA ATC TGT GGT C Lys_3-H	3		
10mer +10mer Duplexes			
$DNA4_{3'\text{-}SH}$ AGT TTG TAC G $(CH_2)_3SH$ $DNA5_{3'\text{-}SH}$ $HS(CH_2)_3$ TCA AAC ATG C -5′	6		
$DNA4_{3'\text{-}SH}$ AGT TTG TAC G $(CH_2)_3SH$ $PNA5_{N\text{-}Lys+C\text{-}SH}$ $HS(CH_2)_3$ TCA AAC ATG C Lys-H	7		
$PNA4_{N\text{-}Lys+C\text{-}SH}$ H–Lys AGT TTG TAC G$(CH_2)_3SH$ $PNA5_{N\text{-}Lys+C\text{-}SH}$ $HS(CH_2)_3$ TCA AAC ATG C Lys-H	8		
20mer +10mer Duplexes			
$DNA1_{3'\text{-}SH}$ CGT ACA AAC T TAG ACA CCA G $(CH_2)_3SH$ $PNA4_{N\text{-}Lys+C\text{-}SH}$ $HS(CH_2)_3$ GCA TGT TTG A Lys-H	9		
$DNA1_{3'\text{-}SH}$ CGT ACA AAC T TAG ACA CCA G $(CH_2)_3SH$ $DNA4_{3'\text{-}SH}$ $HS(CH_2)_3$ GCA TGT TTG A-5′	10		
CONTROL	$PNA3_{N\text{-}Lys}$ H–Lys-CTG GTG TCT A–NH_2		

IV.3. Results

In the first stage of this study we measured the molecular conductance of duplexes that have the same sequence of 10 base pairs, AGTTTGTACG and its complementary strand. Particularly, we compared duplexes that had a pseudopeptide backbone based on aminoethyl-glycine aeg-PNA, a pseudopeptide backbone based on γ-hydroxymethylene-aminoethyl-glycine γ-PNA, and sugar diphosphate DNA (Figure IV.1). We also examined the influence on the molecular conductance of the linker that connected the duplex to the electrode, through the nucleic acid backbone (propylthiol) or the nucleobase stack to the electrode (a thymine 5-C2 amino linker) (Figure IV.2).

IV.3.1. Thiol Location Control

Initially, we planned to have PT thiol linkers on the C-end to be able to study conductances of all duplexes outlined in Table IV.2, since we could only obtain the PT containing DNA strands on the 3' position from commercial sources. However, due to the low synthetic yields of C-end PT linker containing PNA oligomers to improve the oligomer quantities obtained, we attached the PT linker on either C-end or N-end to compare and exclude any effect of the location of the thiol linker used in the conductance measurements. A control was performed in which the aeg-PNA/aeg-PNA duplex was measured with the thiol linker attached on both the C-end and N-end (see Table IV.6). Sample current-distance trajectories are shown in Figure IV.3.

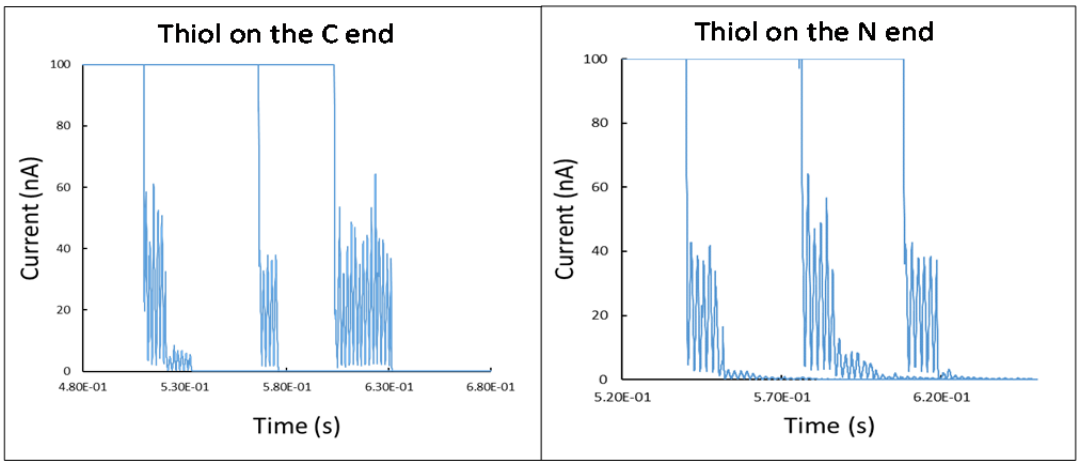

Figure IV.3 Current-time trajectories for aeg-PNA/aeg-PNA duplexes with thiol linkers on the C end and N terminus.

The results of the control showed equivalent current-distance characteristics for both duplexes. For this reason, differences observed between the aeg-PNA/aeg-PNA and γ-PNA/γ-PNA can be attributed to the backbone composition and not the position of the thiol linker.

IV.3.2. Conductance Measurements

Scanning tunneling microscope break junction (STM-BJ) method was utilized to examine the electrical conductance properties of the nucleic acid duplexes.[26] Molecular junctions are formed between a gold substrate and the gold STM tip by way of terminal linkers positioned on the opposing termini of the duplexes (Table IV.2). In this method, as the gold STM tip is withdrawn, a triangular waveform bias voltage is applied;[27] (Figure IV.4(A)). As the STM tip is retracted from the substrate surface, the current between the electrodes is monitored providing a current-time (current-distance) profile or trajectory. Electrical conduction through a purely resistive molecular junction demonstrates a triangular current-time waveform response (Figure IV.4(B)), while the responses of junctions without such molecules are more complex (leaky capacitor). The

standard tip displacement over one period of the applied triangle wave is 20 pm; < 9% of an Au-S bond length. A large set of trajectories for resistive molecular junctions were gathered. Their current responses were fit by an equivalent circuit model to yield a molecular conductance for each period of the waveform (see experimental details). For each duplex, a distribution of molecular conductance values was measured. Figure IV.4 (B) shows a trajectory for an aeg-PNA homo-duplex with propylthiol linkers on each strand. During ~12 periods in which the STM tip is pulled back and a molecular junction is formed with the substrate, the trajectory shows two regimes or modes of conductance. Different relative orientations of the linkers with respect to the gold electrodes and/or to different conformations of the molecule within the molecular junctions may cause the multiple modes seen within a conductance distribution.[28] At early times, a higher conductance mode and the current fluctuations between 30 and 60 nA is observed. The presence of one and two molecules 'wired' in parallel in the junction,[26] or the structural variations of the duplex, which have been shown to affect the conductance of the molecular junction, may cause this fluctuation.[7, 17] Changing the concentration of the nucleic acid duplexes on the surface indicated that a higher molecular coverage causes these fluctuations to occur more frequently in the current response. This supports the interpretation where the fluctuations are attributed to the two molecules in the junction. At later times, the higher conductance regime switches into a much lower conductance mode with a more stable current response. This transition could reproduce a change in the binding of the linker groups to the gold substrate or the partial separating of the nucleic acid strand.[29] However, since single strand molecules give much lower currents (<100 pA) than the ones observed here (5 to 10 nA for the lower conductance) the possibility of

separation is less likely.[8, 16, 30] Albeit only two conductance modes are seen for some of the systems, the terminology of 'high' and 'medium' conductance modes is still kept to be consistent with published data on thiol linkers.[16, 28, 31]

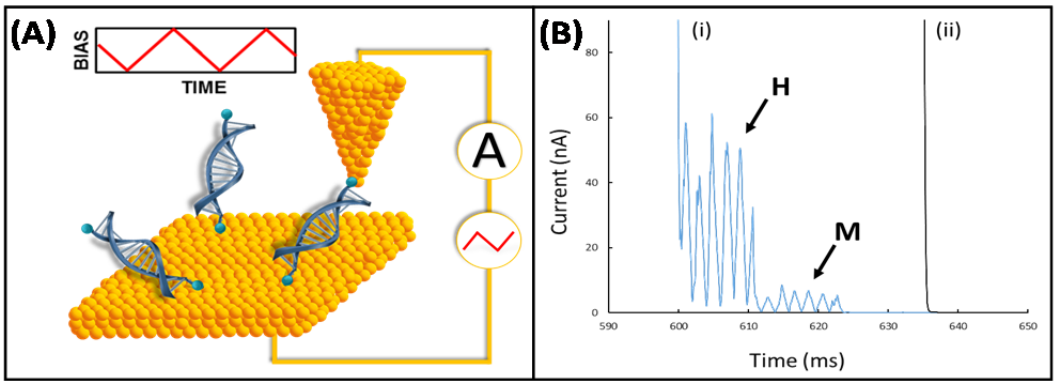

Figure IV.4 (A) The schematic for the single molecule conductance measurements. (B) Example current-time responses for the aeg-PNA homo-duplex showing the triangular wave current response resulting from a molecular junction (i) and an 'empty' current response where a molecular junction does not occur (ii). For the current response showing the molecular junction, a clear transition occurs from the high conductance mode (H) to a lower conductance mode (M).

Backbone Comparison

Conductance distributions for the DNA, the aeg-PNA, the γ-modified PNA homo-duplexes, and the DNA/aeg-PNA hetero-duplex, are shown in Figure IV.5 (B) through Figure IV.5 (E) with propylthiol linker groups in each case. These distributions were obtained from several thousands of measurements and normalized to unit area for comparison. For one of the molecular junctions, an example trajectory is also presented in panel A for each duplex type. The conductance distributions have a multimodal character and extend several orders of magnitude. The data set for the aeg-PNA homo-duplex (Figure IV.5 (C)) shows three modes while the data sets of the other three types of duplexes display two dominant conductance modes. The lowest mode of the DNA, γ-

modified PNA, and DNA/aeg-PNA duplexes were not observed, likely due to the preamplifier sensitivity constraints. The two highest conductance modes, which are observed for all four duplexes were analyzed and compared. The plots in Figure IV.5, present fits to the data by a sum of two Gaussian functions that allows a 'peak' conductance value to be assigned for the two higher conductance modes.

It should be noted that at about twice the conductance of the peak, the high conductance mode generally presents a shoulder on the high conductance side of the peak. Based on the analysis of these trajectories, the current response is shown to be varying between integer multiples of a single value; i.e., the junction has two molecules bound across the junction and they act as two parallel resistors.[27] Therefore, the conductance of a single molecule junction is considered to be the basis for the main peak and a junction containing two or more molecules for the shoulder.

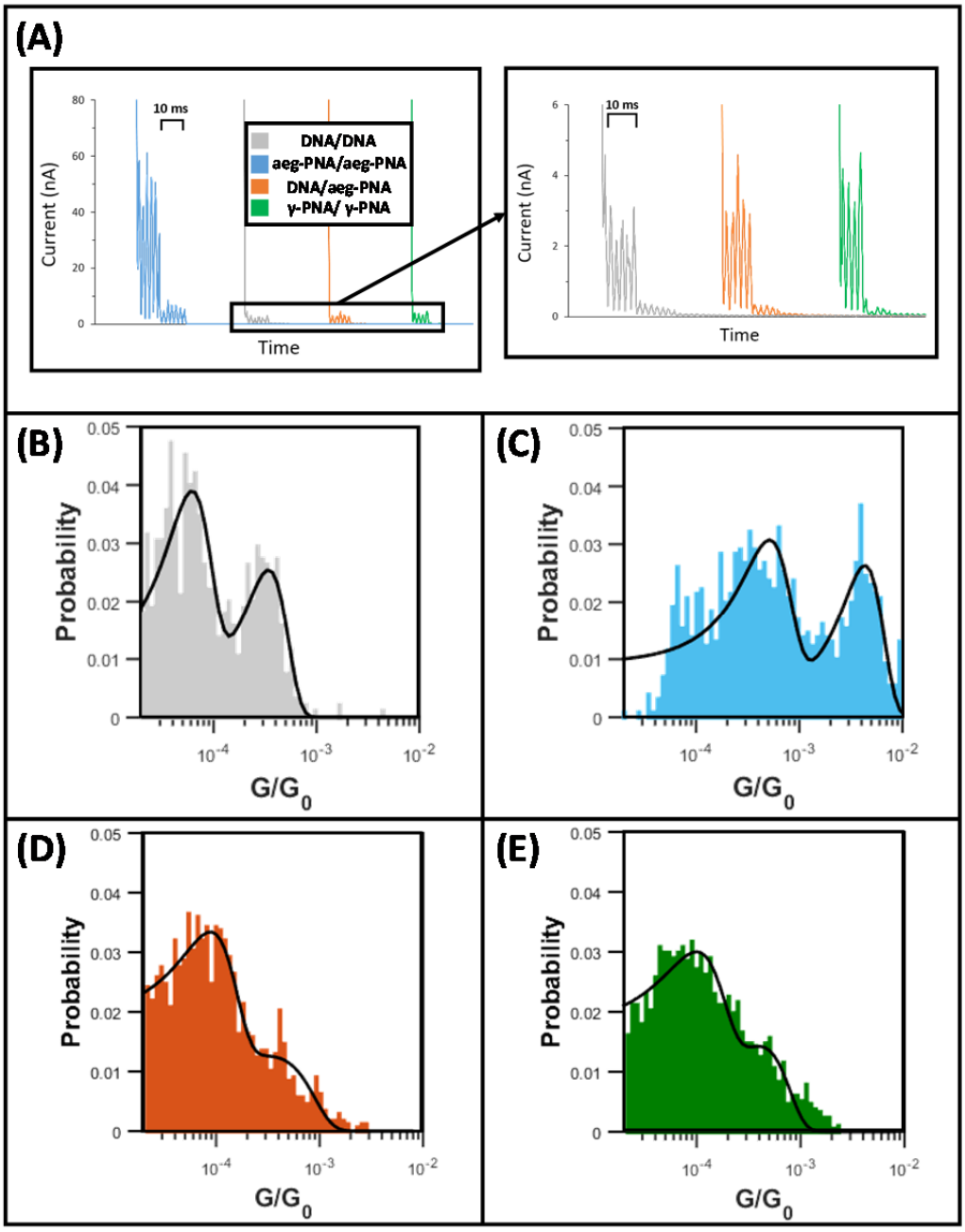

Figure IV.5 Panel A shows example current responses for the duplexes. The conductance histograms are shown for the DNA homo-duplex (B), the aeg-PNA homo-duplex (C), the DNA/aeg-PNA hetero-duplex (D), and the γ-PNA homo-duplex (E). The black curve is a fit of the histogram by a sum of two Gaussian functions. The peaks in the distributions are associated with major conductance modes, referred to as high and medium modes.

In Figure IV.5 (B), the distribution of molecular conductances for the DNA homo-duplex is presented. The conductance for the high conductance mode at the peak

maximum (most probable conductance for the high mode) is 3 x 10^{-4} G_0, where $G_0=2e^2/h$ is the quantum of conductance.[32] This value is in agreement with results reported for other 10-mer DNA duplexes with thiol linkers.[5-6, 29] Following about 20 angstroms of retraction, the magnitude of the current responses decreased significantly, which is consistent with available literature for these molecules.[29] This decrease was attributed to severing of the hydrogen bonds between the two strands of the duplex, the source of the breakdown mechanism of the molecular junction.

The conductance distribution measured for the aeg-PNA homo-duplex is shown in Figure IV.5 (C). For the aeg-PNA, the entire conductance distribution is shifted to higher values than that of DNA (Figure IV.5 (B)). The distribution for the aeg-PNA shows three conductance modes. For the high to medium to low modes, a fit of these three modes using Gaussians yields most probable conductance values in a ratio of approximately 54 to 6 to 1, respectively (see Table IV.8). These ratios are akin to those previously reported for alkanedithiols in Au junctions.[28] The values for the high and medium conductance modes of the aeg-PNA homo-duplex are well in agreement with the previously reported results.[16] The most probable conductance for the high mode of the aeg-PNA duplex (G_H /(10^{-4} G_0)= 43$\pm$21) is ten times larger than the most probable conductance for the high mode of the DNA homo-duplex (G_H /(10^{-4} G_0)=3.4$\pm$ 1.7).

The conductance distributions for the DNA/aeg-PNA hetero-duplex and the γ-PNA homo-duplex are shown in Figure IV.5 (D) and Figure IV.5 (E), respectively. For both duplexes, the most probable conductance for the high mode, about 4 x 10^{-4} G_0, lies between the high conductance mode observed for the DNA and aeg-PNA homo-duplexes. This value is within one-fourth of the DNA homoduplex and around ten times

lower than that observed for the high conductance mode of aeg-PNA. The conductance data for all the duplexes studied are summarized in Table IV.3. The data reveals that the DNA/DNA, DNA/aeg-PNA, and γ-PNA/γ-PNA have similar conductance. This similarity occurs although the backbones of the duplexes are different in chemical nature and have different electrostatic charge (Figure IV.1). Additionally, aeg-PNA and γ-PNA homo-duplexes form a P-type helix whereas the DNA homo-duplexes and the DNA/PNA hetero-duplexes form B-DNA helixes.[20, 22-23, 25]

In a previous study, the γ-PNA was found to have an electrochemical rate constant less than that of aeg-PNA by a factor of two,[16] and change in flexibility of the two duplexes was stated as the basis. The difference in conductance experiments by a factor of ten and in electrochemistry experiments by a factor of two may reflect the nonlinear relationship between the single molecule conductance and electron transfer rate in addition to the difference in electronic decoherence between the aeg-PNA and γ-PNA.

Linker Study

Conductance histograms for DNA and PNA homo-duplexes with amino thymine linkers and a fit to these data by a sum of Gaussians (black line) are shown in Figure IV.6. The DNA homo-duplex has a most probable high conductance value of 1.8×10^{-3} G_0, around five times higher than the same mode of the DNA homo-duplex with a thiol linker (Figure IV.5 (B)). Likewise, the aeg-PNA homo-duplex with the amino thymine linkers has a most probable high conductance mode that is over ten times higher than that observed for the thiol linkers, i.e. 0.062 G_0.

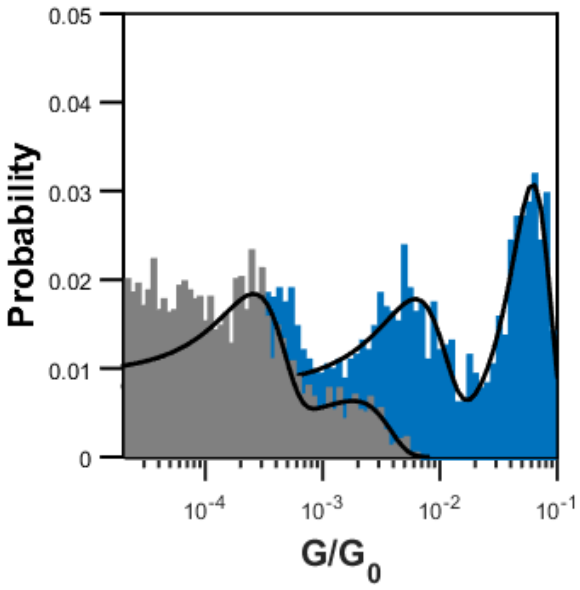

Figure IV.6 The conductance histograms for the DNA homo-duplex (gray) with amine linkers and PNA homo-duplex (blue) with amine linkers. The peaks in the distributions correspond to major conductance modes; the overlaid black curves are fits to the histogram by a sum of Gaussian functions.

Based on these findings, it is believed that the linker has a great effect on the conductance of duplexes. As the overall conductance increases, the histogram presents the development of a low conductance peak for the DNA duplex, verifying the earlier hypothesis that the third, low mode, was not detected for the thiol linkers because of instrumental limitations. Better electronic coupling between the electrode and the nucleobase stack mediated by the former linker is considered to be the basis for the fact that the conductance measured for each duplex with amino thymine linkers is larger than that for the same duplex with propylthiol linkers. It is noteworthy to state that a conductance value as high as six percent of G_0 was previously reported only for molecular junctions of a few angstroms, which are much shorter than the 30 angstrom PNA duplex studied here.[33-34] Structures of those molecular junctions are given in Figure IV.7.

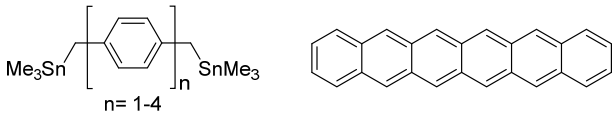

Figure IV.7 Chemical structures of molecular junctions bades on oligophenyls and oligoacene.

Summary

The most probable conductance values for the high (G_H) and medium (G_M) conductance modes observed in this study, along with the ratios of the conductance of the high mode to medium mode are shown in Table IV.3.

The conductance for both the high and medium modes rises from the DNA and γ-PNA homo-duplexes, to the DNA/aeg-PNA hetero-duplex, to the aeg-PNA homo-duplex. The comparative change for the high conductance peak maximum is slightly more than the comparative change in the medium conductance peak maximum for the four duplexes. The less conductive duplexes have a slightly smaller ratio. It may be claimed that different modes of the conductance can stem from different nucleic acid duplex conformations and/or from different linker-gold electrode geometries. For both nucleic acid duplexes and alkanedithiols, the G_H/G_M ratios reported here for the thiol linker are in reasonable agreement with previous findings,[16] suggesting that the different conductance modes originate from linker-gold conformation. Moreover, the comparison of the different conductance modes for the same core structures (especially DNA/DNA and aeg-PNA/aeg-PNA duplexes) but with different linkers G_H(amine)/G_M(amine) and G_H(thiol)/G_M(thiol) points to somewhat different ratios. This trend cannot be described by a conformational effect of the molecular backbone alone since the same 'high' to 'medium' ratios would be preserved when the linker identity is changed. Consequently,

the origin of the modes is assumed to arise from changes in the linker group's binding geometry, at least partly.

Table IV.3 Summary of the single molecule conductance measurements for the nucleic acid duplexes

Linker Type	Duplex	G_H /(10^{-4} G_0)	G_M /(10^{-4} G_0)	G_H / G_M	% G_H
Thiol	DNA/DNA	3.4 ± 1.7	0.60 ± 0.32	5.7	47
	DNA/aeg-PNA	3.6 ± 1.9	0.86 ± 0.48	4.1	33
	γ-PNA/γ-PNA	4.0 ± 3.3	0.92 ± 0.79	4.4	52
	aeg-PNA/aeg-PNA	43 ± 21	5.0 ± 3.0	8.7	53
Amine	DNA/DNA	18 ± 16	2.5 ± 1.9	7.2	31
	aeg-PNA/aeg-PNA	620 ± 240	59 ± 45	10.5	39

The relative probabilities of observing the high and medium modes reasonably agree with each other for the different duplexes. This consistency of the relative amounts of high and medium modes also backs the conception that the modes arise from different binding geometries, as the relative occurrence of the different linker binding geometries would not be expected to change with the molecular backbone drastically.

IV.3.3. Computational Results

Computational studies were used to examine features of the backbone changes in the model system. Molecular dynamics (MD) simulations of the 10-mer duplexes were used to generate structures for the aeg-PNA, DNA, DNA/aeg-PNA, and γ-PNA duplexes. Quantum chemistry calculations (with the ZINDO method in Gaussian 09[35]) of the electronic couplings were performed on the duplex structures generated by the MD simulations.

Computations were performed on central part (six base pairs) of the nucleic acid duplex studied experimentally (marked in blue in Figure IV.8). Figure IV.8 shows the electronic coupling strength between nearest neighbor purine sites and the definitions of V1-V5. Root-mean-square of coupling strengths (in front of ±) and found for the nucleic acid duplexes in eV are given in Table IV.4.

Figure IV.8 Nucleic acid sequence and numbering scheme for the couplings between nearest neighbor purine bases.

Table IV.4 Root-mean-square of coupling strengths (in front of ±) and found for the nucleic acid duplexes in eV

	aeg-PNA	DNA	DNA/aeg-PNA	**γ**-PNA
V1	0.092 ±0.103	0.11 ±0.134	0.086 ±0.106	0.103 ±0.126
V2	0.087 ±0.104	0.11 ±0.136	0.089 ±0.112	0.0981 ±0.120
V3	0.055 ±0.055	0.034 ±0.040	0.037 ±0.053	0.0463 ±0.048
V4	0.013 ±0.022	0.016 ±0.021	0.012 ±0.019	0.0161 ±0.022
V5	0.072 ±0.073	0.043 ±0.051	0.066 ±0.070	0.0767 ±0.077

Backbone Study

The Büttiker-Landauer probe approach was implemented to calculate the molecular conductances.[36-38] Büttiker virtual electrodes were introduced to simulate the dephasing induced by the interaction of the molecule with the environment. In this approach, the conductance is calculated with the Hamiltonian

$$H_M = \sum_{i=1}^{N} \varepsilon_i |i><i| + \sum_{i=1}^{N-1} V_{i,i+1} |i><i+1| + h.c. \qquad \textbf{Eq. 1}$$

where ε_i is the mean site energy of purine site i, which is the HOMO energy. These calculations include the middle six base pairs in the molecular Hamiltonian, while treating the two base pairs at each end as part of the electrodes. The coupling between electrodes and the terminal molecular sites is taken to be 0.1 eV. The coupling between Büttiker probes and the molecular sites is set to 0.003 eV for γ-PNA, DNA/aeg-PNA, and DNA (indicative of slower dephasing) and 0.01 eV for aeg-PNA (indicative of faster dephasing) to reproduce the trend observed in the experimental measurements. Using this methodology, the calculated conductances were $18.9 \times 10^{-9}\ G_0$ for aeg-PNA/aeg-PNA, $2.26 \times 10^{-9}\ G_0$ for DNA/DNA, $2.67 \times 10^{-9}\ G_0$ for γ-PNA/ γ-PNA, and $1.48 \times 10^{-9} G_0$ for DNA/aeg-PNA. The conductance for the aeg-PNA homo-duplex was also calculated using the same Büttiker probe coupling (0.003 eV) that was used for the other duplexes. In this instance, the calculated conductance is $1.87 \times 10^{-9}\ G_0$. This indicates that the increased conductance calculated for the aeg-PNA homo-duplex is representative of the increased dephasing rate and not an increase in the nucleobase coupling for the aeg-PNA/aeg-PNA duplex. The need for a much faster dephasing rate to capture the experimentally observed conductance differences supports the notion that backbone flexibility affects the conductance.

Consideration of the backbone flexibility by simulating structural fluctuations provides a basis for understanding the electronic dephasing in charge transfer.[39-41] The fluctuations in the duplex structures were explored by simulating the thermal fluctuations of the structural parameters.

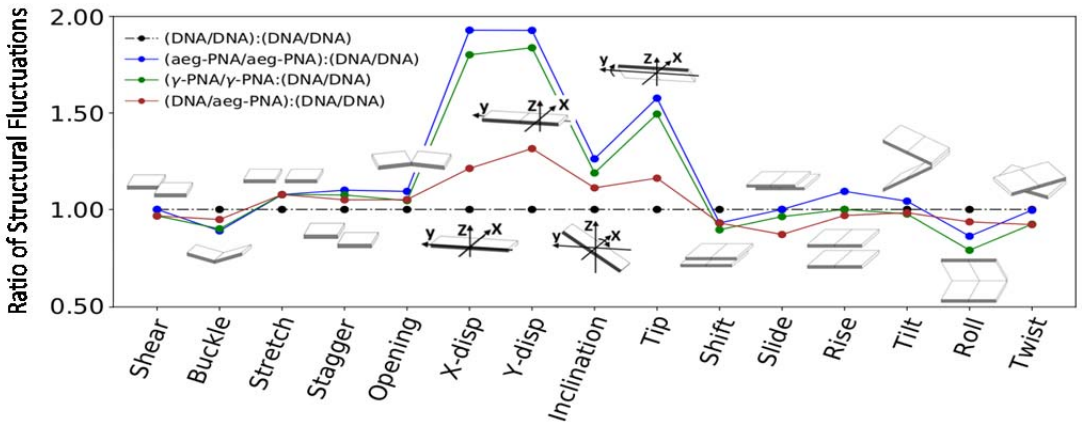

Figure IV.9 The ratio of structural parameter fluctuations (standard deviation of 10,000 MD snapshots, averaged among the middle 6-mers) between different backbone species as compared to DNA. Structural parameters are defined and calculated with x3DNA[42].

Figure IV.9 shows the ratio of the structural parameter fluctuations for the aeg-PNA/aeg-PNA, γ-PNA/γ-PNA, and DNA/aeg-PNA duplexes relative to DNA/DNA. Aeg-PNA has systematically higher fluctuation width in most structural parameters suggesting that aeg-PNA is the most flexible backbone motif. The required Büttiker probe coupling values needed to reproduce the experimentally determined conductance values appear plausible. The γ-PNA duplex has lower parameter fluctuations as compared to aeg-PNA except for the Buckle metric, indicating the effective rigidification of γ-modification. Pairing a DNA strand with an aeg-PNA strand (as in the DNA/aeg-PNA duplex), rigidifies the whole structure as shown in Figure IV.9.

The dephasing rate is a collective result of system-environmental interaction, which is represented by the fluctuations of structural parameters in our case. Dissecting the dephasing rate and assigning a weight to each helical parameter in determining the dephasing rate is difficult or may be conceptually impossible. Our qualitative study found that dephasing from molecular flexibility is another essential parameter in controlling charge transfer rate, other than the energy landscape and electronic coupling strength.

Note that the effective charge injection between the STM tip and the guanine for the amine modified structures is mediated by a thymine base, which should enhance the effective coupling as compared to the thiol modified structures. Lastly, we note that the magnitude of the computed conductance is much lower than that measured and likely arises from the Fermi level's and electrode couplings that were used to ensure the computations correspond to the non-adiabatic limit.

Linker Study

We examined the effect of the linker group on the overall conductance by examining the average contact distance between the heteroatom of the linker (the thymine N atom and the thiol S atom) that is believed to bind to the Au and the nearest guanine base; see Figure IV.4. Molecular dynamics (MD) simulations were run and the distribution of through space distances for the atom linked to Au (S in thiol linker and N in amino linker) and the center of the closest guanine base were calculated and are presented in Figure IV.10. The center of the closest guanine base was defined as the geometric center of the heavy atoms (C, N and O) on the guanine ring. Because the electronic coupling is known to change exponentially with distance through saturated bonds and the saturated groups are similar for the two linkers, the through space distance calculated here is presumed to reflect the difference in coupling strengths qualitatively. A more rigorous treatment would evaluate the through space and through bond contributions explicitly, however it is not clear that the data warrant such a treatment, as the junction geometry is likely to change from measurement to measurement.

The distance distributions shown in Figure IV.10 reveal significant differences among the three different duplexes: DNA homo-duplex, aeg-PNA homo-duplex, and γ-

PNA homo-duplex. The PNA and γ-PNA display a multi-mode distance distribution between the S atom and the center of the guanine, whereas the DNA duplex shows one dominant mode. For the PNA duplexes, the distributions display a short distance mode at around 4 Å and another somewhat longer one at ~about 8 Å. In addition, the PNAs have significant population in the distance range from 9 to 13 angstroms, which encompasses the unimodal distance distribution peaking at ~11 Å for the DNA. In general, the PNA duplexes have significant population in which the G base is closer to the metal (thiol as surrogate).

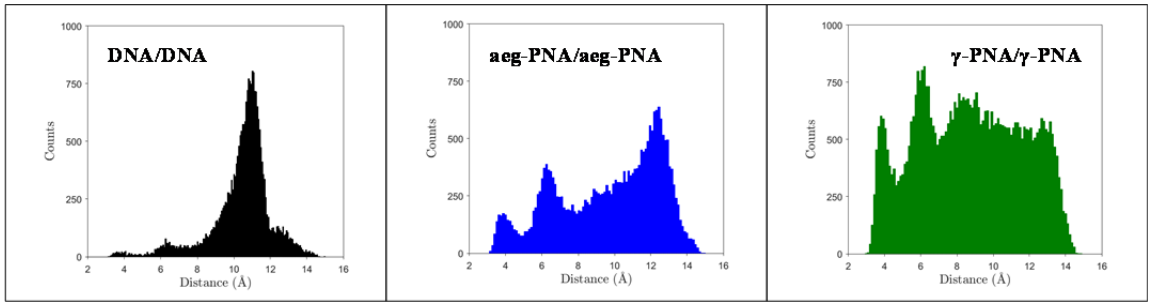

Figure IV.10 The contact distance distributions for DNA/DNA (left), aeg-PNA/aeg-PNA (middle) and γ-PNA/ γ-PNA (right).

The PNA and γ-PNA can access a van der Waals contact regime (~4 Å) and a typical snapshot showing this interaction is shown in Figure IV.11. We recorded the time evolution of the contact distance and found that the lifetime of each mode is on the time scale of several nanoseconds.

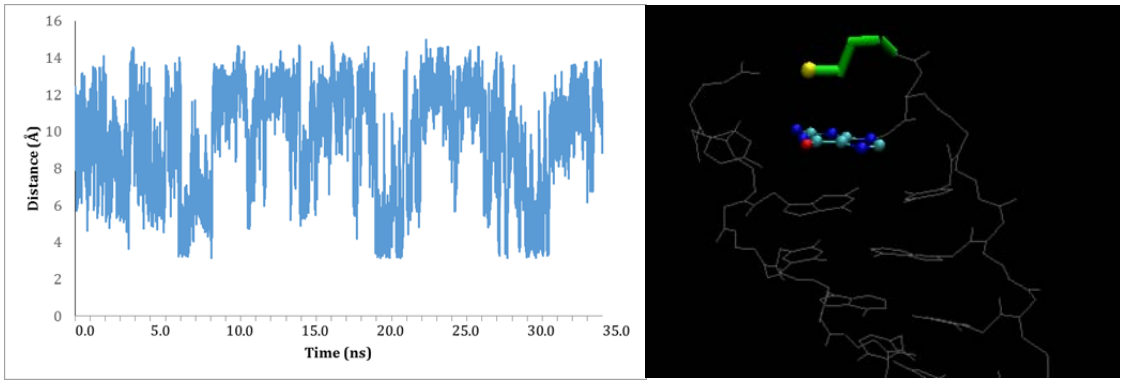

Figure IV.11 Time evolution of the contact distance (left); A typical snapshot of the vDW contact between the S atom (colored in yellow) on the thiol linker (green) and the guanine (colored as atom type) (right).

For the amine linked PNA and DNA duplexes the molecular dynamics simulations gave a unimodal distribution for the contact distance (Figure IV.12) with average contact distances of 9.2 Å ± 1.4 Å for DNA and 9.0 Å ± 1.2 Å for PNA. Both are shorter than the average contact distance in the thiol modified structures.

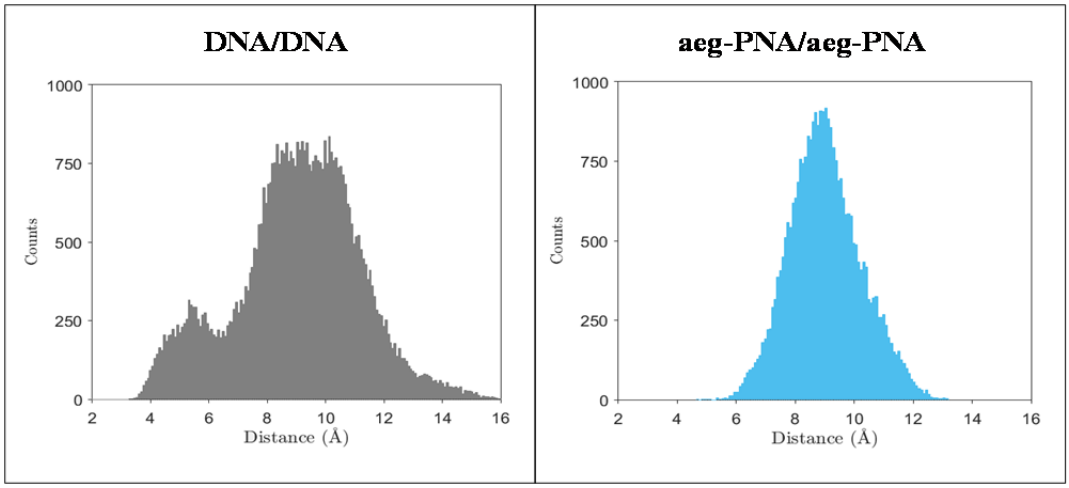

Figure IV.12 Contact distance distributions for amine modified DNA (top) and PNA (bottom).

These findings suggest that the amino linker structures have a stronger effective injection coupling with the Au because of their closer average proximity to the electrode;

however, the thiol modified PNA and γ-PNA can access conformations that place the G base in van der Waals contact with the Au tip.

Table IV.5 Summary of the contact distance calculations for the measured duplexes

Contact distance	Average	Distribution mode	Coupling type	Number of snapshots
Thiol modified DNA	10.4 Å ± 1. 7 Å	Unimodal	Through space	25,000
Thiol modified PNA	9.6 Å ± 2.8 Å	Multiple peaks	Through space	35,000
Thiol modified γ-PNA	8.7 Å ± 2.9 Å	Multiple peaks	Through space	49,000
Amine modified DNA	9.2 Å ± 1.4 Å	Unimodal	Base mediated	52,000
Amine modified PNA	9.0 Å ± 1.2 Å	Unimodal	Base mediated	30,000

IV.4. Conclusions

The most probable molecular conductance of 10-base pair nucleic acid duplexes that have identical nucleobase sequence but different backbones show a 200-fold range. The value of 0.06 G_0 measured for the aeg-PNA duplex is unprecedented for a molecule that is ~ 30-Å long. The aeg-PNA has a high mode conductance that is 13 times higher than that of the corresponding DNA duplex when the linker is propylthiol linker and 34 times higher than the DNA when the linker is amino-C2-thymine. These findings show that both the linker and the nucleic acid backbone play critical roles in determining the overall magnitude of the measured conductance. Hence, the molecular conductance for these ~30-Å long nucleic acid duplexes cannot be modeled as an incoherent sum of charge injection, charge transport, and charge escape steps, but must be treated as coherent (or semi-coherent) transport through the molecule.

IV.5. Materials and Methods

IV.5.1. General Procedures

All reactions were performed under nitrogen atmosphere unless otherwise stated. All commercial available materials were used without further purification unless otherwise specified. Anhydrous solvents, purchased from EMD Millipore, such as DMF, DCM and THF, were dried by standard methods and freshly distilled prior to use. All anhydrous reagents were purchased from Aldrich. Common reagents purchased from either Chem-Impex or Alfa Aesar. ^{1}H-NMR and ^{13}C-NMR spectra were acquired on a Bruker Avance AV-300 or 500 MHz NMR spectrometer using standard Bruker software.

Boc/Z and Fmoc/Bhoc PNA monomers were purchased from PolyOrg Inc. and ASM Research Chemicals and used without further purification.

IV.5.2. Synthesis of PNA Oligomers

The Boc-protected γ-PNA monomers were synthesized according to slightly changed published procedures (as described in Chapter II). The oligomers were synthesized on MBHA resin according to the published protocol. Upon completion of the last monomer coupling, the oligomers were cleaved from the resin (and the protecting groups were simultaneously removed) by immersing the resin in a cocktail containing m-cresol/thioanisole/TFA/TFMSA (150/150/900/300 μL for 100 mg of resin) for 2 h. The crude mixture was eluted and precipitated in ethyl ether, dissolved in water, purified by reversed-phase HPLC using a C18 column (5 μm; 19 × 100 mm and characterized by MALDI-TOF on an Applied Biosystems Voyager Biospectrometry Workstation using R-cyano-4-hydroxycinnamic acid matrix (10 mg/mL in 1:1 water/acetonitrile, 0.1% TFA).

The observed mass of each synthesized PNA agreed well with the expected mass (Table IV.6). Concentrations of the oligomers were determined by UV absorption at 260 nm at 90 ^{o}C in water.

Synthesis of Propylthiol Linker Containing PNAs

4-(Tritylthio)butyric acid, which was necessary for the N-end modification of PNA with the thiol linker, was synthesized using a published procedure.[43] The PNA oligomers with N-end propylthiol were synthesized using the Boc strategy; the PNA oligomers with C-end propylthiol were synthesized by Fmoc strategy. A p-methyl-benzhydrylamine (MBHA) resin purchased from Peptide International was used for the Boc strategy and PNA oligomers were synthesized manually by standard solid phase peptide synthesis methods. The MBHA resin (1.0 g) was down-loaded to 0.1 mmol/g with the first monomer.

The PT modification at C-end of PNA was afforded by using 2-chlorotrityl resin purchased from AnaSpec, and this resin was downloaded with 3-Amino-1-propanethiol hydrochloride was purchased from Sigma Aldrich as described in a published protocol (Figure IV.13).[44] 3-Amino-1-propanethiol hydrochloride (2 eq.) and DIPEA (2 eq.) dissolved in anhydrous (DCM/DMF 1:1) (10 ml per gram of resin) were added to 2-chlorotrityl resin. The suspension was stirred at RT for 5 h. At end of the reaction, the resin was filtered, washed with 3xDCM. To ensure that 3-Amino-1-propanethiol was not attached to the resin through its amino group, resin was treated with a mixture of acetic acid AcOH/trifluoroethanol (TFE)/DCM (1:2:7) for 30 min at rt. This mixture cleaves the aminotrityl bond effectively. Unreacted remaining trityl chlorides were converted to the corresponding inert tritylmethyl ethers by washing resin with DCM/MeOH/DIPEA

(80:15:5). A qualitative positive Kaiser test [in a 1.5 mL centrifuge tube, added a few beads of resin 1 drop of Monitor 1 (8g of phenol dissolved in 2 mL EtOH) and 2 drops of Monitor 2 (13 mg KCN/20 mL water. Dilute 200 µL of KCN aqueous solution with 9800 µL L pyridine)] and 1 drops Monitor 3 (1 g ninhydrin in 20 mL ethanol) was used to confirm the presence of free amines on the 2-chlorotrityl resin. In order to check the loading of the 2-chlorotrityl resin with the PT linker, PT downloaded resin was coupled with Boc-Lys(Fmoc)-OH. After, deprotection of the Fmoc- group on an accurately weighed sample, amount of released Fmoc- was measured by UV-vis spectrometry photometrically.

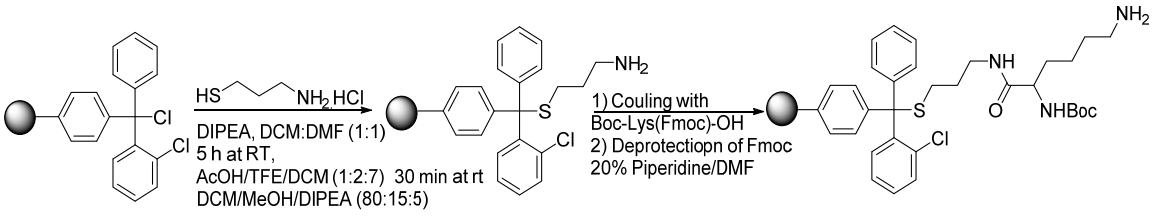

Figure IV.13 Loading of the 2-chlorotrityl resin with the PT linker.

The PNA was cleaved using TFMSA/TFA/m-cresol/thioanisole (20:60:10:10) and TFA/triisopropylsilane/water (95:2.5:2.5) for Boc and Fmoc strategy, respectively. Cleaved PNA was precipitated with cold diethyl ether. PNA strands were purified by reverse-phase HPLC and were lyophilized. Characterization of the oligomers was performed by MALDI-TOF using R-cyano-4-hydroxycinnamic acid matrix (10 mg/mL in 1:1 water/acetonitrile, 0.1% TFA). The observed mass of each synthesized PNA agreed well with the expected mass (Table IV.6).

Synthesis of $T_{(C2\text{-}NH2)}$ Linker Containing PNAs

The $T_{(C2\text{-}NH2)}$ functionalized PNA oligomers were synthesized manually on Rink-amide AM resin purchased from Novabiochem following the standard Fmoc procedures of solid-phase peptide synthesis. $T_{(C2\text{-}NH2)}$ acedic acid linker was added on the N-end of a PNA oligomer as the side chain of the Boc-DAP(Fmoc)-OH (Boc-3-(Fmoc-amino)-L-alanine) amino acid which was purchased from Sigma-Aldrich.

Upon completion of the oligomer synthesis, the oligomers were cleaved from the resin by immersing the resin in a cocktail containing TFA:DCM:TIS (50:50:1, TIS used as scavenger) for 1.5 h. Cleaved PNA was precipitated with cold diethyl ether. PNA strands were purified by reverse-phase HPLC and were lyophilized. Characterization of the oligomers was performed by MALDI-TOF using R-cyano-4-hydroxycinnamic acid matrix (10 mg/mL in 1:1 water/acetonitrile, 0.1% TFA). The observed mass of each synthesized PNA agreed well with the expected mass (Table IV.6).

Table IV.6 PNA Sequences and MALDI data

Oligomer sequences N to C end			
Thiol on the C end Lys on the N end		**Cal. MW**	**Obs. MW**
$PNA4_{N\text{-}Lys+C\text{-}SH}$	H–Lys AGT TTG TAC G $(CH_2)_3SH$	2959.98	2983.81
$PNA5_{N\text{-}Lys+C\text{-}SH}$	H-Lys CGT ACA AAC T $(CH_2)_3SH$	2921.33	2921.63
Thiol on the C end			
$PNA4_{C\text{-}SH}$	Ac AGT TTG TAC G$(CH_2)_3SH$	2874.67	2875.25
$PNA5_{C\text{-}SH}$	Ac CGT ACA AAC T$(CH_2)_3SH$	2814.65	2814.78
Thiol on the N end			
$PNA4_{N\text{-}SH}$	$HS(CH_2)_3$ AGT TTG TAC G NH_2	2860.67	2858.00
$PNA5_{N\text{-}SH}$	$HS(CH_2)_3$ CGT ACA AAC T NH_2	2798.65	2797.03
Thiol on the N end (gamma modified)			
$\gamma PNA4_{N\text{-}SH}$	$HS(CH_2)_3$ AGT TTG TAC G-NH_2	3160.67	3159.71
$\gamma PNA5_{N\text{-}SH}$	$HS(CH_2)_3$ CGT ACA AAC T-NH_2	3098.65	3098.34
GC Block PNA with thiol and amino linker on the N –end			
$PNA6_{N\text{-}SH}$	$HS(CH_2)_3$ GGG GGC CCC C Lys NH_2	2960.81	2959.10
$PNA7_{N\text{-}T\text{-}C2\text{-}NH2}$	H-$T_{(C2\text{-}NH2)}$ (dap) GGG GGC CCC C A NH_2	3356.24	3354.14
Amino linker on the N end			
$PNA4_{N\text{-}T\text{-}C2\text{-}NH2}$	H-$T_{(C2\text{-}NH2)}$ (dap) AGT TTG TAC G A-NH_2	3384.38	3381.43
$PNA5_{N\text{-}T\text{-}C2\text{-}NH2}$	H-$T_{(C2\text{-}NH2}$ (dap) CGT ACA AAC T A-NH_2	3322.26	3319.62

* Ac shows N-end acetylation
** Underlined letters shows γ-modified PNA monomers
*** SH stands for propylthiol linker
**** Dap= 3-amino-L-Alanine

IV.5.3. Preparation of Samples for Conductance Measurements

Nucleic Acid Duplexes

The DNA strands were purchased from Integrated DNA Technologies or Alpha DNA, and the PNA strands were synthesized by the aforementioned procedure. Duplexes were hybridized by heating a solution containing 20 μM of each nucleic acid strand in a pH = 7.0 Tris-EDTA buffer and 50 mM NaCl. The solution was heated to 90 ^{o}C for 10 minutes and then allowed to cool to room temperature over 2-3 hours. This procedure yields duplexes, which was confirmed by absorbance and circular dichroism spectroscopy.

Gold Substrate

The ultraflat gold substrates were prepared using the template-stripping process.[45] 100 nm gold films were evaporated onto freshly-cleaved mica using an AJA ATC-T Series Thermal Evaporation System. Piranha-cleaned glass slips (10 mm x 25 mm) were glued to the gold films using epoxy resin (Epo-Tek). The glass slips were peeled off the gold film prior to each experiment and the film was transferred to the glass to expose an atomically flat gold surface. 50 μL of the hybridized nucleic acid solution is deposited on the gold surface and the terminal linkers on the nucleic acid duplexes are allowed to bond to the gold surface for approximately 10 seconds. The gold substrates are then washed once with water and washed once with ethanol before complete drying under a stream of argon. Prolonged incubation of the substrate with the nucleic acid solution was shown to increase the coverage of the deposited duplexes and more commonly result in current-distance trajectories that included multiple molecules in the junction.

Conductance Measurements and Analysis

All measurements were performed using an Agilent 5500 Scanning Probe Microscope system equipped with an environmental chamber. The chamber was housed in a homemade acoustically isolated Faraday cage seated on an anti-vibrational system (Table Stable) that was mounted on an optical table. Data collection was performed using a modified version of the STM-controlled break junction method.[5, 27] An STM tip was repeatedly driven to the surface of the gold substrates and withdrawn at a constant speed of 10 nm s^{-1}. During the retraction period, molecular junctions can form as molecules bridge the gap between the gold substrate and the gold tip. Thousands of trajectories were collected for each duplex, requiring multiple substrates and STM tips to collect a full set. The gold STM tips (0.25 mm, 99.95% gold wire, Alfa Aesar) were freshly cut prior to each experiment. All experiments were performed under an argon atmosphere and the substrates were immersed in mesitylene. The applied bias was a triangular waveform with a modulation frequency of 500 Hz (Stanford Research Systems, DS345 Function Generator). A bias of 50 ± 50 mV was applied in the measurement of every duplex with the exception of the aeg-PNA/aeg-PNA duplex with amine linkers; for these measurements, the applied bias was 5 ± 5 mV. All measurements were performed using a 10 nA/V preamplifier.

Data filtering and analysis were performed using a custom Matlab code. The current-distance trajectories were filtered to remove trajectories that did not display molecular junctions. The trajectories were partitioned into periods established by the applied bias and fit to current responses generated using a library of resistance values

based on a previous protocol.[27] For certain duplexes, multiple bias ranges were used to ensure that the highest conductance mode was observable in each instance.

Data sets for each duplex included several thousand current-distance trajectories. The data sets were manually filtered to exclude trajectories that did not have molecular junctions or did not have an exponential decay with distance. The procedure for fitting the current-distance trajectories can be found in reference 22.

Table IV.7 The applied bias for each measured duplex

Duplex	**Applied Bias (mV)**
DNA/DNA (thiol)	50±50
DNA/aeg-PNA (thiol)	50±50
γ-PNA/γ-PNA (thiol)	50±50
aeg-PNA/aeg-PNA (thiol)	50±50
DNA/DNA (amine)	50±50
aeg-PNA/aeg-PNA (amine)	5±5

Mode Analysis

Analysis of the probability of the high conductance mode shows relative agreement among the studied duplexes (see Figure IV.14). The absolute counts are totaled for each conductance mode based on the fitted Gaussian functions and the fractions of the counts corresponding to the high mode are given relative to the total counts. With the exception of the DNA/aeg-PNA duplex, the thiol linkers appear to have roughly an even probability of occupying the high mode and medium mode. For the amine linkers, the relative probability of the high mode appears to be lower.

Table IV.8 The relative fraction of the high conductance mode calculated for the studied duplexes using the fitted Gaussian functions.

Duplex	High Mode Fraction
DNA/DNA (thiol)	0.47
DNA/aeg-PNA (thiol)	0.33
γ-PNA/γ-PNA (thiol)	0.52
aeg-PNA/aeg-PNA (thiol)	0.53
DNA/DNA (amine)	0.31
aeg-PNA/aeg-PNA (amine)	0.39

Mode Fitting in aeg-PNA

The aeg-PNA conductance histogram displays three modes: high, medium, and low. However, for the purposes of comparison with the other studied duplexes, the analysis only focuses on the high and medium modes. Figure IV.14 shows a comparison of the aeg-PNA conductance histogram with both 2 and 3 fitted Gaussian functions. The calculated high and medium Gaussian functions shown in Figure IV.14 (B) represent the same as those calculated for the fit to three Gaussians, but the fit to the low conductance mode is simply omitted.

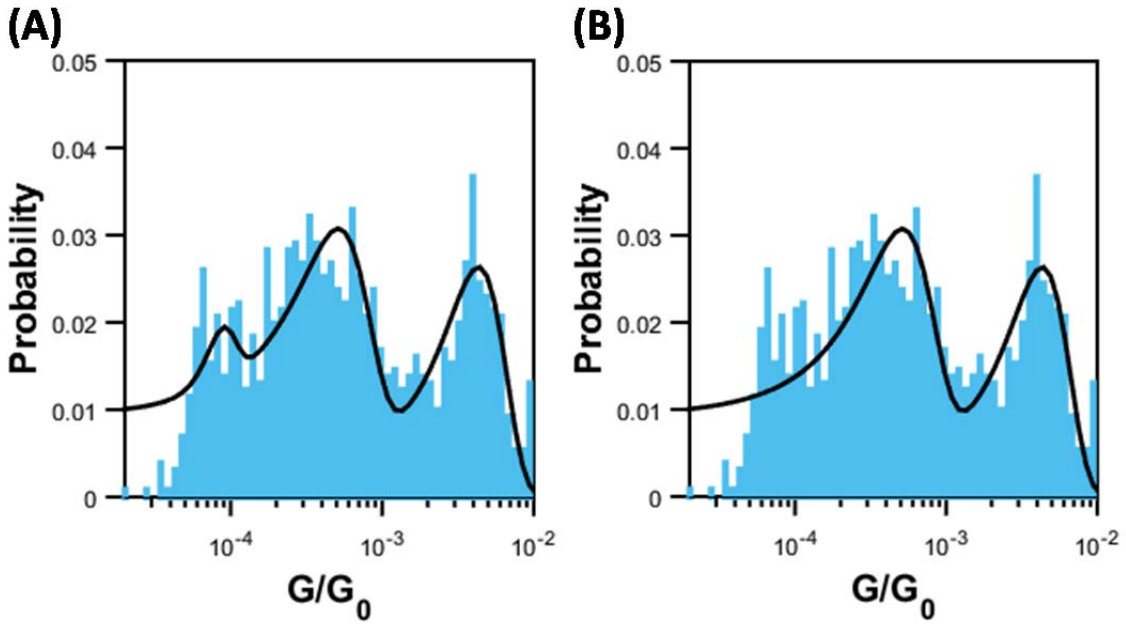

Figure IV.14 The aeg-PNA conductance histograms with three Gaussian fits (A) and two Gaussian fits (B).

IV.5.4. Molecular Dynamics

The initial structures of DNA are obtained with an x3DNA webserver.[46] PNA structures for this sequence were generated by a custom program. The γ-PNA structures were assembled by replacing the H2'' atom on the PNA structures backbone with a C atom. The CHARMM force field[47] was used and CGenFF[48] was used to find force field parameters for the amine linker. DNA/aeg-PNA was built in GaussView,[49] starting from PDB:1PDT. [23]

For each structure, multiple MD simulations were performed and snapshots were taken at 1frame/ps. Two nucleobases (donor and acceptor bases in coupling calculations) are extracted from each snapshot. Backbones, solvent molecules, and counter-ions are removed. Hydrogen atoms are patched to dangling bonds.[12] Coupling calculations were

performed with the block diagonalization method[50] based on the Fock matrix obtained from the ZINDO semi-empirical quantum method embedded in Gaussian 09.[35]

Conductance Calculations

To explore the conductivity of all the nucleic acids, we implemented the Büttiker-Landauer model,[51] where Büttiker probes perturb the coherence and introduce the incoherent charge transfer mechanisms. The Büttiker-Landauer model is widely used in simulating molecular junction conductance.[52-54] Because the measured conductance is mainly contributed by hole transfer in our experimental setup[55-56] and hole transfer is mostly mediated by purine bases, we only consider purine bases (guanine and adenine) in our model.

In our model, the site energy of guanine (HOMO) is 0.35 eV higher than the site energy of adenine (HOMO).[57] The Fermi level of the Au electrodes was placed 0.8 eV higher in energy than the guanine HOMO.[13] The electronic coupling strength between nearest neighbor purine sites $V_{i,i+1}$is obtained from quantum calculations and averaged from 1000 MD snapshots. The coupling calculation results for nucleic acids of all backbone species are listed in Table IV.5.

IV.6. References

1. Barbara, P. F.; Meyer, T. J.; Ratner, M. A., Contemporary Issues in Electron Transfer Research. *J. Phys. Chem.* **1996,** *100* (31), 13148-13168.
2. Moser, C. C.; Keske, J. M.; Warncke, K.; Farid, R. S.; Dutton, P. L., Nature of biological electron transfer. *Nature* **1992,** *355* (6363), 796-802.
3. Nishitani, S.; Kurata, N.; Sakata, Y.; Misumi, S.; Karen, A.; Okada, T.; Mataga, N., A new model for the study of multistep electron transfer in photosynthesis. *J. Am. Chem. Soc.* **1983,** *105* (26), 7771-7772.
4. Choi, D.; Kim, H.; Persson, N.; Chu, P.-H.; Chang, M.; Kang, J.-H.; Graham, S.; Reichmanis, E., Elastomer–Polymer Semiconductor Blends for High-Performance Stretchable Charge Transport Networks. *Chem. Mater.* **2016,** *28* (4), 1196-1204.
5. Xu; Zhang; Li; Tao, Direct Conductance Measurement of Single DNA Molecules in Aqueous Solution. *Nano Lett.* **2004,** *4* (6), 1105-1108.
6. van Zalinge, H.; Schiffrin, D. J.; Bates, A. D.; Haiss, W.; Ulstrup, J.; Nichols, R. J., Single-Molecule Conductance Measurements of Single- and Double-Stranded DNA Oligonucleotides. *ChemPhysChem* **2006,** *7* (1), 94-98.
7. Wierzbinski, E.; Arndt, J.; Hammond, W.; Slowinski, K., In Situ Electrochemical Distance Tunneling Spectroscopy of ds-DNA Molecules. *Langmuir* **2006,** *22* (6), 2426-2429.
8. Nogues, C.; Cohen, S. R.; Daube, S.; Apter, N.; Naaman, R., Sequence Dependence of Charge Transport Properties of DNA. *J. Phys. Chem. B* **2006,** *110* (18), 8910-8913.
9. Nogues, C.; Cohen, S. R.; Daube, S. S.; Naaman, R., Electrical properties of short DNA oligomers characterized by conducting atomic force microscopy. *PCCP* **2004,** *6* (18), 4459-4466.
10. Meggers, E.; Michel-Beyerle, M. E.; Giese, B., Sequence Dependent Long Range Hole Transport in DNA. *J. Am. Chem. Soc.* **1998,** *120* (49), 12950-12955.
11. Kubař, T.; Elstner, M., What Governs the Charge Transfer in DNA? The Role of DNA Conformation and Environment. *J. Phys. Chem. B* **2008,** *112* (29), 8788-8798.
12. Hatcher, E.; Balaeff, A.; Keinan, S.; Venkatramani, R.; Beratan, D. N., PNA versus DNA: Effects of Structural Fluctuations on Electronic Structure and Hole-Transport Mechanisms. *J. Am. Chem. Soc.* **2008,** *130* (35), 11752-11761.
13. Paul, A.; Bezer, S.; Venkatramani, R.; Kocsis, L.; Wierzbinski, E.; Balaeff, A.; Keinan, S.; Beratan, D. N.; Achim, C.; Waldeck, D. H., Role of Nucleobase Energetics and Nucleobase Interactions in Single-Stranded Peptide Nucleic Acid Charge Transfer. *J. Am. Chem. Soc.* **2009,** *131* (18), 6498-6507.
14. Venkatramani, R.; Davis, K. L.; Wierzbinski, E.; Bezer, S.; Balaeff, A.; Keinan, S.; Paul, A.; Kocsis, L.; Beratan, D. N.; Achim, C.; Waldeck, D. H., Evidence for a Near-Resonant Charge Transfer Mechanism for Double-Stranded Peptide Nucleic Acid. *J. Am. Chem. Soc.* **2011,** *133* (1), 62-72.
15. Wierzbinski, E.; de Leon, A.; Davis, K. L.; Bezer, S.; Wolak, M. A.; Kofke, M. J.; Schlaf, R.; Achim, C.; Waldeck, D. H., Charge Transfer through Modified Peptide Nucleic Acids. *Langmuir* **2012,** *28* (4), 1971-1981.
16. Wierzbinski, E.; Venkatramani, R.; Davis, K. L.; Bezer, S.; Kong, J.; Xing, Y.; Borguet, E.; Achim, C.; Beratan, D. N.; Waldeck, D. H., The Single-Molecule Conductance and Electrochemical Electron-Transfer Rate Are Related by a Power Law. *ACS Nano* **2013,** *7* (6), 5391-5401.

17. O 'Neill, M. A.; Barton, J. K., DNA-mediated charge transport requires conformational motion of the DNA bases: elimination of charge transport in rigid glasses at 77 K. *J. Am. Chem. Soc.* **2004,** *126* (41), 13234-13235.
18. Thazhathveetil, A. K.; Vura-Weis, J.; Trifonov, A.; Wasielewski, M. R.; Lewis, F. D., Dynamics and efficiency of hole transport in LNA: DNA hybrid diblock oligomers. *J. Am. Chem. Soc.* **2012,** *134* (39), 16434-16440.
19. Dragulescu-Andrasi, A.; Rapireddy, S.; Frezza, B. M.; Gayathri, C.; Gil, R. R.; Ly, D. H., A Simple γ-Backbone Modification Preorganizes Peptide Nucleic Acid into a Helical Structure. *J. Am. Chem. Soc.* **2006,** *128* (31), 10258-10267.
20. He, W.; Crawford, M. J.; Rapireddy, S.; Madrid, M.; Gil, R. R.; Ly, D. H.; Achim, C., The structure of a γ-modified peptide nucleic acid duplex. *Mol. Biosyst.* **2010,** *6* (9), 1619-1629.
21. He, W.; Hatcher, E.; Balaeff, A.; Beratan, D. N.; Gil, R. R.; Madrid, M.; Achim, C., Solution Structure of a Peptide Nucleic Acid Duplex from NMR Data: Features and Limitations. *J. Am. Chem. Soc.* **2008,** *130* (40), 13264-13273.
22. Watson, J. D.; Crick, F., Molecular structure of nucleic acids: a structure for deoxyribose nucleic acid. JD Watson and FHC Crick. Published in Nature, number 4356 April 25, 1953. *Nature* **1974,** *248* (5451), 765.
23. Eriksson, M.; Nielsen, P. E., Solution structure of a peptide nucleic acid–DNA duplex. *Nature Structural & Molecular Biology* **1996,** *3* (5), 410-413.
24. Yeh, J. I.; Shivachev, B.; Rapireddy, S.; Crawford, M. J.; Gil, R. R.; Du, S.; Madrid, M.; Ly, D. H., Crystal Structure of Chiral γPNA with Complementary DNA Strand: Insights into the Stability and Specificity of Recognition and Conformational Preorganization. *J. Am. Chem. Soc.* **2010,** *132* (31), 10717-10727.
25. Rasmussen, H.; Kastrup, J. S.; Nielsen, J. N.; Nielsen, J. M.; Nielsen, P. E., Crystal structure of a peptide nucleic acid (PNA) duplex at 1.7 A resolution. *Nat Strut Biol.* **1997,** *4* (2), 98-101.
26. Xu, B.; Tao, N. J., Measurement of single-molecule resistance by repeated formation of molecular junctions. *Science* **2003,** *301* (5637), 1221-1223.
27. Beall, E.; Yin, X.; Waldeck, D. H.; Wierzbinski, E., A scanning tunneling microscope break junction method with continuous bias modulation. *Nanoscale* **2015,** *7* (36), 14965-14973.
28. Li, C.; Pobelov, I.; Wandlowski, T.; Bagrets, A.; Arnold, A.; Evers, F., Charge transport in single Au| alkanedithiol| Au junctions: coordination geometries and conformational degrees of freedom. *J. Am. Chem. Soc.* **2008,** *130* (1), 318-326.
29. Bruot, C.; Xiang, L.; Palma, J. L.; Tao, N., Effect of mechanical stretching on DNA conductance. *ACS nano* **2014,** *9* (1), 88-94.
30. Guo, X.; Gorodetsky, A. A.; Hone, J.; Barton, J. K.; Nuckolls, C., Conductivity of a single DNA duplex bridging a carbon nanotube gap. *Nat. Nanotechnol.* **2008,** *3* (3), 163-167.
31. Haiss, W.; Martín, S.; Leary, E.; Zalinge, H. v.; Higgins, S. J.; Bouffier, L.; Nichols, R. J., Impact of junction formation method and surface roughness on single molecule conductance. *J. Phys. Chem. C* **2009,** *113* (14), 5823-5833.
32. Van Wees, B.; Van Houten, H.; Beenakker, C.; Williamson, J. G.; Kouwenhoven, L.; Van der Marel, D.; Foxon, C., Quantized conductance of point contacts in a two-dimensional electron gas. *Phys. Rev. Lett.* **1988,** *60* (9), 848.

33. Chen, W.; Widawsky, J. R.; Vázquez, H.; Schneebeli, S. T.; Hybertsen, M. S.; Breslow, R.; Venkataraman, L., Highly conducting π-conjugated molecular junctions covalently bonded to gold electrodes. *J. Am. Chem. Soc.* **2011,** *133* (43), 17160-17163.
34. Yelin, T.; Korytár, R.; Sukenik, N.; Vardimon, R.; Kumar, B.; Nuckolls, C.; Evers, F.; Tal, O., Conductance saturation in a series of highly transmitting molecular junctions. *Nat. Mater.* **2016,** *15* (4), 444-449.
35. Frisch, M.; Trucks, G.; Schlegel, H.; Scuseria, G.; Robb, M.; Cheeseman, J.; Scalmani, G.; Barone, V.; Mennucci, B.; Petersson, G., Gaussian 09, Revision B. 01. Wallingford, CT: Gaussian. *Inc.,(2)* **2004**.
36. Büttiker, M., Small normal-metal loop coupled to an electron reservoir. *Phys. Rev. B* **1985,** *32* (3), 1846.
37. Büttiker, M., Role of quantum coherence in series resistors. *Phys. Rev. B* **1986,** *33* (5), 3020.
38. Venkatramani, R.; Wierzbinski, E.; Waldeck, D. H.; Beratan, D. N., Breaking the simple proportionality between molecular conductances and charge transfer rates. *Farad. Discuss.* **2014,** *174*, 57-78.
39. Liu, C.; Beratan, D. N.; Zhang, P., Coarse-grained theory of biological charge transfer with spatially and temporally correlated noise. *J. Phys. Chem. B* **2016,** *120* (15), 3624-3633.
40. Rebentrost, P.; Mohseni, M.; Kassal, I.; Lloyd, S.; Aspuru-Guzik, A., Environment-assisted quantum transport. *New J. Phys* **2009,** *11* (3), 033003.
41. Weiss, U., *Quantum dissipative systems*. World Scientific: 2012; Vol. 13.
42. Lu, X.-J.; Olson, W. K., 3DNA: a software package for the analysis, rebuilding and visualization of three-dimensional nucleic acid structures. *Nucleic Acids Res.* **2003,** *31* (17), 5108-5121.
43. Qvit, N.; Reuveni, H.; Gazal, S.; Zundelevich, A.; Blum, G.; Niv, M. Y.; Feldstein, A.; Meushar, S.; Shalev, D. E.; Friedler, A.; Gilon, C., Synthesis of a novel macrocyclic library: discovery of an IGF-1R inhibitor. *J. Comb. Chem.* **2008,** *10* (2), 256-66.
44. Mourtas, S.; Katakalou, C.; Nicolettou, A.; Tzavara, C.; Gatos, D.; Barlos, K., Resin-bound aminothiols: synthesis and application. *Tetrahedron Lett* **2003,** *44* (1), 179-182.
45. Hegner, M.; Wagner, P.; Semenza, G., Ultralarge atomically flat template-stripped Au surfaces for scanning probe microscopy. *Surf. Sci.* **1993,** *291* (1-2), 39-46.
46. Lu, X. J.; Olson, W. K., 3DNA: a software package for the analysis, rebuilding and visualization of three‐dimensional nucleic acid structures. *Nucleic Acids Res.* **2003,** *31* (17), 5108-5121.
47. MacKerell Jr, A. D.; Bashford, D.; Bellott, M.; Dunbrack Jr, R. L.; Evanseck, J. D.; Field, M. J.; Fischer, S.; Gao, J.; Guo, H.; Ha, S., All-atom empirical potential for molecular modeling and dynamics studies of proteins. *J. Phys. Chem. B* **1998,** *102* (18), 3586-3616.
48. Vanommeslaeghe, K.; Hatcher, E.; Acharya, C.; Kundu, S.; Zhong, S.; Shim, J.; Darian, E.; Guvench, O.; Lopes, P.; Vorobyov, I., CHARMM general force field: A force field for drug‐like molecules compatible with the CHARMM all‐atom additive biological force fields. *J. Comput. Chem.* **2010,** *31* (4), 671-690.
49. Dennington, R.; Keith, T.; Millam, J., GaussView, version 5. *Semichem Inc., Shawnee Mission, KS* **2009**.

50. Scholes, G. D., Long-range resonance energy transfer in molecular systems. *Annu. Rev. Phys. Chem.* **2003,** *54* (1), 57-87.
51. Qi, J.; Edirisinghe, N.; Rabbani, M. G.; Anantram, M., Unified model for conductance through DNA with the Landauer-Büttiker formalism. *Phys. Rev. B* **2013,** *87* (8), 085404.
52. Kilgour, M.; Segal, D., Tunneling diodes under environmental effects. *J. Phys. Chem. C* **2015,** *119* (45), 25291-25297.
53. Kilgour, M.; Segal, D., Charge transport in molecular junctions: From tunneling to hopping with the probe technique. *J. Chem. Phys.* **2015,** *143* (2), 024111.
54. Korol, R.; Kilgour, M.; Segal, D., Thermopower of molecular junctions: Tunneling to hopping crossover in DNA. *J. Chem. Phys.* **2016,** *145* (22), 224702.
55. Liu, C.; Xiang, L.; Zhang, Y.; Zhang, P.; Beratan, D. N.; Li, Y.; Tao, N., Engineering nanometre-scale coherence in soft matter. *Nat. Chem.* **2016**.
56. Xiang, L.; Palma, J. L.; Bruot, C.; Mujica, V.; Ratner, M. A.; Tao, N., Intermediate tunnelling–hopping regime in DNA charge transport. *Nat. Chem.* **2015,** *7* (3), 221-226.
57. Zhang, Y.; Liu, C.; Balaeff, A.; Skourtis, S. S.; Beratan, D. N., Biological charge transfer via flickering resonance. *Proceedings of the National Academy of Sciences* **2014,** *111* (28), 10049-10054.

CHAPTER V. CONCATENATION OF PNA OLIGOMERS THROUGH COORDINATION

V.1. Introduction

Watson-Crick base pairing organizes nucleic acids duplex formation that is necessary for genetic information storage in biological systems. In the last decade and half, nucleic acid recognition properties have also been extended to non-biological systems, where exquisite specificity of DNA base pairing has been used to design complex nanostructures and novel materials.[1] By replacing nucleic acid base pairs with ligands, hybrid nucleic acid structures with new topologies are obtained. Furthermore, tailoring the electronic and magnetic properties of the nucleic acid-ligand hybrids with metal ions, desired molecular architecture and the function can be achieved. The structure and the electronic properties of the dsDNA can be easily modified by altering the hydrogen-bond base pairing motif with different pairing interactions, such as site-specific metal coordination.[2-3]

Transition metals can be inserted into nucleic acids by substitution of the natural nucleobases with ligands. The most common synthetic method of ligand containing monomers is forming an acetyl carbonyl linker between the Aeg backbone and the nucleobase. In the presence of the metal ions, ligand-nucleic acid conjugates form supramolecular structures based on a combination of coordination and hydrogen bonds. In our lab, successful incorporation of mono-, di and tridentate ligands to peptide nucleic acids have been shown.[4-7] To make ligand containing PNAs, nucleobase moiety of the monomer is replaced by a ligand that requires the synthesis of ligand modified building-blocks. Using this methodology insertion of one or more ligands into PNA oligomers was successfully shown on relatively short PNA oligomers. However, inserting more ligands

and increasing the length of the PNA oligomers, oligomer synthesis becomes less efficient and low yielding oligomers are obtained.

However, in this chapter to minimize the number of synthetic steps, ligands were introduced as a side chain of a known amino acid on shorter PNA oligomers. Aligning two ligand-modified PNA strands on a complementary PNA template under appropriate conditions allows hybridization to occur. Using templated hybridization, a variety of ligand-metal conjugates can be inserted at the different positions within the oligomer. The results of this study can be useful for designing functional PNA oligomers for different applications such as PNA-based molecular electronic devices.

A variety of oligonucleotide templated reactions have been reported in the last two decades. In these reactions, a long nucleic acid template aligns reactive functionalities in close proximity to each other by linking them to two short complementary strands. This methodology has been used to translate nucleic acid instructions into diverse collections of small molecules,[8] synthetic oligomers,[9] and functional nanomaterials[10] or to uncage fluorophore or bioactive molecules.[11] DNA was shown to support the template-directed formation of phosphoramidates,[12] nucleophilic substitution[13] and conjugate addition;[13] amine acylation,[14] reductive amination,[14] nitro-aldol and nitro-Michael addition,[14] Wittig olefination,[14] transition metal-catalyzed cross-coupling,[14] heterocycle formation,[15] cycloadditions,[15-16] and azide-alkyne cycloaddition (click reaction).[17]

A few examples on the nucleic acid template-directed synthesis of coordination complexes have also been reported.[18] High affinity of Schiff bases for metals makes them suitable ligands. The N,N′-bis(salicylidene)ethylendiamine or salen (SALEN) is

commonly used due to its catalytic properties. Since Salen formation from salicylaldehyde (Sal) and ethylenediamine is a reversible process, a driving force, such as metal ion coordination, for the reductive amination to occur is required in aqueous solution. The preorganization of an aldehyde and an amine close to each other onto a template entropically favors the formation of the condensation product in dilute samples, a strategy used early on in Inorganic Chemistry to form Salen complexes. In 1997, for the condensation of a 3′-end aldehyde group with the 5′-end amino group of two different oligonucleotides a ssDNA template was used in the absence of a metal ion.[19] Adjacent portions of the shorter ssDNA's were aligned on a complementary DNA template.

In a similar manner but in the presence of a metal ion, Czlapinski and Sheppard showed the formation of metallosen-DNA conjugates (Scheme V.1). Two salicylaldehyde fragments (**1** and **2**) situated at the opposite ends, either at the 3′ or 5′ end and directly attached to the terminal phosphate group of each strand, were preorganized on the DNA template **3**. Then the metallosalen conjugate was constructed by addition of a suitable metal, Mn^{2+} and diamine.

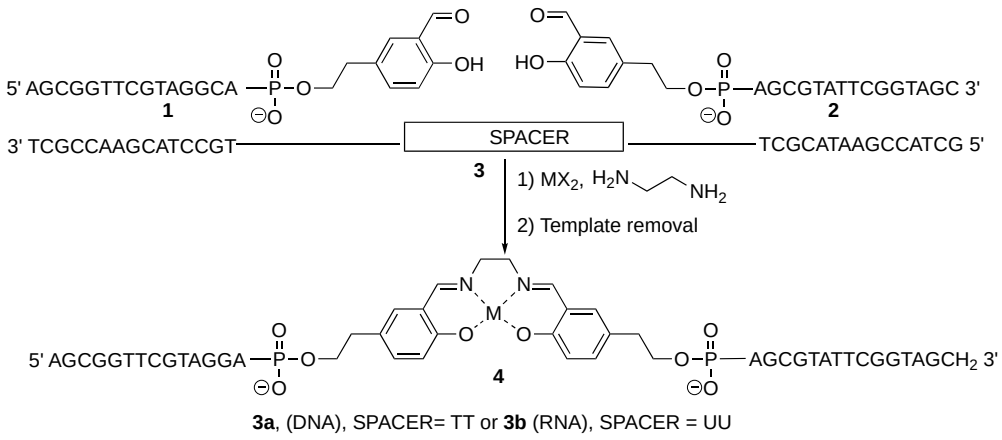

Scheme V.1 Template directed Metallosalen-DNA assembly

In a related approach, Czlapinski and Sheppard also showed the formation of non-

metallated and metallated Salen between two salicylaldehydes situated at the end of opposite strands in a 15-bp DNA duplex in the presence of ethylenediamine.[19] The two salicylaldehyde ligands **1** and **5** (Scheme V.2) were attached directly to the terminal phosphate group of each strand rather than to a sugar moiety; this type of anchoring of the ligands is likely to favor π-stacking of the ligands with the adjacent nucleobase pairs in a way similar to that in which overhang nucleobases stack at the end of a nucleic acid duplex.

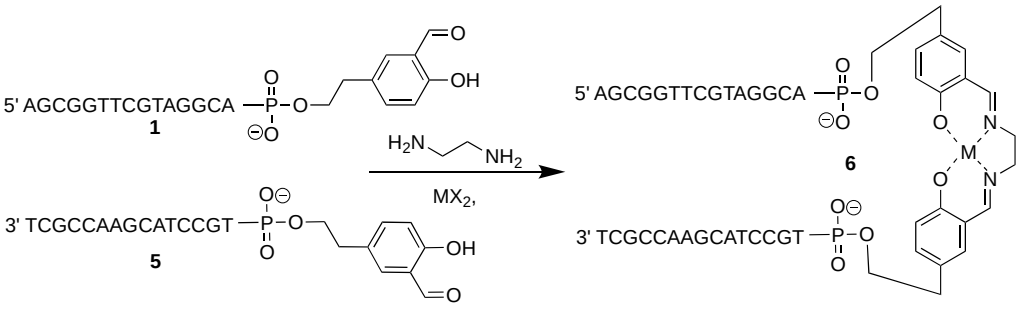

Scheme V.2 Template-directed assembly of metallosalen-DNA hairpins

V.2. Research Design

This project focused on the study of the use of metal coordination as means to "glue" concatenated short PNA strands organized on a long PNA template. Figure V.1a shows cartoon representation of the assembly with the two short PNAs in pink and light blue (*1*) hybridized to the purple long template and (*2*) connected to each other by a metal complex (red circle). The metal complex is formed with ligands attached to adjacent ends of the two short PNAs. This position of the metal complex within a strand of the duplex is in contrast to previous work from our lab that described formation of inter-strand coordination complexes that connected ligands situated in complementary positions in "opposite" strands of homo PNA/PNA duplexes (Figure V.1b).

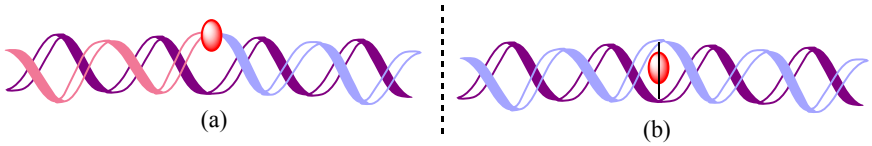

Figure V.1 Cartoon representation of, (a) a PNA-templated, intra-strand metal complex in a PNA/PNA homo-duplex and (b) PNA duplex that contains an inter-strand coordination complex

The assembly process is shown in Figure V.2. Two ligand-modified PNA strands are aligned on a complementary PNA template. The PNA/PNA hybridization brings the ligands in close proximity of each other in the duplex. Once the duplex was formed, a PNA-metal complex can form between the ligands **L** upon addition of a transition metal ion. Similar work was reported by Sheppard using DNA strands. [18] In his work, a Schiff base complex was formed upon addition of Mn^{2+} and between two 15-bp ssDNAs bearing aldehydes hybridized to a complementary 30-bp DNA template.

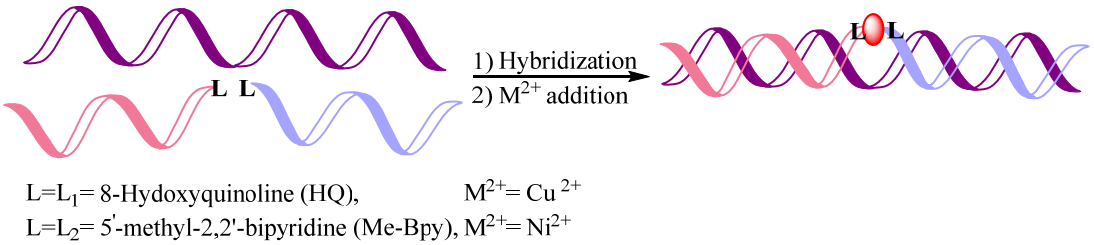

Figure V.2 Cartoon representation of PNA-metal duplex formation

Table V.1 shows the sequence of the PNA strands used in the study. The sequence of the short 9-mer PNAs and of the template were similar to those used for concatenation in Chapter III. The PNA Duplex 1 is "ligand-free. PNA Duplexes 2 and 6 are Q-modified. Duplexes 3 and 7 are Bpy-modified. PNA Duplexes 4 and 5 contain a pair of (Q, Bpy) ligands. After hybridization of the two 9-mer strands on the 20-bp PNA template to form a duplex, ligands were coordinated by Cu^{2+} and Ni^{2+} (Figure V.2). The ligands and metal ions were identified based on the stability constants for- and the size

of- the complexes they form (Table V.2). Either 8-hydoxyquinoline (Q) or 5'-methyl-2,2'-bipyridine (B) was inserted at the N- or C-end of 9-mer PNAs to obtain strands termed Q-PNA or Bpy-PNA, respectively. The ligands were attached to the side chain of Boc-DAP(Fmoc)-OH using solid phase strategy. This approach for inserting the ligand is similar to that used in an earlier study in which a bipyridine was attached to the side chain of an lysine.[20]

Table V.1 Sequences of PNA Duplexes

$PNA1_{C\text{-}Lys}$	NH_2-Lys_3-GAC CAC AGA T-T CAA ACA TGC-H	
$PNA3_{N\text{-}Lys}$	H-Lys-CTG GTG TCT A/A GTT TGT ACG-Lys-NH_2 $PNA4_{C\text{-}Lys}$	Duplex 1
$PNA1_{C\text{-}Lys}$	NH_2-Lys_3-GAC CAC AGA T-T CAA ACA TGC-H	
$PNA3_{C\text{-}A/Q}$	H-Lys-CTG GTG TCT Q/Q GTT TGT ACG-Lys-NH_2 $PNA4_{N\text{-}A/Q}$	Duplex 2
$PNA1_{C\text{-}Lys}$	NH_2-Lys_3-GAC CAC AGA T-T CAA ACA TGC-H	
$PNA3_{C\text{-}A/B}$	H-Lys-CTG GTG TCT B/B GTT TGT ACG-Lys-NH_2 $PNA4_{N\text{-}A/B}$	Duplex 3
$PNA1_{C\text{-}Lys}$	NH_2-Lys_3-GAC CAC AGA T-T CAA ACA TGC-H	
$PNA3_{C\text{-}A/B}$	H-Lys-CTG GTG TCT B/Q GTT TGT ACG-Lys-NH_2 $PNA4_{N\text{-}A/Q}$	Duplex 4
$PNA1_{C\text{-}Lys}$	NH_2-Lys_3-GAC CAC AGA T-T CAA ACA TGC-H	
$PNA3_{C\text{-}A/Q}$	H-Lys-CTG GTG TCT Q/B GTT TGT ACG-Lys-NH_2 $PNA4_{N\text{-}A/B}$	Duplex 5
$PNA1_{C\text{-}Lys}$	NH_2-Lys_3-GAC CAC AGA T-T CAA ACA TGC-H	
$PNA3_{C\text{-}A/Q}$	H-Lys-CTG GTG TCT Q	Duplex 6
$PNA1_{C\text{-}Lys}$	NH_2-Lys_3-GAC CAC AGA T-T CAA ACA TGC-H	
$PNA3_{C\text{-}A/B}$	H-Lys-CTG GTG TCT B	Duplex 7

Table V.2 Binding constants to HQ and Bpy[22]

	Ni^{2+}			r(Å)	Cu^{2+}			r(Å)
	Log β_1	**Log β_2**	**Log β_3**		**Log β_1**	**Log β_2**	**Log β_3**	
Q	9.27	26.1	-	0.69/0.55	12.1	22.9	-	0.73/0.57
B	7.0	13.9	20.2		8.0	13.5	16.9	

The UV spectra of Q-PNA oligomers in pH 7 sodium phosphate buffer are dominated by absorption bands at 260 and 247 nm, which correspond to π-π* transitions

of the nucleobases and the Q-ligand, respectively.[23-25] A broad band at 320 nm is due to π-π* transitions of Q. Addition of Cu^{2+} to Q-PNA duplexes is expected to induce a bathochromic shift of the ligand absorption band from 247 to 260 nm, the disappearance of the ligand π-π* band at 320 nm, and the appearance of a metal-to-ligand charge transfer band at 400 nm.[26] The stoichiometry of Cu^{2+} binding to Q-PNA can be determined from titration curves monitored at the wavelengths mentioned above if they show sharp inflection points which in turn is due to the complexes formed between Cu^{2+} and Q-PNA having large stability constants. If the titration curves show gradual changes, the stoichiometry of the complexes and the stability constants may be determined using simulations of the curves with Hypspec.

The UV spectra of Bpy-PNA oligomers are dominated by a broad, intense absorption band at 260 nm, which corresponds to π-π* transitions of the nucleobases. Metal coordination to bipyridine shifts the π-π* bands of the ligand from 235 nm and 280 nm to 245 nm and 295-320 nm.[27-28] The absorption band appearing at 295-320 nm is the only one that does not overlap significantly with the nucleobase absorption. To determine the stoichiometry of Ni^{2+} binding to Bpy-PNA, spectrophotometric titrations of Bpy-PNA with Ni^{2+} were performed by monitoring changes in absorbance at the wavelengths mentioned above.

In contrast to B-DNA, which has a chiral backbone, PNA has an achiral backbone. Consequently, B-DNA adopts a right handed helical structure while PNA duplexes show a preference for a given handedness only upon chiral induction by an enantiomerically pure component, such as an L-amino acid attached to the carboxy terminus of the PNA oligomers or a chiral center built into the aeg backbone.[29-30] In the

study described in this chapter, the chiral induction effect arises from the incorporation of L-Lys into the PNA oligomers. The chiral induction effect depends on the type of base pair that is adjacent to the chiral component of the PNA duplex, herein the L-Lys. Previous studies have shown that a GC base pair transmits the chiral effect of L-Lys more efficiently than an AT base pair, an observation that was attributed to the stronger hydrogen binding of GC base pair.[29]

V.3. Results

V.3.1. Variable-Temperature UV-Vis Spectroscopy

Variable temperature UV-Vis spectroscopy was used to evaluate changes in the stability of the PNA duplexes upon Cu(II) and Ni(II) binding. All the UV melting experiments have been monitored at 260 nm. Substitution of AT base pair with ligands that cannot form hydrogen bonds generally leads to destabilization of the PNA duplexes. Binding of these ligands can partially or totally reestablish the thermal stability.

Thermal denaturation experiments were performed for the Duplexes 1-7 in the absence and presence of transition metal (Figure V.3). Melting temperatures of each duplex in the absence and in the presence of a metal ion can be found in Table V.3. In the absence of any transition metal, the melting temperature T_m of Duplexes 1-7 varied between 71-76 ^oC. Addition of Cu^{2+} had a significant stabilization effect on Duplex 2 that contained 2 adjacent Q ligands and a smaller stabilization effect on Duplexes 4 and 5 that contained a mixed pair of Q/Bpy ligands. Addition of Ni^{2+} had a significant stabilization effect on Duplex 3 that contained 2 adjacent Bpy ligands. The stabilization by Cu^{2+} of Duplex 2 ($\Delta T_m = +9$) was larger than that by Ni^{2+} of Duplex 3 ($\Delta T_m = +5$).

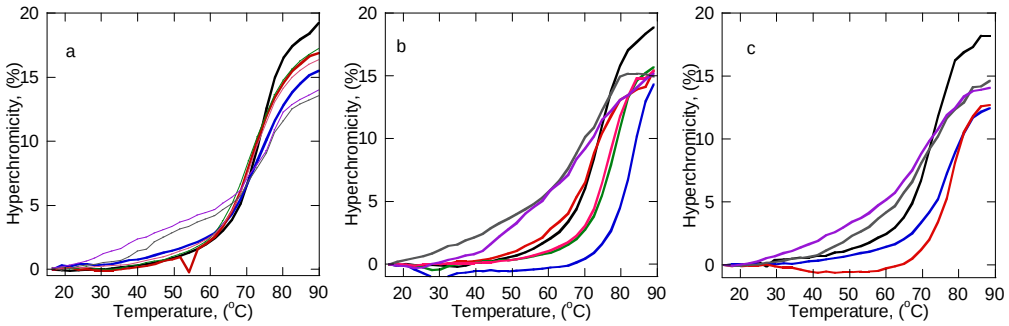

Figure V.3 Denaturation profiles measured at 260 nm for Duplexes 1-7 in the absence of metal ions (a) and in the presence of 1eq. M^{2+} $CuCl_2$ (b) and $NiCl_2$ (c). Solutions were prepared in pH 7 10 mM sodium phosphate buffer. The total concentration of ss PNA in each sample was 3 µM. (Black Line: Duplex 1); (Blue Line: Duplex 2); (Red Line: Duplex 3); (Green Line: Duplex 4); (Pink Line: Duplex 5); (Gray Line: Duplex 6); (Purple Line: Duplex 7).

Table V.3 Melting temperatures T_m (^oC) and change in the melting temperatures ΔT_m (^oC) for non-modified, Q-PNA and Bpy-PNA duplexes in the absence or presence of the metal ions.*

Duplex	**Type**	**without M^{2+}**	**1eq.Cu^{2+}**	**ΔT_m/Cu**	**1eq.Ni^{2+}**	**ΔT_m/Ni**
Duplex 1	No Ligand	73	74	+1	72	-1
Duplex 2	QQ	75	84	+9	77	+2
Duplex 3	Bipy-Bipy	72	71	-1	77	+5
Duplex 4	Q-Bipy	72	78	+6	-	-
Duplex 5	Bipy-Q	71	75	+4	-	-
Duplex 6	Q	77	74	-3	72	-5
Duplex 7	Bipy	76	73	-3	72	-4

*The total concentration of ssPNA in each sample was 3 µM. Solutions were prepared in pH 7 10 mM NaPi buffer. ΔT_m represents the difference between the melting temperature of the duplex formed in the presence and absence of the metal ion.

V.3.2. CD Spectroscopy

We have measured the CD spectra of ligand-modified PNA homo-duplexes in the absence and in the presence of the transition metal ions (Figure V.4). Duplex 1 had an L-Lysine and formed a left-handed helical structure as revealed by the negative features at

242 nm, 255 nm and positive feature at 276 nm in the CD spectra in the presence and absence of Cu^{2+} or Ni^{2+}.

The Q-PNA and Bpy-PNA Duplexes 2-7 contained an L-Lysine, which was anticipated to lead to a left-handed helical structure in the absence of any metal ion. However, upon addition of Cu^{2+} or Ni^{2+} to Duplexes 2 and 3-7, we observed distinct exciton coupling patterns with minima at 242 and 276 nm and maxima at 255 nm indicative of a right-handed helix structure. Addition of Ni^{2+} to Duplex 3 led to a left-handed helix, which suggests that the Bpy-Ni^{2+} complex significantly influences the transmission of the chiral effect through the duplex.

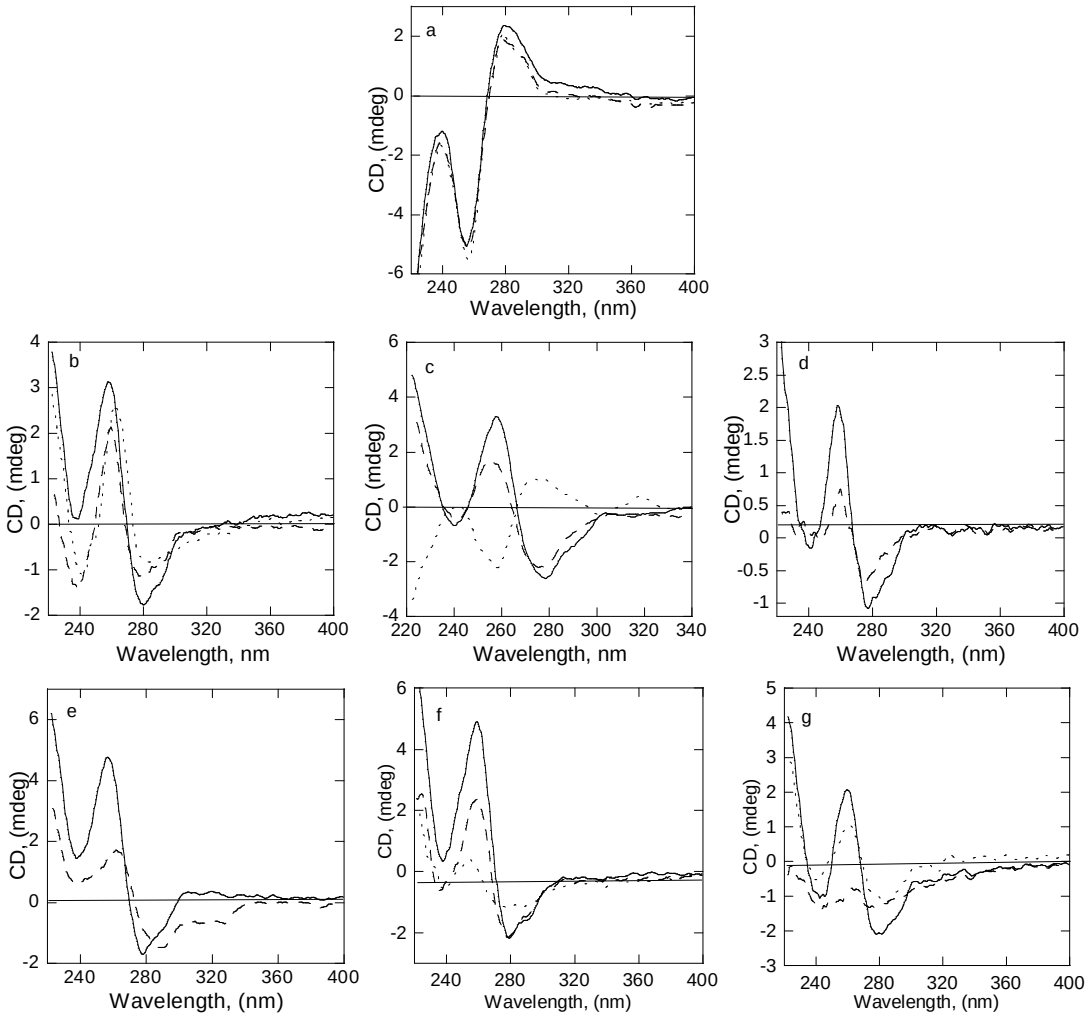

Figure V.4 CD spectra of annealed 3 μM a-g are for Duplexes 1-7, respectively. In the absence of metal ion (solid line); in the presence of 1 eq. of $CuCl_2$ (dashed line) and in the presence of 1 eq. of $NiCl_2$ (dotted line). Solutions were prepared in pH 7 10 mM sodium phosphate buffer.

V.3.3. Spectrophotometric Titrations

Spectrophotometric titrations with Cu^{2+} and Ni^{2+} were carried out for the free Q, free Bpy ligand, the Q-PNA, Q/Bpy-PNA and Bpy-PNA duplexes.

Titrations of Free Ligands Me_2Bpy and Q with Cu(II)

UV-visible titrations of Q and Bpy with Cu^{2+} were performed to determine the relative stability and the stoichiometry of metal complexes, as well as to provide reference spectra for titrations of ligand-modified PNA duplexes. Titrations of Q with

Cu^{2+} caused a bathochromic shift of the π-π* transitions of Q from 240 nm and 314 nm to 256 and 378 nm, respectively, which establishes that Cu^{2+} binds to Q.[24, 31] The titration curve of Q with Cu^{2+} monitored at 243 nm and 380 nm showed an inflection point at a Cu^{2+}/Q ratio of 1:2, indicating the formation of a $[CuQ_2]$ complex (Figure V.5).

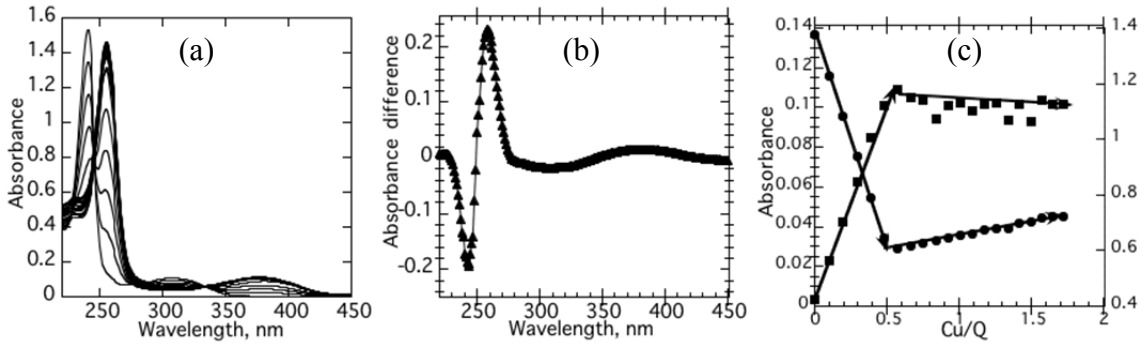

Figure V.5 Spectrophotometric titration of 40 μM Q with 500 μM Cu^{2+}, 10 mM NaPi buffer (a) Titration spectra (b) difference spectrum (c) and titration curves at 380 nm (filled square) and 243 nm (filled circle).

Complexation of free Bpy with Cu^{2+} caused a bathochromic shift of the ligand π-π* transitions situated at 277 nm to 302 nm-310 nm. The titration curve of Bpy with Cu^{2+} showed an inflection point at a Cu^{2+}/Bpy ratio of 1:1, indicating the formation of a $[CuBpy]^{2+}$ complex (Figure V.6). Note that the coordination of Cu^{2+} will be higher than 2, with the other 3-4 ligands being water, buffer molecules and/or nucleobases adjacent to Bpy.

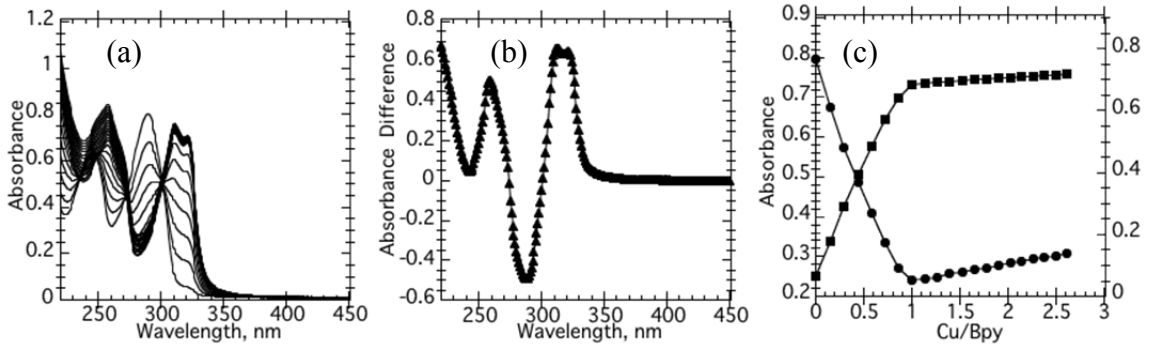

Figure V.6 Spectrophotometric titration of 50 μM Bpy with 1000 μM Cu(II), 10 mM NaPi buffer (a) Titration spectra (b) difference spectra (c) and titration curves at 316 nm (filled square) and 289 nm (filled circle).

The titration curve of Q and Bpy with Ni^{2+} showed an inflection point at a Ni^{2+}:Q ratio of 1:2 and at a Ni^{2+}:Bpy ratio of 1:2, indicating the formation of $[NiQ_2]$ and $[Ni(Bpy)_2]$ complexes (Figure V.12 and Figure V.13).

Titrations of Q-PNA and Bpy-PNA Duplexes

The UV-Vis spectra of the Q-PNA duplexes in the presence of increasing amounts of Ni^{2+} and Cu^{2+} are shown in Figure V.7a and Figure V.8a, Figure V.14 and Figure V.16. The intensity of the absorption bands at 246 nm and 320 nm, which arise from π-π* transitions of the non-coordinated Q ligands, and of the 410 nm band caused by π-π* transitions of the coordinated Q, decreased and increased, respectively. These spectral changes establish that Ni^{2+} and Cu^{2+}coordinate to the Q ligands in the Q- PNA duplexes. The UV-Vis spectra of the Bpy-PNA duplexes in the presence of increasing amounts of Cu^{2+} and Ni^{+2} and the corresponding titration curves are shown in Figure V.7b, Figure V.8b, Figure V.13 and Figure V.15. The absorbance band at 260 nm is caused by π-π* transitions of the nucleobases; its intensity changed upon addition of the metal ions. New absorption bands arising from π-π* transitions of the coordinated Bpy are observed at 300-330 nm upon addition of the metal ions.

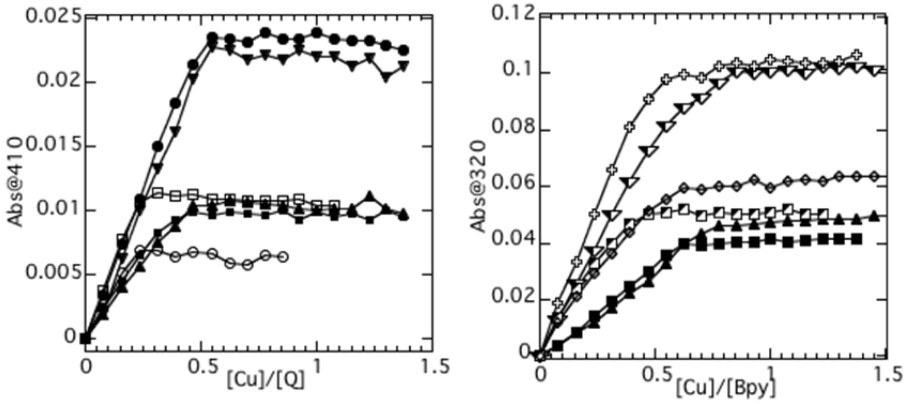

(a) (b)

Figure V.7 Spectrophotometric titrations of 5 μM solutions of Q-PNA (a) and Q-Bpy duplexes (b) in pH 7 10 mM NaPi buffer with $CuCl_2$. The titration curves were monitored at 410 and 320 nm. (Duplex 2: filled circle and down pointing triangle; Duplex 3: half-filled triangle and plus sign; Duplex 4: filled square; Duplex 5: up pointing triangle; Duplex 6: unfilled square and unfilled circle; Duplex 7: half-filled square and diamond)

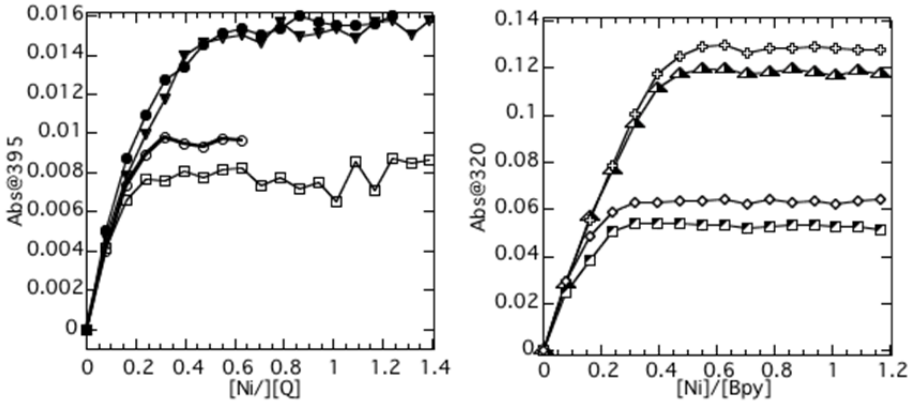

(a) (b)

Figure V.8 Spectrophotometric titrations of 5 μM (a) Q-PNA and (b) Q-Bpy duplexes in pH 7 10 mM NaPi buffer with $NiCl_2$. The titration curves with Ni^{2+} were monitored at 410 and 320 nm. (Duplex 2: filled circle and down pointing triangle; Duplex 3: half-filled triangle and plus sign; Duplex 6: unfilled square and unfilled circle; Duplex 7: half-filled square and diamond).

Examination of the Figure V.7a shows that the titration curves for Duplex 2 shows an inflection point at Cu/Q = 1:2 ratio, which is indicative of the formation of $[CuQ_2]$ complexes, as expected if a metal complex forms with the two Q ligands situated at adjacent ends of the two short 10-base Q-PNA hybridized onto the complementary 20-

mer PNA oligomer. An inflection point at the same Cu/Q= 1:2 ratio is observed for duplexes 4 and 5, which contain only one Q ligand per concatenated duplex. This result is in agreement with the coordination of one Cu^{2+} per pair of Q, Bpy ligands to form mixed ligand [CuQ(Bpy)] complexes. This coordination of Cu in Duplexes 2, 4, and 5 is also supported by the fact that the change in absorbance at 410 nm for Duplex 2 is ~twice as large than for the change in absorbance measured at the same wavelength for Duplexes 4 and 5.

Examination of the Figure V.7b and Figure V.8b reveals that the titration curves monitored at 320 nm for Duplex 3, 4, 5 show a less sharp inflection point than those monitored at 410 nm, suggesting that the CuQ complexes formed with the duplexes are more stable than the CuBpy complexes. This makes it problematic to determine the stoichiometry of the $[M(Bpy)_n]^{2+}$ complexes from titration curves. Nevertheless, an inflection point is apparent at Cu/Bpy = 1:2 ratio, which is indicative of the formation of $[CuBpy_2]$ complexes, as expected if a metal complex forms with the two Bpy ligands situated at adjacent ends of the two short 10-base B-PNA hybridized onto the complementary 20-mer PNA oligomer. An inflection point at the same Cu/B = 1:2 ratio is observed for duplexes 4 and 5, which contain only one Bpy ligand per concatenated duplex. This result is in agreement with the coordination of one Cu^{2+} per pair of Q, Bpy ligands to form mixed ligand [CuQ(Bpy)] complexes. This coordination of Cu in Duplexes 3, 4, and 5 is also supported by the fact that the change in absorbance at 320 nm for Duplex 3 is ~twice as large than for the change in absorbance at the same wavelength measured for Duplexes 4 and 5.

Table V.4. Stoichiometry for complexes formed between metal ions and Bpy and Q-PNA oligomers and duplexes based on inflection points of UV titrations.

Ligands/Duplex	Ligand	[Cu]/[L]	[Ni]/[L]
Free ligands	Q	0.5	0.5
	Bpy	1	0.5
Duplex 2	Q-Q	0.5	0.5
Duplex 3	Bipy-Bipy	0.5	0.5
Duplex 4	Q-Bipy	0.5	-
Duplex 5	Bipy-Q	0.5	-

The stability constants for metal complexes formed with the free Bpy ligand and with several types of Bpy-PNA duplexes have been obtained from UV-Vis data using Hypspec. These constants are shown in Table V.5 and the corresponding duplexes are shown in Figure V.9.

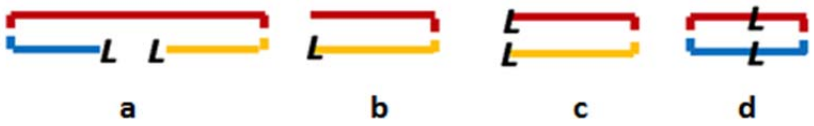

Figure V.9 Cartoon representation of the Bpy-PNA duplexes for which stability constants were obtained from UV titrations using Hypspec. (a) Duplex 3; (b) Duplex 7; (c) 10bp-dsPNA(MeBpy) (d) 10bp-dsPNA(MeBpy)$_2$end (e) 10bp-dsPNA(MeBpy)$_2$center

Table V.5 The stability constants for metal complexes formed with the free ligands or Bpy-PNA obtained from UV-Vis data using Hypspec.

Ligand	logβ_2
MeBpy	10.74
MeBpy$_2$	10.90
Duplex 3	12.88
10bp-dsPNA(MeBpy)	10.35
10bp-dsPNA(MeBpy)$_2$end	9.2
10bp-dsPNA(MeBpy)$_2$center	11.16

The stability constants measured for complexes of Ni^{2+} with the free MeBpy and $MeBpy_2$ are smaller than those reported in the literature ($\log\beta_2 = 13.9$).[22] We attribute this difference to the fact that our stability constants are apparent and have been measured by UV-Vis spectroscopy under different experimental conditions than the ones used in the earlier studies, which were measured by potentiometric titration. The solutions for the potentiometric titration contained sodium acetate, hydrochloric acid and potassium chloride[32] whereas solutions for our UV-Vis titrations were in pH 7.0 10 mM sodium phosphate buffer.

The substitution of a natural base pair situated near the center of a PNA duplex with a pair of ligand is known to decrease the duplex's stability; this is in contrast to a ligand modification near the end of the duplex, which does not affect much the duplex stability.[4] Previous research also showed that the introduction of a metal base pair that has a non-planar geometry disturbs the base stacking of adjacent nucleobases and reduces the stability of the duplex. Therefore, we would expect to see a decrease in the complex stability when ligands were placed in the center. Interestingly, binding constants for duplexes a and d (Table V.5), where the ligands were located in complementary position in the duplexes, were $\log\beta_2 = 12.88$ and 11.16, respectively. The binding constants for duplexes b and c where the ligands were located at the end of the duplexes, were $\log\beta_2 =$ 10.35 and 9.2, respectively.

To evaluate the effect of temperature on binding constants, we measured the UV-absorption spectra of duplexes at high and low temperature the presence and absence of metal ions. Figure V.10 is representation of these spectra obtained for Duplex 2 and Duplex 3 in the presence or absence of metal ions at different temperatures. Presence of

absorptions bands corresponding to Cu(Bpy-PNA)$_2$ or Cu(Bpy-PNA)$_2$ demonstrates Cu^{2+} binds to Q and Bpy at both temperatures.

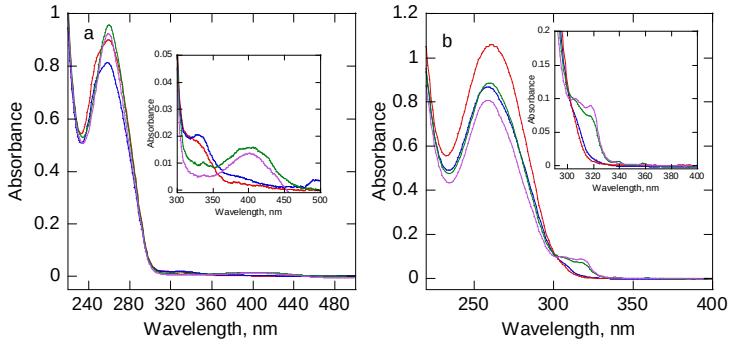

Figure V.10 UV absorption spectra of (a) Duplex 2 and (b) Duplex 3 with and without Cu^{2+} ion at 90 ^{o}C and 15 ^{o}C. Red and blue lines are showing the absorptions at 90 ^{o}C and 15 ^{o}C without metal ion, respectively; green and purple lines are showing the absorptions at 90 ^{o}C and 15 ^{o}C in the presence of Cu^{2+} ion, respectively.

V.4. Conclusions

Inclusion of ligands at adjacent ends of two 10-base PNAs hybridized to a template has a very small effect on the stability of the concatenated duplex. T_m of Q- and Bpy-containing concatenated PNA duplexes were between 71 and 76 ^{o}C. Metal coordination increased the thermal stability of ligand-modified concatenated PNA duplexes, which supports the idea that a metal complex bridges the two short PNAs hybridized to the long PNA template. Upon addition of the metal, T_m's of Q and Bpy containing PNA duplexes increased. The bridges between hybridized ligand-containing 10 base PNA strands are ML_2 complexes. The metal complex formed in the middle of the duplex can affect the handedness of the concatenated duplex. In the absence and in the presence of a metal ion Q-containing PNA duplexes showed a right-handed helical structure. The same is true for Bpy-containing duplexes except for the Bpy pair containing duplex in the center, which has right-handed helical structure in the absence of metal ion and left- handed only upon addition of the Ni^{2+}. The binding constants for the

concatenated duplexes by metal complexes are similar to those of duplexes that contain the same metal complexes as alternative base pair.

V.4.1. Materials and Methods

Oligomer Synthesis

Boc-PNA monomers were purchased from PolyOrg, Inc and used without further purification. PNA oligomers were synthesized manually on methyl benzhydryl amine (MBHA) resin (0.45 meq/g) by standard solid-phase peptide synthesis methods. The MBHA resin (1.0 g) was down-loaded to 0.1 mmol/g with Boc-Dap(Fmoc)-OH or with the first monomers for the Boc-PNA oligomers (100 mg resin). The resin was first swelled in DCM for 1 h. The following solutions were prepared: 0.2 M Boc-Dap(Fmoc)-OH or Boc-Lys-(2-Cl-Z)-OH in NMP (A), 0.2 M HATU in NMP (B), and 0.5 M DIEA in NMP (C). These solutions were then combined appropriately to give two additional solutions: 0.45 mL of A + 0.46 mL of C + 1.59 mL NMP (Solution I), and 0.55 mL of B + 1.95 mL NMP (Solution II). Solutions I and II were pre-mixed for 1 min and then added to the resin. The resulting mixture was agitated for 4hours. The resin was subsequently washed with DMF (2x), DCM (4x), once with 5% DIEA in DCM (agitate 30 seconds), and again with DCM (4x). The remaining active sites were then capped with a 1:2:2 solution of Ac_2O:NMP:pyridine (1.5 h), followed by DCM (4x) washes and a qualitative Kaiser test [in a 1.5 mL centrifuge tube, added a few beads of resin 1 drop of Monitor 1 (8g of phenol dissolved in 2 mL EtOH) and 2 drops of Monitor 2 (13 mg KCN/20 mL water. Dilute 200 μL of KCN aqueous solution with 9800 μL L pyridine)] and 1 drops Monitor 3 (1 g ninhydrin in 20 mL ethanol) to confirm that all the unreacted primary amines were capped. The resin was allowed to dry under vacuum. The loaded

resin was stored at -20 ^{o}C for further use. To make, C-end ligand (HQ or 5'-Me Bipy) containing PNA oligomers, resin downloaded with Fmoc-Dap(Boc)-OH was used. For introducing the ligand moity either 2-(8-(hydroxymethyl)quinolin-5-yl)acetic acid or 2-(5'-methyl-[2,2'-bipyridin]-5-yl)acetic acid, the loaded resin (100 mg) was swelled in DCM for 1 h. The solvent was drained using positive air pressure and to deprotect Fmoc-group from the side chain of the Boc-Dap(Fmoc)-OH, a solution of 20% Piperidine in DMF was added to the resin. The resin was shaken for 5 min, and the solution was removed using positive air pressure. The Fmoc deprotection was repeated (2x 10 min). This was followed by subsequent washes with DMF (2x), DCM (2x), DMF (2x). Kaiser test was performed to verify the effectiveness of deprotection. After positive Kaiser test, 150 μL of 0.2 M monomer solution in NMP was premixed with 150 μL of 0.8 M MDCHA in pyridine and 300 μL of 0.1 M HBTU in DMF for 1 min and then added immediately to the resin. The resin was shaken for 30 min. Following coupling, the solution was removed using positive air pressure and the resin was washed with DMF (3x), 5% DIEA/DCM (1x 30 sec) and DCM (2x). Once more, a qualitative Kaiser test was performed and, if negative, the resin was capped with a 1:25:25 mixture of Ac_2O: NMP: piperidine (2 x 2 min). The capping step was followed by washes with DCM (1x), 20% piperidine/DMF (1x) and then DCM (3x). After inserting the ligand to the resin, for rest of the steps regular boc-methodology was applied.

The following is a representative coupling cycle for one Boc-PNA monomer. A solution of 5% m-cresol in TFA was added to the resin. The resin was shaken for 4 min, and the solution was removed using positive air pressure. The TFA deprotection was repeated (2x 4 min). This was followed by subsequent washes with DCM (2x), DMF

(2x), DCM (2x), and pyridine (1x). Kaiser test was performed to verify the effectiveness of deprotection. After positive Kaiser test, 150 μL of 0.2 M monomer solution in NMP was premixed with 150 μL of 0.8 M MDCHA in pyridine and 300 μL of 0.1 M HBTU in DMF for 1 min and then added immediately to the resin. The resin was shaken for 30 min. Following coupling, the solution was removed using positive air pressure and the resin was washed with DMF (3x), 5% DIEA/DCM (1x 30 sec) and DCM (2x). Once more, a qualitative Kaiser test was performed and, if negative, the resin was capped with a 1:25:25 mixture of Ac_2O: NMP: pyridine (2 x 2 min). The capping step was followed by washes with DCM (1x), 20% piperidine/DMF (1x) and then DCM (3x). This cycle was then repeated until the last monomer was coupled.

In order to make, N-end ligand (HQ or 5'-Me Bipy) containing PNA oligomers, resin downloaded with Boc-Lys-(2-Cl-Z)-OH(100 mg) was used and until the addition of the last monomer regular Boc-strategy was applied. After introducing the last Boc-PNA monomer, Boc-group was deprotected and coupled with Fmoc-Dap(Boc)-OH. Next, a negative Kaiser test was followed by capping. To remove the Fmoc-deprotection group, Fmoc-deprotection procedure described above was followed. After washings and the positive Kaiser test, side chain of the Boc-Dap(NH_2)-OH was coupled either with 2-(8-(hydroxymethyl)quinolin-5-yl)acetic acid (Q-CH_2COOH) or 2-(5'-methyl-[2,2'-bipyridin]-5-yl)acetic acid (Me-Bpy-CH_2COOH).

Upon completion of the last monomer coupling, the oligomers were cleaved from the resin (and the protecting groups were simultaneously removed) by immersing the resin in a cocktail containing m-cresol/thioanisole/TFA/TFMSA (1:1:2:6; 150/150/900/300 μL for 100 mg of resin) for 1 h and precipitated with cold diethyl ether.

PNA strands were purified by reverse-phase HPLC using a C18 column (5 μm; 19 × 100 mm; Waters Corporation, Milford, MA) and were subsequently lyophilized for long-term storage. Characterization of the oligomers was performed by MALDI-TOF on an Applied Biosystems Voyager Biospectrometry Workstation using R-cyano-4-hydroxycinnamic acid matrix (10 mg/mL in 1:1 water/acetonitrile, 0.1% TFA).

Table V.6 PNA Oligomer sequences and duplexes

Oligomer	Oligomer sequence N to C	Cal. MW	Obs. MW
$PNA1_{C\text{-}Lys}$	H-CGT ACA AAC T TAG ACA CCA G Lys_3-NH_2	5783.55	5782.34
$PNA3_{N\text{-}Lys}$	H-Lys-CTG GTG TCT A-NH_2	2861.83	2861.82
$PNA3_{C\text{-}A/Q}$	H-Lys-CTG GTG TCT Dap(Q)-NH_2	2857.83	2877.83
$PNA3_{C\text{-}A/B}$	H-Lys-CTG GTG TCT Dap(B)-NH_2	2882.89	2903.02
$PNA4_{C\text{-}Lys}$	H-AGT TTG TAC G-Lys-NH_2	2885.85	2886.97
$PNA4_{N\text{-}A/Q}$	H-Dap(Q) GTT TGT ACG NH_2	2881.84	2902.52
$PNA4_{N\text{-}A/B}$	H-Dap(B) GTT TGT ACG NH_2	2906.90	2928.23

***** Dap= 3-amino-L-Alanine

Variable Temperature UV Spectroscopy

Melting temperature experiments were performed in 10-mm path length quartz cells on a Varian Cary 300 spectrophotometer equipped with a programmable temperature block. PNA stock solutions were prepared in deionized water and were stored at -18 °C. The PNA solutions for UV and CD experiments were in pH 7.0 10 mM phosphate buffer. The concentration of these solutions was determined by UV absorption at 95 °C using the sum of the published extinction coefficients at 260 nm; ε_{260} of the constituent PNA monomers were taken to be 8600 M^{-1} cm^{-1} for T, 6600 M^{-1} cm^{-1} for C , 13700 M^{-1} cm^{-1} for A, and 11700 M^{-1} cm^{-1} for G.[33-34]

UV melting curves were recorded in the temperature range 15°C to 95°C. The rate of both cooling and heating was 1°C/min. Prior to the measurement of the melting profiles, the solutions were kept at 15°C for at least 10 min. The melting temperature T_m was taken at the inflection point of the Boltzmann sigmoidal fit function, which assumes a two-state model.

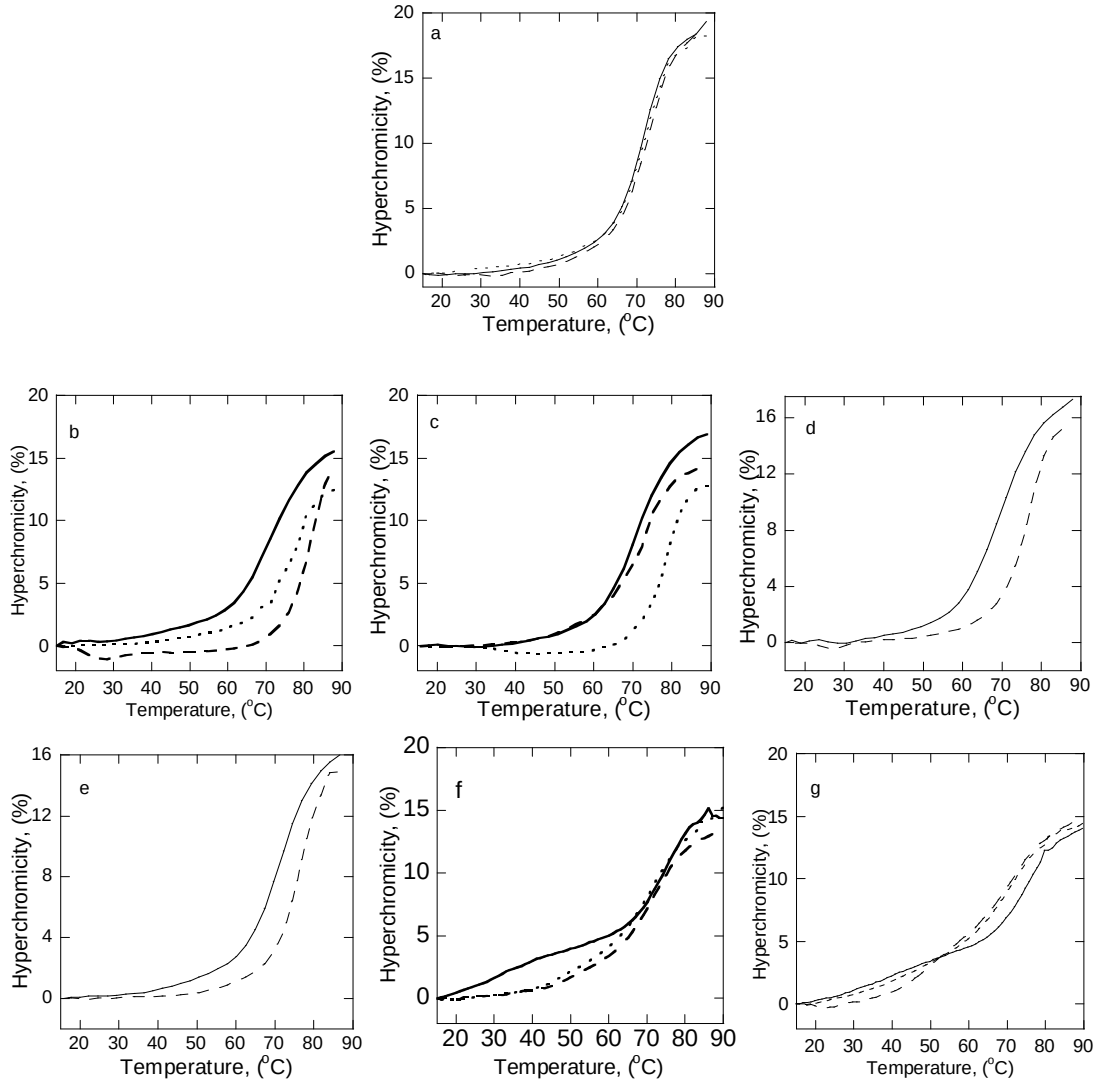

Figure V.11 Denaturation profiles a-g measured at 260 nm for Duplexes 1-7 in the absence of metal ions (solid line) and in the presence of 1eq. M^{2+} $CuCl_2$ (dashed line) and $NiCl_2$ (dotted). Solutions were prepared in pH 7 10 mM sodium phosphate buffer. The total concentration of ss PNA in each sample was 3 μM. (a-g/ Duplex 1/Duplex 7, respectively.

Spectrophotometric Titrations

The UV-Vis spectra were recorded on a Varian Cary 50 spectrophotometer as a function of the metal concentration. PNA stock solutions have been prepared with nanopure water and have been stored at -18 ^{o}C. The concentration of PNA oligomers was determined by UV absorption at 90 ^{o}C using the sum of the extinction coefficients of the constituent nucleosides ε260 taken from the literature.[33] The extinction coefficient for 8-hydroxyquinoline and 5-methyl bipyridine (ε260 = 2570 M cm^{-1} and 9770 M cm^{-1}, respectively at pH = 7.0) were also taken from literature.[4-5] PNA solutions for melting curves and titrations had concentrations in the micromolar range (3-5 μM) and have been prepared in 10 mM pH 7.0 phosphate buffer; the samples were annealed prior to titrations by slow cooling from 90 to 20 °C. UV-Vis titrations have been carried out by addition of standard 11.5 mM $CuCl_2$ and 10.3mM $NiCl_2$ solutions in water to PNA solutions. The ΔAbs values were obtained by correcting the absorbance measured after each addition for dilution and PNA absorption.

UV-Vis titration curves of the free Bpy ligand and Duplex 3 and Duplex 7 were analyzed using Hypspec and obtained stability constants were used to calculate the corresponding speciation diagrams.[21]

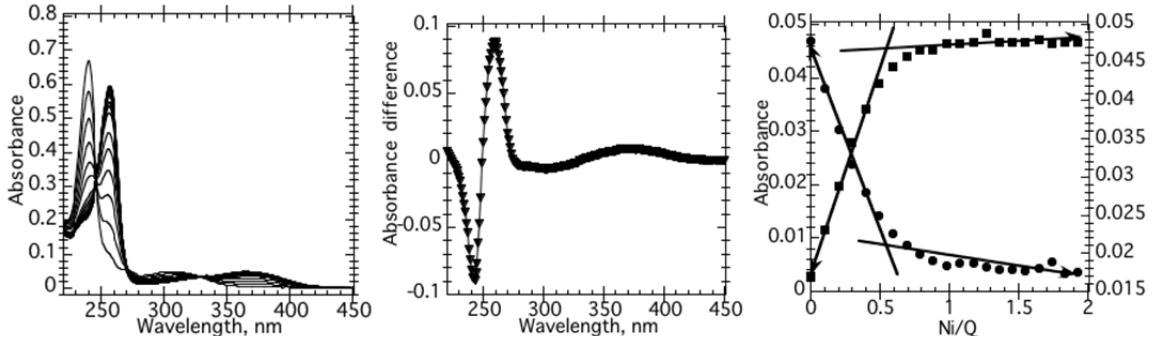

(a) (b) (c)

Figure V.12 Spectrophotometric titration of 20 μM Q with 1000 μM Ni(II), 10 mM NaPi buffer (a) Titration spectra (b) difference spectra (c) and titration curves at 372 nm (filled square) and 303 nm (filled circle).

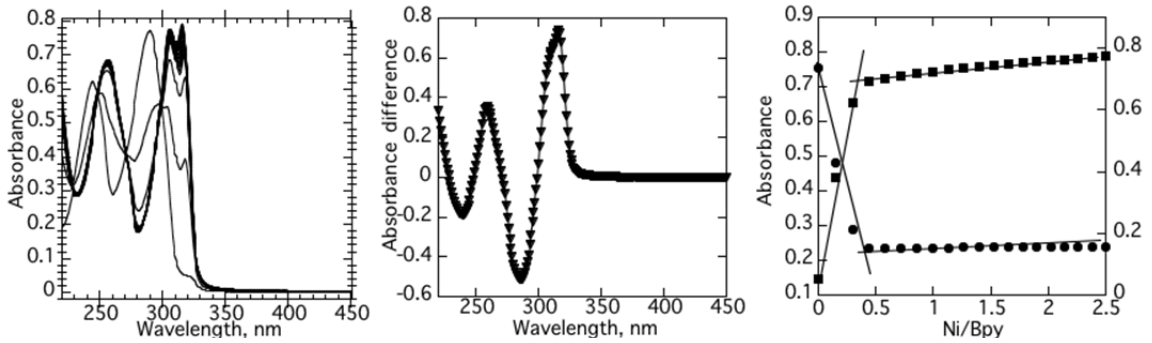

(a) (b) (c)

Figure V.13 Spectrophotometric titration of 50 μM Bpy with 1000 μM Ni(II), 10 mM NaPi buffer (a) Titration spectra (b) difference spectra (c) and titration curves at 317 nm (filled square) and 303 nm (filled circle).

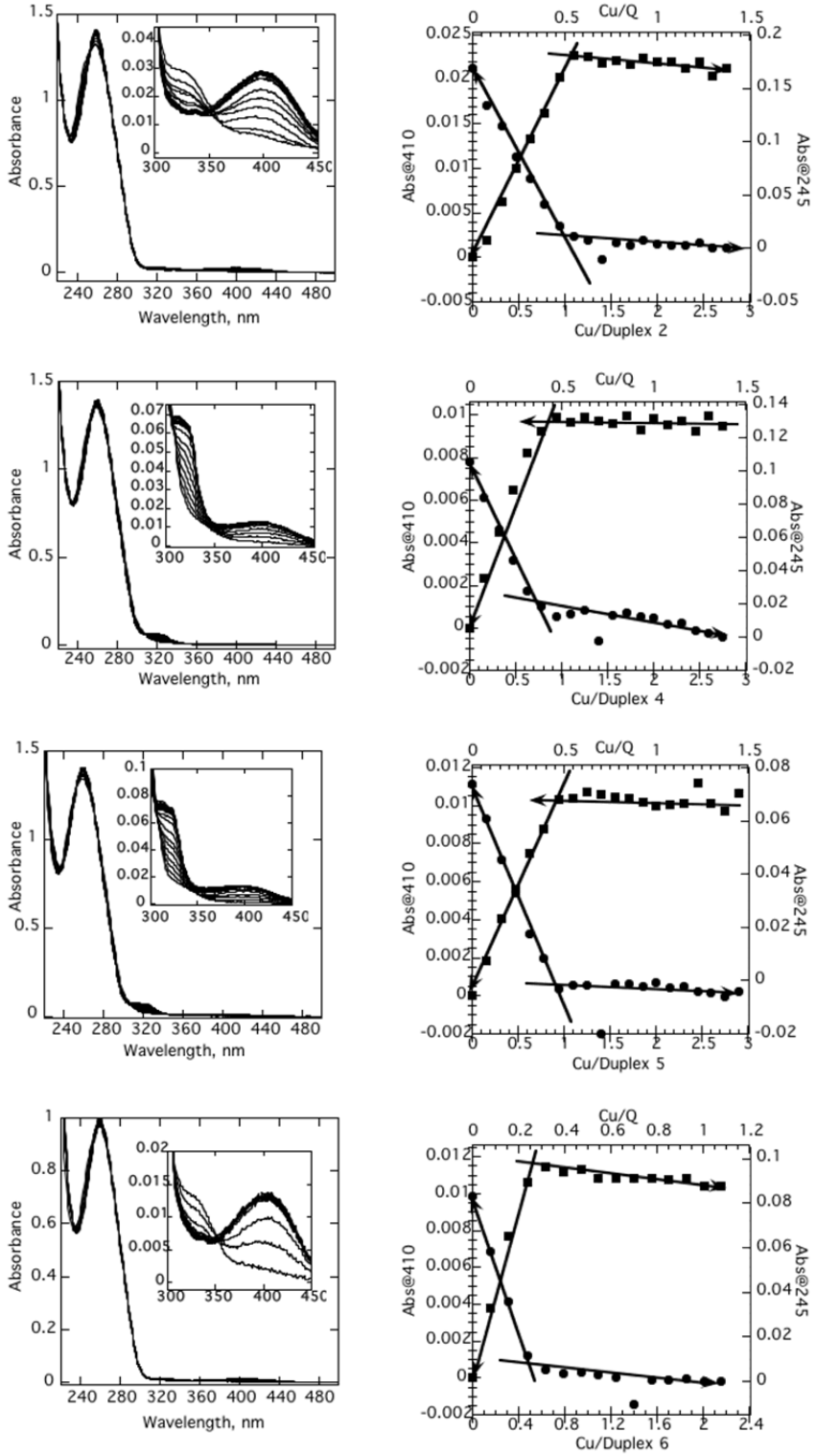

Figure V.14 Spectrophotometric titrations of 5 μM Q-PNA duplexes in pH 7 10 mM NaPi buffer with $CuCl_2$. The titration curves with Cu^{2+} were monitored at 410 and 245 nm.

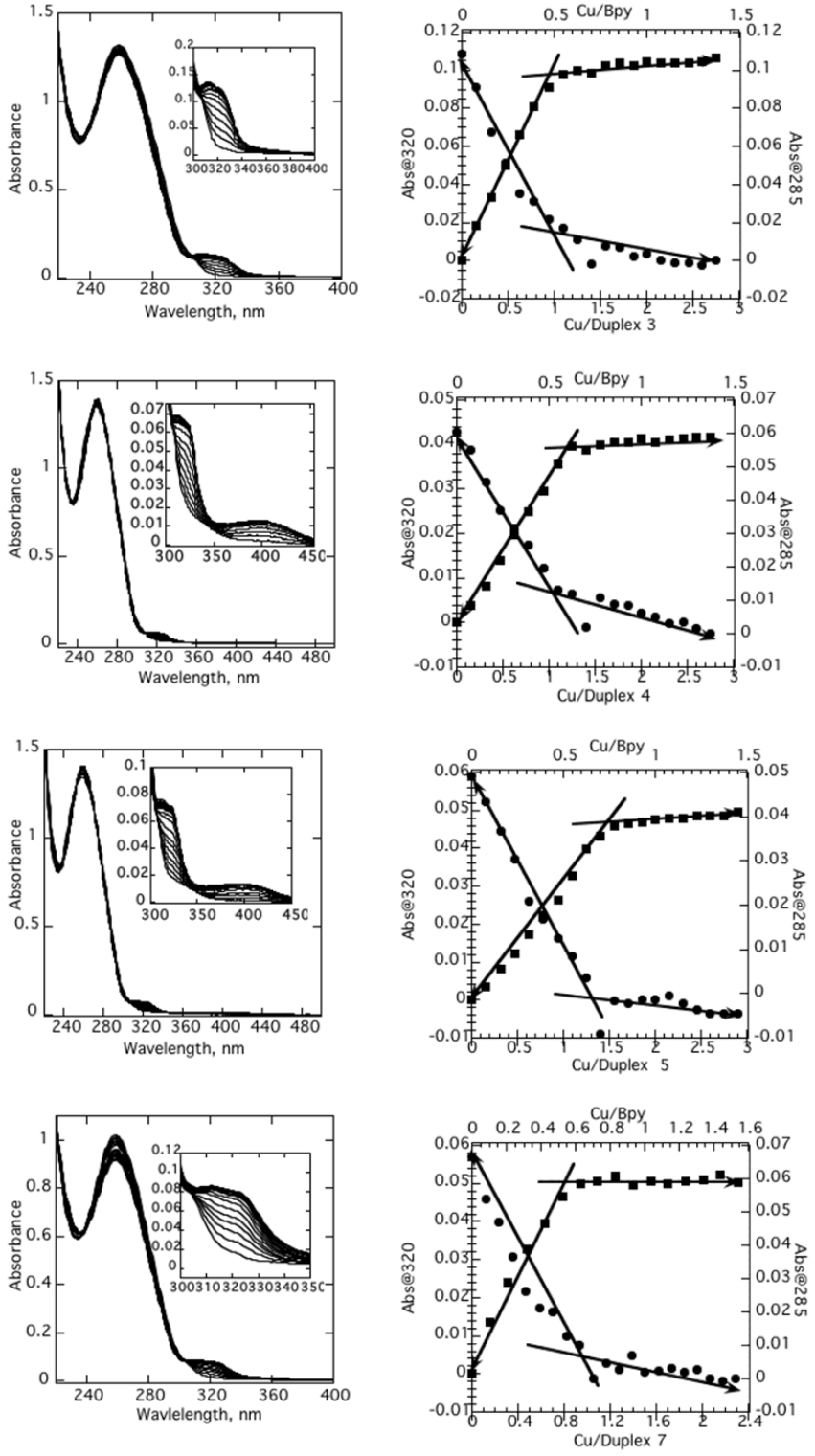

Figure V.15 Spectrophotometric titrations of 5 μM Bpy-PNA duplexes in pH 7 10 mM NaPi buffer with $CuCl_2$. The titration curves with Cu^{2+} were monitored at 320 and 285 nm.

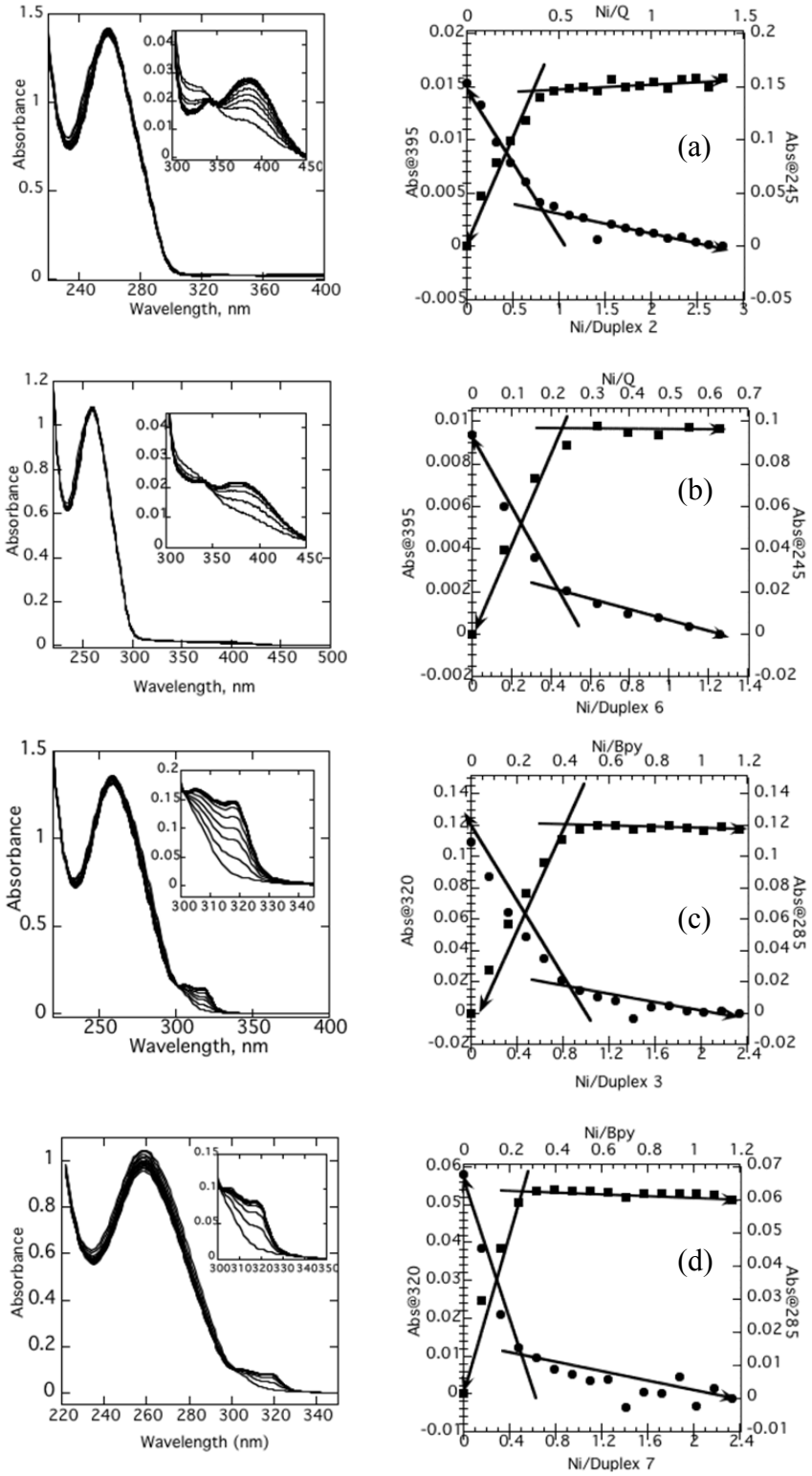

Figure V.16 Spectrophotometric titrations of 5 μM Q-PNA duplexes in pH 7 10 mM NaPi buffer with $NiCl_2$. The titration curves with Ni^{2+} were monitored at 395 and 245 nm (a and b) and at 320 and 285 nm (c and d).

Circular Dichroism (CD)

CD spectra have been measured for 3-5 μM total PNA concentration in pH 7.0 10 mM sodium phosphate buffer solutions. In the case where complementary PNA strands have been used, solutions have been equimolar in the two strands. CD measurements have been conducted on a JASCO J-715 spectropolarimeter equipped with a thermoelectrically controlled, single-cell holder. CD spectra have been collected using bandwidth 1 nm, response time 1 s, speed 50 nm/min, sensitivity 20 mdeg, and scan accumulation 20. All CD data were recorded at 20 ^{o}C. All spectra represent, an average of at least 10 scans recorded from 400 to 220 nm, were processed using KaleidaGraph software.

V.5. References

1. Rothemund, P. W. K., Folding DNA to create nanoscale shapes and patterns. *Nature* **2006,** *440* (7082), 297-302.
2. Liu, S.; Clever, G. H.; Takezawa, Y.; Kaneko, M.; Tanaka, K.; Guo, X.; Shionoya, M., Direct Conductance Measurement of Individual Metallo-DNA Duplexes within Single-Molecule Break Junctions. *Angew. Chem. Int. Ed.* **2011,** *50* (38), 8886-8890.
3. Wierzbinski, E.; de Leon, A.; Davis, K. L.; Bezer, S.; Wolak, M. A.; Kofke, M. J.; Schlaf, R.; Achim, C.; Waldeck, D. H., Charge Transfer through Modified Peptide Nucleic Acids. *Langmuir* **2012,** *28* (4), 1971-1981.
4. Franzini, R. M.; Watson, R. M.; Patra, G. K.; Breece, R. M.; Tierney, D. L.; Hendrich, M. P.; Achim, C., Metal Binding to Bipyridine-Modified PNA. *Inorg. Chem.* **2006,** *45* (24), 9798-9811.
5. Ma, Z.; Olechnowicz, F.; Skorik, Y. A.; Achim, C., Metal Binding to Ligand-Containing Peptide Nucleic Acids. *Inorg. Chem.* **2011,** *50* (13), 6083-6092.
6. Popescu, D.-L.; Parolin, T. J.; Achim, C., Metal Incorporation in Modified PNA Duplexes. *J. Am. Chem. Soc.* **2003,** *125* (21), 6354-6355.
7. Watson, R. M.; Skorik, Y. A.; Patra, G. K.; Achim, C., Influence of Metal Coordination on the Mismatch Tolerance of Ligand-Modified PNA Duplexes. *J. Am. Chem. Soc.* **2005,** *127* (42), 14628-14639.
8. Calderone, C. T.; Liu, D. R., Nucleic-acid-templated synthesis as a model system for ancient translation. *Curr. Opin. Chem. Biol.* **2004,** *8* (6), 645-653.
9. McKee, M. L.; Milnes, P. J.; Bath, J.; Stulz, E.; Turberfield, A. J.; O'Reilly, R. K., Multistep DNA-Templated Reactions for the Synthesis of Functional Sequence Controlled Oligomers. *Angew. Chem. Int. Ed.* **2010,** *49* (43), 7948-7951.
10. Mandal, M.; Bandyopadhyay, A., Engineering of DNA templated tri-functional nano-chain of Fecore–Aushell and a preliminary study for cancer cell labeling and treatment. *J Adv Res.* **2012,** *3* (4), 359-363.
11. Gorska, K.; Winssinger, N., Reactions Templated by Nucleic Acids: More Ways to Translate Oligonucleotide-Based Instructions into Emerging Function. *Angew. Chem. Int. Ed.* **2013,** *52* (27), 6820-6843.
12. Luther, A.; Brandsch, R.; von Kiedrowski, G., Surface-promoted replication and exponential amplification of DNA analogues. *Nature* **1998,** *396* (6708), 245-248.
13. Gartner, Z. J.; Liu, D. R., The Generality of DNA-Templated Synthesis as a Basis for Evolving Non-Natural Small Molecules. *J. Am. Chem. Soc.* **2001,** *123* (28), 6961-6963.
14. Gartner, Z. J.; Kanan, M. W.; Liu, D. R., Expanding the Reaction Scope of DNA-Templated Synthesis. *Angew. Chem. Int. Ed.* **2002,** *41* (10), 1796-1800.
15. Li, X.; Gartner, Z. J.; Tse, B. N.; Liu, D. R., Translation of DNA into synthetic N-acyloxazolidines. *J. Am. Chem. Soc.* **2004,** *126* (16), 5090-5092.
16. Poulin-Kerstien, A. T.; Dervan, P. B., DNA-Templated Dimerization of Hairpin Polyamides. *J. Am. Chem. Soc.* **2003,** *125* (51), 15811-15821.
17. Peng, X.; Li, H.; Seidman, M., A Template-Mediated Click–Click Reaction: PNA–DNA, PNA–PNA (or Peptide) Ligation, and Single Nucleotide Discrimination. *Eur. J. Org. Chem.* **2010,** *2010* (22), 4194-4197.
18. Czlapinski, J. L.; Sheppard, T. L., Nucleic Acid Template-Directed Assembly of Metallosalen−DNA Conjugates. *J. Am. Chem. Soc.* **2001,** *123* (35), 8618-8619.

19. Zhan, Z.-Y. J.; Lynn, D. G., Chemical Amplification through Template-Directed Synthesis. *J. Am. Chem. Soc.* **1997,** *119* (50), 12420-12421.
20. Sugiyama, T.; Kuwata, K.; Imamura, Y.; Demizu, Y.; Kurihara, M.; Takano, M.; Kittaka, A., Peptide Nucleic Acid with a Lysine Side Chain at the β-Position: Synthesis and Application for DNA Cleavage. *Chem. Pharm. Bull.* **2016,** *64* (7), 817-823.
21. Gans, P.; Ienco, A.; Peters, D.; Sabatini, A.; Vacca, A. H., A Utility Program for the Investigation of Equilibria Involving Soluble and Partially Soluble Species. *Coord. Chem. Rev.* **1999,** *184*, 311-318.
22. d Martell, A.; Smith, R., Critical Stability Constants, Vol. 5, First Supplement. Plenum Press, New York and London: 1982.
23. Phillips, J. P.; Huber, W. H.; Chung, J. W.; Merritt, L. L., Ultraviolet Absorption Spectra of 2-Substituted 8-Quinolinols. *J. Am. Chem. Soc.* **1951,** *73* (2), 630-632.
24. Sone, K., Absorption Spectra of Some Metallic Chelate Compounds. *J. Am. Chem. Soc.* **1953,** *75* (21), 5207-5211.
25. Stone, K. G.; Friedman, L., The Ultraviolet Absorption Spectrum and the Acid Ionization Constant of 8-Hydroxyquinoline. *J. Am. Chem. Soc.* **1947,** *69* (2), 209-211.
26. Amundsen, A. R.; Whelan, J.; Bosnich, B., Biological analogs. Nature of the binding sites of copper-containing proteins. *J. Am. Chem. Soc.* **1977,** *99* (20), 6730-6739.
27. Jørgensen, C. K., Spectroscopy of Transition-Group Complexes. In *Adv. Chem. Phys.*, John Wiley & Sons, Inc.: 2007; pp 33-146.
28. Sone, K.; Krumholz, P.; Stammreich, H., Studies on the Coördinate Bond. III. Absorption Spectra of Mono-α,α″-dipyridyl and Mono-o-phenanthroline Complexes1. *J. Am. Chem. Soc.* **1955,** *77* (3), 777-780.
29. Wittung, P.; Eriksson, M.; Lyng, R.; Nielsen, P. E.; Norden, B., Induced Chirality in PNA-PNA Duplexes. *J. Am. Chem. Soc.* **1995,** *117* (41), 10167-10173.
30. Wittung, P.; Nielsen, P. E.; Buchardt, O.; Egholm, M.; Nordén, B., DNA-like double helix formed by peptide nucleic acid. *Nature* **1994,** *368* (6471), 561-563.
31. Ewing, G. W.; Steck, E. A., Absorption Spectra of Heterocyclic Compounds. I. Quinolinols and Isoquinolinols1. *J. Am. Chem. Soc.* **1946,** *68* (11), 2181-2187.
32. Irving, H.; Mellor, D. H., 1002. The stability of metal complexes of 1,10-phenanthroline and its analogues. Part I. 1,10-Phenanthroline and 2,2[prime or minute]-bipyridyl. *J. Chem. Soc.* **1962,** (0), 5222-5237.
33. Nielsen, P. E., *Peptide Nucleic Acids: Protocols and Applications*. Horizon Bioscience: Wyndmondham, 2004.
34. Franzini, R. M.; Watson, R. M.; Patra, G. K.; Breece, R. M.; Tierney, D. L.; Hendrich, M. P.; Achim, C., Metal Binding to Bipyridine-Modified PNA. *Inorganic Chemistry* **2006,** *45*, 9798-9811.